Computer Modeling in Engineering & Sciences

Tech Science Press

Doi:10.32604/cmes.2025.071629

ARTICLE

Demographic Heterogeneities in a Stochastic Chikungunya Virus Model with Poisson Random Measures and Near-Optimal Control under Markovian Regime Switching

Maysaa Al-Qurashi[1], **Ayesha Siddiqa**[2], **Shazia Karim**[3], **Yu-Ming Chu**[4,5,*] **and Saima Rashid**[2,*]

[1]Department of Mathematics, College of Science, King Saud University, P.O. Box 2455, Riyadh, 11451, Saudi Arabia
[2]Department of Mathematics, Government College University, Faisalabad, 38000, Pakistan
[3]Department of Basic Sciences and Humanities, University of Engineering and Technology Lahore, Faisalabad Campus, Faisalabad, 38000, Pakistan
[4]Institute for Advanced Study, Honoring Chen Jian Gong Hangzhou Normal University, Hangzhou, 311121, China
[5]Department of Mathematics, Huzhou University, Huzhou, 313000, China

*Corresponding Authors: Yu-Ming Chu. Email: chuyuming@zjhu.edu.cn; Saima Rashid. Email: saimarashid@gcuf.edu.pk

Received: 08 August 2025; Accepted: 22 October 2025; Published: 26 November 2025

ABSTRACT: Chikungunya is a mosquito-borne viral infection caused by the chikungunya virus (CHIKV). It is characterized by acute onset of high fever, severe polyarthralgia, myalgia, headache, and maculopapular rash. The virus is rapidly spreading and may establish in new regions where competent mosquito vectors are present. This research analyzes the regulatory dynamics of a stochastic differential equation (SDE) model describing the transmission of the CHIKV, incorporating seasonal variations, immunization efforts, and environmental fluctuations modeled through Poisson random measure noise under demographic heterogeneity. The model guarantees the existence of a global positive solution and demonstrates periodic dynamics driven by environmental factors. A key contribution of this study is the formulation of a stochastic threshold parameter, $\mathbb{R}_{0L}$, which characterizes the conditions for disease persistence or extinction under random environmental influences. Although our analysis highlights age-specific heterogeneities to illustrate differential transmission risks, the framework is general and can incorporate other vulnerable demographic groups, ensuring broader applicability of the results. Using the Monte Carlo Markov Chain (MCMC) method, we estimate $\mathbb{R}_{0L} = 1.4978$ (95% C-I: 1.4968–1.5823) based on CHIKV data from Florida, USA, spanning 2005 to 2017, suggesting that the outbreak remains active and requires targeted control strategies. The effectiveness of immunization, screening, and treatment strategies varies depending on the prioritized demographic groups, due to substantial differences in CHIKV incidence across age categories in the USA. Numerical simulations were conducted using the truncated Euler–Maruyama method to robustly capture the stochastic dynamics of CHIKV transmission with Poisson-driven jumps. Employing an iterative approach and assuming mild convexity conditions, we formulated and solved a parameterized near-optimality problem using the Ekeland variational principle. Our findings indicate that vaccination campaigns are significantly more effective when focused on vulnerable adults over the age of 66, as well as individuals aged 21 to 25. Furthermore, enhancements in vaccine efficacy, diagnostic screening, and treatment protocols all contribute substantially to minimizing infection rates compared to current standard approaches. These insights support the development of targeted, age-specific public health interventions that can significantly improve the management and control of future CHIKV outbreaks.

KEYWORDS: Chikungunya virus; mathematical modeling; age-structure; poisson random measure; monto-carlo markov chain; extinction; persistence in mean; stochastic near-optimal control; Ekeland's variational principle

Copyright © 2025 The Authors. Published by Tech Science Press.
This work is licensed under a Creative Commons Attribution 4.0 International License, which permits unrestricted use, distribution, and reproduction in any medium, provided the original work is properly cited.

1 Introduction

The *Aedes* mosquito-borne *alphavirus* (family Togaviridae), known as the CHIKV, has recently resurfaced in several regions worldwide, leading to widespread epidemics. Chikungunya fever is primarily characterized by symptoms such as fever, arthralgia, and, in some cases, a *maculopapular* rash. Bioactive compounds found in hops (*Humulus lupulus, Cannabaceae*), particularly *acylphloroglucinols*—commonly referred to as α- and β-acids—have demonstrated significant antiviral activity against CHIKV without exhibiting cytotoxic effects. Vector-borne diseases are infections transmitted to humans via vectors harboring microbial organisms, viruses, or bacteria. CHIKV, an arthropod-borne alphavirus, is propagated predominantly by *Aedes aegypti* and *Aedes albopictus* mosquitoes—the same vectors responsible for Zika, dengue, and yellow fever transmission [1]. CHIKV is a positive-sense, single-stranded RNA virus (11.8 kb) that encodes four nonstructural proteins (nsP1, nsP2 [helicase], nsP3, nsP4 [RNA-dependent RNA polymerase]) and six structural proteins (C, E3, E2, E1, 6K, and TF) [2]. Characterized clinically by arthralgia, myalgia, and tachycardia, CHIKV has expanded from its African origins to South America, particularly Brazil. Between 2013 and 2019, the Pan American Health Organization (PAHO) recorded over 600 CHIKV-related deaths in Latin America, likely underestimating the true global mortality burden.

Recent outbreaks of CHIKV have been markedly distinct from previous ones, characterized by accelerated transmission and broader geographic spread, often originating in migrant communities from regions where the virus remains endemic. A nationwide epidemic in Malaysia in 1998, primarily driven by workforce migration, exemplifies this trend [3]. Following a 20-year hiatus, Indonesia experienced a significant resurgence from 2001 to 2003 [4]. The 2005 global outbreak in India, affecting 1.4 million individuals, represents one of the most severe in recent history, occurring 32 years after the region's last major CHIKV event [5]. The national economic impact of this epidemic was estimated at 45.26 disability-adjusted life years per million, approximately equating to 26,000 cases. In 2006, Réunion Island, located southwest of Madagascar in the Indian Ocean, witnessed an epidemic that impacted one-third of its population [6]. This outbreak was particularly severe, with a notably high fatality rate and significant neurological, hepatocellular, and cardiovascular complications. CHIKV, while similar to Zika and dengue, shows distinct clinical features. In endemic areas, 10%–70% are infected and 50%–97% develop symptoms after 4–7 days [7]. Neonates are highly vulnerable, and individuals over 65 have a five-fold higher fatality rate. The disease has an acute phase (7 days) and a persistent/recurrent phase lasting months or years, with acute polyarthralgia affecting 30%–90% of cases; some patients may also experience coronary, neurological, or ocular complications [8]. Chronic CHIKV infection poses ongoing health challenges. During the Réunion Island epidemic, 43%–75% had symptoms one year post-infection, including arthritic pain, fatigue, and neuralgia. Up to 50% may experience persistent pain, often linked to osteoarthritis and ankylosing spondylitis, affecting joints and cartilage [9].

CHIKV transmission occurs in two distinct phases: the forest and city transmission cycles. In the urban cycle, propagation follows a mosquito-mediated human-to-human transmission, while the forest cycle involves a mosquito-borne transmission from animals to humans route [10]. The forest phase is the initial mechanism for the virus's persistence in Africa [11], whereas the urban cycle dominates in densely populated areas, where *Aedes* mosquitoes, particularly *Aedes aegypti* and *Aedes albopictus*, act as the primary vectors, and humans are the principal hosts [9]. Although *Ae. aegypti* has traditionally been the dominant vector, the significance of *Ae. albopictus* has increased, particularly in recent outbreaks in Europe, Gabon, and Réunion [12]. However, as evidenced by the 2013 Caribbean epidemic, *Ae. aegypti* remains a major vector despite this shift [13]. The spread of *Ae. albopictus* as a prominent vector has been linked to a genetic variation in the virus's E1 protein (A226V polymorphism), which enhances the virus's transmissibility to this mosquito species [9]. Additionally, vertical transmission of CHIKV, particularly in cases following the 2005 epidemic, has been observed, though its validity remains debated [14]. This mode of transmission is considered particularly concerning when the mother remains infected in the days following childbirth [9,11,13].

In humans, the transmission process of CHIKV is well understood, with certain cell types exhibiting heightened susceptibility. Human endothelial and epidermal cells, primordial fibroblasts, and monocyte-derived lymphocytes are particularly prone to infection, facilitating viral propagation. Conversely, CHIKV replication is generally not supported by major lymphocytes, monocytes, lymphoma cells, monocytoid cells, or dendritic cells derived from monocytes [9]. However, this finding remains contentious, as CHIKV-confirmed fibroblasts have been observed *in vivo* in virus-contaminated individuals [11]. Following initial infection, the host mounts an immune activation, however the infection subsequently spreads to lymphocytes and circulates through various organs [13]. This parasitic phase, marked by widespread viral dissemination, is when mosquitoes can acquire the virus from infected hosts during feeding, facilitating further transmission.

Several aspects of the immune response to CHIKV remain unresolved. To eliminate the virus, CHIKV activates non-hematopoietic mitochondria, primarily fibroblasts, triggering a type I interferon response at the site of infection [15]. The interferon response is regulated by factors 3 and 7, which are less effective in older individuals but are crucial for defending against infection in neonates who lack these factors [15]. Brito and Teixeira [16] highlighted that CHIKV-related fatalities were often underreported within healthcare systems, largely due to limited awareness of the virus's clinical manifestations and complications. This underrecognition is understandable, given that CHIKV had only recently emerged in the Americas. The authors noted that secondary causes of death—such as cardiac, respiratory, or metabolic conditions—were frequently documented without acknowledging CHIKV infection as the primary or contributing factor. In individuals with persistent symptoms, CD4+ T-cells are more prevalent in synovial tissues, while CD8+ T-cells are found in the skin during the critical phase of the illness [16]. In addition, bone marrow mesenchymal antigen-2 may help mitigate autoimmune responses triggered by CHIKV and protect lymphoid tissue from damage [17].

To better understand biophysical phenomena and the unpredictable nature of transmission of infections, mathematical models have been extensively used [18,19]. Additionally, they are essential instruments for assessing and choosing the best means of control [20]. Sir Ronald Ross's groundbreaking research on plasmodium established the groundwork for viral infection modeling. Plenty of models have been created since then. Deterministic ordinary differential equations (ODEs) were commonly employed for initial simulations, which assumed consistent death rates and ignored the effects of demographic characteristics and density of the population on morbidity. In [21], Bellan showed that the consequences of vector prevention techniques might be greatly overestimated if age-independent morbidity is assumed. The propagation of many ailments, such as dengue fever, human liver, tumor cells in immunogenetic tumour, HIV with CD4+ t-cells, SARS (severe acute respiratory syndrome), Zika virus, and, most recently, Nipah virus, is also known to be significantly impacted by density of population [18,20]. Recently, Olayiwola and Oluwafemi [22] modeled Tuberculosis dynamics with awareness and vaccination using the Laplace-Adomian method. Olayiwola et al. [23] studied the impact of booster vaccines on managing a new COVID-19 variant using the Laplace-Adomian decomposition method. Mohamed Ali et al. [24] examined stability criteria and optimal control measures for a fractional-order model of human papillomavirus (HPV) infection and cervical cancer. El-Mesady et al. [25] investigated optimal control strategies to reduce HPV transmission in a fractional-order mathematical model.

Meanwhile, the effects of population density have been incorporated into various simulations of insect-borne disease transmission [20]. In [21], the authors considered density-dependent larval mortality rates, but did not account for density effects on transitions between aquatic developmental stages. Although density-dependent mortality during the aquatic phase was included in the basic model of *Aedes aegypti* population dynamics proposed in [9], the three distinct aquatic stages were merged into a single class. This simplification

poses challenges when assessing the impact of specific vector control strategies, as pharmaceutical treatments may affect eggs and larvae differently [14].

Similarly, although Buonomo [26] incorporated mortality driven by population density in humans and mosquitoes within a malaria transmission model, the model did not differentiate between the various aquatic stages of mosquito development via critical aspect for designing effective mosquito control measures. In the same vein, Chitnis et al. [27] studied the propagation processes of the CHIKV by considering only the egg and larval stages of the mosquito population, modeling the effects of density solely on recruitment rates and developmental progression. However, they did not address the impact of larval density on mortality rates, instead focusing exclusively on density-dependent stage advancement during the aquatic maturation process.

Achieving probabilistic optimal control becomes particularly challenging when strict constraints are present. In simpler cases, it may even be impossible to realize true optimal control due to the inherent unpredictability of the system, as highlighted in certain studies [28]. Nevertheless, even in such complex environments, it is often possible to attain near-optimal solutions for stochastic processes [29]. In many applications—such as economics, technology, and beyond developing near-optimal control strategies within an appropriate framework is crucial for achieving desired outcomes. The growing demand for probabilistic near-optimal control has driven significant advancements in this field, establishing it as a key component of dynamic regulation [28,29].

To address these challenges, researchers have developed controlled frameworks based on continuous-time models and finite-state Markov chains, particularly for systems where stochastic differential equations (SDEs) experience abrupt changes phenomena frequently encountered in fields like financial markets, risk management, and asset allocation [30]. Moreover, necessary conditions for ensuring near-optimal control in such complex systems have been rigorously established [30]. It is also widely recognized that environmental perturbation contributes a crucial role in the spread of viral diseases in real-world settings [31]. Since SDEs can more accurately capture the randomness inherent in infection patterns, simulating epidemic outbreaks within a stochastic framework is considered a more reliable approach. Consequently, numerous studies have explored how external noise influences epidemic dynamics [32]. Dereich et al. [33] investigated the behavior of a multilevel Monte Carlo algorithm within an epidemiological framework where population growth remains stable, independent of disease incidence. Their findings demonstrated that the system sustains at least one robust and favorable recurring pattern, ensuring the persistence of the epidemic in a stable environment.

Beyond white noise, Poisson noise is a critical factor in epidemiological simulations, inducing transitions between distinct environmental states [33,34]. In this work, we account for the influence of Poisson noise [35], which drives regime shifts corresponding to varying environmental conditions. For example, fish population growth rates can differ substantially between dry and wet seasons. These transitions, typically following an exponential waiting time distribution, are characterized by a memoryless property [36].

Inspired by the aforementioned literature, we propose a novel model for CHIKV transmission that incorporates density-dependent mortality rates within the human population. This model is calibrated using demographic data from a major CHIKV outbreak in Florida, USA, through the MCMC method. To more effectively quantify the influence of key parameters, a global sensitivity analysis is conducted, focusing on the primary thresholds that govern the model's dynamics. Incorporating a Poisson random measure, we extend the model to a stochastic framework that accounts for dual infection dynamics, environmental noise with random jumps, and a saturated transmission rate. This stochastic model establishes sufficient conditions for both the persistence and potential eradication of the virus, offering a robust foundation for analyzing long-term disease behavior under fluctuating environmental conditions. Additionally, we

address the near-optimal control problem in random frameworks influenced by Poisson noise and regime-switching, without the restrictive requirement of second-order continuous differentiability in the drift and diffusion coefficients. Necessary and sufficient requirements for achieving near-optimal control strategies—such as targeted vaccination and optimized intervention timing—are derived, demonstrating that any ϵ-optimal insight minimizes the Hamiltonian function involving error of order $\epsilon^{3/16}$. Furthermore, the model establishes that an ϵ-minimum condition guarantees near-optimality with an error order of $\epsilon^{1/2}$. This comprehensive framework significantly enhances the ability to design efficient and effective public health interventions against vector-borne diseases such as Chikungunya.

The organization of the work is as follows: Section 2 introduces our autonomous model, which incorporates the adaptive immune response and latently infected cells, and is then extended to a stochastic CHIKV model involving Gaussian white noise and Poisson random measure. Section 3 focuses on the mathematical analysis of the model in relation to the Poisson random measure. Section 4 presents and analyzes the near-optimality control conditions, including numerical simulations and an efficiency analysis. Section 5 discusses model calibration, population stratification, and the contact matrix for the CHIKV model. Section 6 conducts a sensitivity analysis and further examines the optimal control model, including numerical simulations and supporting arguments. Finally, the paper concludes with a summary in the last section. By rigorously analyzing individual class behaviors and leveraging advanced methodologies like Possion random measure, the entire procedurehas been illustrated in the flowchart presented in Fig. 1.

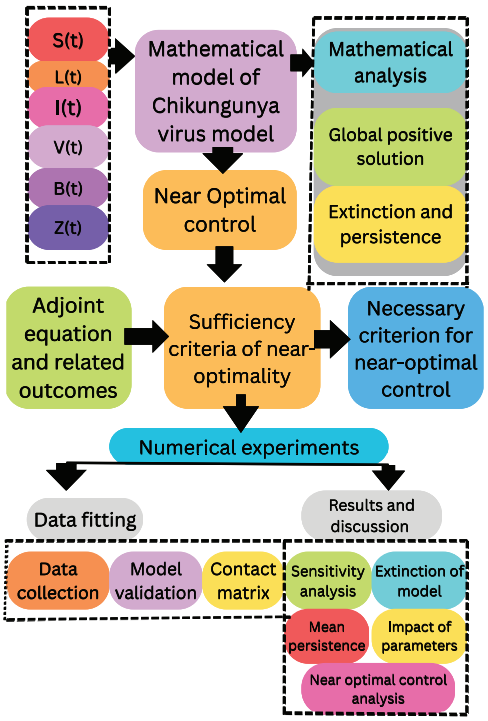

Figure 1: Flow diagram of the overall methodology

2 Model Description

In what follows, the development of CHIKV is dependent on the transmission properties of the virus. Chikungunya fever, which is caused by the CHIKV, an *alphavirus* spread by mosquitoes, is distinguished by an acute fever that appears suddenly, along with eruption, extreme arthritis in the joints, and exhaustion. The Asian continent, the European Union, and the Americas have all seen occurrences of such illness,

which is mostly propagated by *Aedes aegypti* and *Aedes albopictus* mosquitoes [1,3,4]. Research indicates a clear pattern in the spread of CHIKV [14]. To better understand this phenomenon, we propose two models as follows: Firstly, the interaction between the infectious agent, host cells, and immune components such as T cells and antibodies—is modeled within an adaptive immune response framework for CHIKV. This framework helps explain immune variability during infection and fluctuations in transmission. We proceed by presenting the adaptive immune response model, represented by the following system of ODEs:

$$\begin{cases} \dfrac{dS(t)}{dt} = \pi - \varpi_1 S(t) - \beta S(t)V(t), \\ \dfrac{dI(t)}{dt} = \beta S(t)V(t) - \varpi_2 I(t) - \epsilon I(t)Z(t), \\ \dfrac{dV(t)}{dt} = \varpi_3 I(t) - \varpi_4 V(t) - \varpi_5 V(t)B(t), \\ \dfrac{dB(t)}{dt} = \varpi_6 + \varpi_7 B(t)IV(t) - \delta B(t), \\ \dfrac{dZ(t)}{dt} = \varpi_8 + \varpi_9 I(t)Z(t) - \varpi_{10} Z(t), \end{cases} \tag{1}$$

subject to the ICs: $S(0) = S_0, I(0) = I_0, V(0) = V_0, B(0) = B_0$ and $Z(0) = Z_0$. However, system (1) operates on the following assertions:

(i) The number of sensitive cells, $S(t)$, decreases due to natural loss and interaction with virus particles $V(t)$, and fresh vulnerable cells are injected at a steady rate (see Shu et al. [37]).

(ii) Infected cells, $I(t)$, are formed through virus-cell interaction and can be removed naturally or destroyed by cytotoxic T-lymphocytes, $Z(t)$ (see Dubey et al. [38]).

(iii) Infected cells emit $V(t)$, which are neutralized through interactions with antibodies. $B(t)$ cells are activated by infection and eventually die. The population of cytotoxic T cells, $Z(t)$, grows and then decreases at a steady rate (see Handel and Antia [39]).

Secondly, by accounting for lymphocytes that have been infected but are not yet infectious, a CHIKV model incorporating latently infected cells offers a more accurate representation of transmission dynamics. This enhancement captures the latent period between viral entry and active replication, improving the precision of predictive algorithms. The incubation phase influences viral propagation potential, timing of immune responses, and viral load buildup. Including this stage strengthens estimates for outbreak control and therapeutic intervention strategies. The following extended framework of ODEs builds upon the previous model by incorporating latently infected cells:

$$\begin{cases} \dfrac{dS(t)}{dt} = \pi - \varpi_1 S(t) - \beta S(t)V(t), \\ \dfrac{dL(t)}{dt} = (1-\rho)\beta S(t)V(t) - (\Theta + \varphi)L(t), \\ \dfrac{dI(t)}{dt} = \rho\beta S(t)V(t) + \varphi L(t) - \varpi_2 I(t) - \epsilon I(t)Z(t), \\ \dfrac{dV(t)}{dt} = \varpi_3 I(t) - \varpi_4 V(t) - \varpi_5 V(t)B(t), \\ \dfrac{dB(t)}{dt} = \varpi_6 + \varpi_7 V(t)B(t) - \delta B(t), \\ \dfrac{dZ(t)}{dt} = \varpi_8 + \varpi_9 I(t)Z(t) - \varpi_{10} Z(t). \end{cases} \tag{2}$$

subject to the ICS: $S(0) = S_0, L(0) = L_0, V(0) = V_0, B(0) = B_0, Z(0) = Z_0$. These values determine the initial population sizes of each compartment. The dynamics of the compartmental model, capturing the transitions between the five key compartments.

The formulation of the proposed CHIKV models is grounded in established immunological and epidemiological modeling frameworks. The first model (1) focuses on the interaction between susceptible host cells, infected cells, virus particles, and immune responses (T-cells and antibodies). Such compartmental structures have been widely adopted in viral dynamics research (see Shu et al. [37]; Dubey et al. [38]; Handel and Antia [39]) as they capture the essential mechanisms of infection progression and immune regulation.

However, to provide a more realistic description of CHIKV transmission, it is crucial to account for the latent phase of infection, where cells are infected but not yet producing new virions. This motivates the extension presented in (2), where a new compartment for latently infected cells is introduced. Similar extensions have been successfully employed in the study of other mosquito-borne viral infections (see e.g., Buonomo [26], Chitnis et al. [27], Shu et al. [37]; Dubey et al. [38]). Incorporating latency reflects the biological reality that the virus requires an incubation period before active replication, thereby improving predictive accuracy for outbreak size, timing, and intervention strategies.

Thus, the transition from the baseline model (1) to the extended model (2) is justified both biologically and mathematically, ensuring that the formulation aligns with state-of-the-art approaches in infectious disease modeling. This refinement allows the model to better capture observed CHIKV transmission dynamics and provides a more solid foundation for evaluating control measures.

This second model (2) modifies the initial system (1) by incorporating the latently infected cells class $L(t)$. All the parameters are described in Table 1.

The basic reproductive number

$$\mathbb{R}_0 = \frac{\beta\delta\pi\varpi_3\varpi_{10}}{\varpi_1(\varpi_5\varpi_6 + \delta)(\epsilon\varpi_8 + \varpi_2\varpi_{10})},$$

serves as a threshold: if $\mathbb{R}_0 > 1$, infection can spread, while $\mathbb{R}_0 < 1$ indicates eventual eradication. Public health relevance lies in its components: reducing β (vector control), lowering ϖ_3 (antivirals), or enhancing immune clearance terms in the denominator (vaccination, improved diagnostics) all decrease $\mathbb{R}_0$. Thus, $\mathbb{R}_0$ guides which interventions most effectively reduce transmission, although under regime switching and stochastic effects the refined threshold $\mathbb{R}_{0L}$ provides a more realistic measure. Effective control requires a combined strategy, where vector reduction lowers transmission opportunities while immune-strengthening interventions (e.g., vaccination or therapeutics) enhance host resistance, together providing the most impactful reduction in spread.

Table 1: Definition of model state variables and parameters associated with the CHIKV model (2)

Symbol	Biological interpretation
$S(t)$	Number of susceptible (healthy target) cells at time t
$L(t)$	Number of latently infected cells (infected but not yet infectious) at time t
$I(t)$	Number of actively infected (productively infectious) cells at time t
$V(t)$	Population of free virus particles (CHIKV virions) at time t
$B(t)$	Population of antibody-producing B cells/antibodies at time t
$Z(t)$	Population of Cytotoxic T Lymphocytes (CTLs) at time t
π	Rate of influx of new susceptible cells into the system

(Continued)

Table 1 (continued)

Symbol	Biological interpretation
ϖ_1	Natural attrition rate of susceptible cells
β	Infection rate of susceptible cells due to contact with CHIKV
ϖ_2	Mortality rate of infected cells
ϵ	Clearance rate of infected cells by CTL immune response
ϖ_3	Mean number of viral particles produced per infected cell
ϖ_4	Clearance rate of free viral particles from the host
ϖ_5	Efficiency of antibody neutralization of viral particles
ϖ_6	Baseline production rate of antibodies
ϖ_7	Proliferation rate of antibodies in response to infection
δ	Natural degradation rate of antibodies
ϖ_8	Baseline generation rate of CTLs
ϖ_9	Expansion rate of CTLs via contact with infected cells
ϖ_{10}	Natural attrition rate of CTLs
ρ	Fraction of infections that immediately progress to active infection
Θ	Death rate of latently infected cells
φ	Activation rate of latent cells transitioning to infectious cells

For the latently infected cells, we have $\bar{\aleph} = \mathrm{S(t)} + \mathrm{L(t)} + \mathrm{I(t)} + \mathrm{V(t)} + \mathrm{B(t)} + \mathrm{Z(t)}$. Now we convert the classical latently infected model to a Gaussian white noise version as follows:

$$\begin{cases} d\mathrm{S(t)} = [\pi - \varpi_1\mathrm{S(t)} - \beta\mathrm{S(t)V(t)}]\,d\mathrm{t} + \sigma_1\mathrm{S(t)}d\mathbb{B}_1(\mathrm{t}), \\ d\mathrm{L(t)} = [(1-\rho)\beta\mathrm{S(t)V(t)} - (\Theta+\varphi)\mathrm{L(t)}]\,d\mathrm{t} + \sigma_2\mathrm{L(t)}d\mathbb{B}_2(\mathrm{t}), \\ d\mathrm{I(t)} = [\rho\beta\mathrm{S(t)V(t)} + \varphi\mathrm{L(t)} - \varpi_2\mathrm{I(t)} - \epsilon\mathrm{I(t)Z(t)}]\,d\mathrm{t} + \sigma_3\mathrm{I(t)}d\mathbb{B}_3(\mathrm{t}), \\ d\mathrm{V(t)} = [\varpi_3\mathrm{I(t)} - \varpi_4\mathrm{V(t)} - \varpi_5\mathrm{V(t)B(t)}]\,d\mathrm{t} + \sigma_4\mathrm{V(t)}d\mathbb{B}_4(\mathrm{t}), \\ d\mathrm{B(t)} = [\varpi_6 + \varpi_7\mathrm{V(t)B(t)} - \delta\mathrm{B(t)}]\,d\mathrm{t} + \sigma_5\mathrm{B(t)}d\mathbb{B}_5(\mathrm{t}), \\ d\mathrm{Z(t)} = [\varpi_8 + \varpi_9\mathrm{I(t)Z(t)} - \varpi_{10}\mathrm{Z(t)}]\,d\mathrm{t} + \sigma_6\mathrm{Z(t)}d\mathbb{B}_6(\mathrm{t}). \end{cases} \tag{3}$$

In spite of the inherent advantages associated with Poisson random measure perturbations, their utility may be further amplified if noise-modulated drift velocity remains inside an optimal threshold domain. The integration of both local and nonlocal Lipschitz criteria underscores that embedding Poisson random measure disturbances can significantly enhance the fidelity and variability of transmitted information, particularly in feedback-driven epidemic models governed by arbitrary SDEs. As highlighted in previous studies [40], Poisson random measure noise exhibits notable advantages over conventional Gaussian disturbances in the context of theoretical epidemiological modeling. Nevertheless, its implementation introduces elevated computational complexity, which poses additional analytical challenges. The jump-diffusion framework incorporating Poisson random measures extends classical formulations by providing a more precise depiction of phenomena such as the abrupt firing of neuronal membrane potentials. Furthermore, the incorporation of such noise mechanisms has been shown to improve the robustness and temporal precision of recurrent neural network (RNN) architectures. When applied to the system described in Eq. (3), the use of Poisson random measure noise leads to a system of compound Poisson-driven SDEs, as detailed in [41].

$$\begin{cases} dS(t) = [\pi - \varpi_1 S(t) - \beta S(t)V(t) + \sigma_1 S(t) d\mathbb{B}_1(t)]\, dt + \int_\Phi \Theta_1(\Psi) S(t^-) \bar{\aleph}(dt, d\Psi), \\ dL(t) = [(1-\rho)\beta S(t)V(t) - (\theta + \varphi)L(t)]\, dt + \sigma_2 L(t) d\mathbb{B}_2(t) + \int_\Phi \Theta_2(\Psi) L(t^-) \bar{\aleph}(dt, d\Psi), \\ dI(t) = [\rho\beta S(t)V(t) + \varphi L(t) - \varpi_2 I(t) - \epsilon I(t)Z(t)]\, dt + \sigma_3 I(t) d\mathbb{B}_3(t) + \int_\Phi \Theta_3(\Psi) I(t^-) \bar{\aleph}(dt, d\Psi), \\ dV(t) = [\varpi_3 I(t) - \varpi_4 V(t) - \varpi_5 V(t)B(t)]\, dt + \sigma_4 V(t) d\mathbb{B}_4(t) + \int_\Phi \Theta_4(\Psi) V(t^-) \bar{\aleph}(dt, d\Psi), \\ dB(t) = [\varpi_6 + \varpi_7 V(t)B(t) - \delta B(t)]\, dt + \sigma_5 B(t) d\mathbb{B}_5(t) + \int_\Phi \Theta_5(\Psi) B(t^-) \bar{\aleph}(dt, d\Psi), \\ dZ(t) = [\varpi_8 + \varpi_9 I(t)Z(t) - \varpi_{10} Z(t)]\, dt + \sigma_6 Z(t) d\mathbb{B}_6(t) + \int_\Phi \Theta_6(\Psi) Z(t^-) \bar{\aleph}(dt, d\Psi), \end{cases} \tag{4}$$

whereas

$$\Omega_1 = \sigma_1 S(t) d\mathbb{B}_1(t) + \int_\Phi \Theta_1(\Psi) S(t^-) \bar{\aleph}(dt, d\Psi), \quad \Omega_2 = \sigma_2 L(t) d\mathbb{B}_2(t) + \int_\Phi \Theta_2(\Psi) L(t^-) \bar{\aleph}(dt, d\Psi),$$
$$\Omega_3 = \sigma_3 I(t) d\mathbb{B}_3(t) + \int_\Phi \Theta_3(\Psi) I(t^-) \bar{\aleph}(dt, d\Psi), \quad \Omega_4 = \sigma_4 V(t) d\mathbb{B}_4(t) + \int_\Phi \Theta_4(\Psi) V(t^-) \bar{\aleph}(dt, d\Psi),$$
$$\Omega_5 = \sigma_5 B(t) d\mathbb{B}_5(t) + \int_\Phi \Theta_5(\Psi) B(t^-) \bar{\aleph}(dt, d\Psi), \quad \Omega_6 = \sigma_6 Z(t) d\mathbb{B}_6(t) + \int_\Phi \Theta_6(\Psi) Z(t^-) \bar{\aleph}(dt, d\Psi).$$

A new scheme of the associated SDE model is built to clarify the dynamical interconnections across the CHIKV propagation system, specifically in the occurrence of latently infectious cell compartments. The chronological progression of every demographic compartment with deterministic and stochastic consequences involving Gaussian white noise and Poisson random measure disruptions. Nonlinear prevalence factors control compartment transitions, and stochastic stimuli are included to account for unpredictable interaction occurrences and modifications in the environment. In particular, the abrupt activation of persistent lymphocytes is represented by a Poisson jump mechanism and a delay differential term, which effectively characterize the pattern of latent infections. Transitions such as infection, latency stimulation, virus generation, immune system stimuli, and natural eradication are indicated in the aforementioned system.

However, the compensated Poisson random measure indicated by $\bar{\aleph}$, it can be described as

$$\bar{\aleph}(dt, dT) = \aleph(dt, dT) - \alpha(dt) d\Psi.$$

The expression $\Theta(t)$ represents the left limit. The terms $B_\jmath(t) \forall \jmath \in \{1, \ldots, 6\}$ represent autonomous classical Brownian motions, started at $B_\jmath(0) = 0$. The parameters $\xi_\jmath$, where $\jmath \in \{1, \ldots, 6\}$, indicate the intensity of the stochastic perturbations, which incorporate Gaussian white noise effects into the epidemiological model. All additional components retain the identical interpretation. The Poisson random measure in this case is $\bar{\aleph}$, and the strength of its estimate becomes $\alpha(.)$. Also, the mapping α stated on measure set $\Psi[0, \infty)$ possessing the features $\alpha(\Psi) < \infty$ and $\Theta_\omega \geq 0$, $(\omega = \{1, \ldots, 6\})$.

2.1 Basic Concept

This section presents the foundational definitions and lemmas pertinent to stochastic analysis. The notation and structural conventions adopted here align with those outlined in [42], and will be consistently employed throughout this study.

$$\langle \mathbb{Q}(t) \rangle = \frac{1}{t} \int_0^t \mathbb{Q}(\jmath) d\jmath. \tag{5}$$

Lemma 1: *([43]) To facilitate our investigation, we shall employ two essential presumptions, denoted* $(\mathbf{A_1}(t))$ *and* $(\mathbf{A_2}(t))$*. Such requirements are necessary for establishing existence-uniqueness for global non-negative outcome for framework (3).*

$(\mathbf{A_1}(t))$: *for all* $\mathsf{M} > 0\ \exists \mathbb{L}_{\mathsf{M}} > 0$ *such that*

$$\int_{\Phi} |\Lambda_I(\Psi_1, \mho) - \Lambda_I(\Psi_2, \mho)|^2 d\alpha(\Psi) \leq \mathbb{L}_{\mathsf{M}} |\mho_1 - \mho_2|^2, \jmath = \{1, 2, \ldots, 6\}, \tag{6}$$

with $|\mho_1| \vee |\mho_2| \leq \mathbb{S}$, *where*

$$\begin{aligned}
&\Lambda_1(\mho, \Psi) = \Theta_1(\Psi)\mho \ for\ \mho = S(t^-),\\
&\Lambda_2(\mho, \Psi) = \Theta_2(\Psi)\mho \ for\ \mho = L(t^-),\\
&\Lambda_3(\mho, \Psi) = \Theta_3(\Psi)\mho \ for\ \mho = I(t^-),\\
&\Lambda_4(\mho, \Psi) = \Theta_4(\Psi)\mho \ for\ \mho = V(t^-),\\
&\Lambda_5(\mho, \Psi) = \Theta_5(\Psi)\mho \ for\ \mho = B(t^-),\\
&\Lambda_6(\mho, \Psi) = \Theta_6(\Psi)\mho \ for\ \mho = Z(t^-),
\end{aligned} \tag{7}$$

where t *represents the compensated stochastic parameter.*

$(\mathbf{A_2}(t))$: $|\log(1 + \Theta_\jmath(\mho))| \leq \complement$ *for* $\Theta_\jmath(\mho) > -1, \jmath = \{1, 2, \ldots, 6\}$, *where* $\complement$ *is a fixed non-negative number.*

Theorem 1: *For a stochastic model (4)* $(S(t), L(t), I(t), V(t), B(t), Z(t))$ *is a solution containing ICs* $(S(0), L(0), I(0), V(0), B(0), Z(0)) \in \mathbb{R}_6^+$, *then*

$$\lim_{t\to\infty} \frac{S(t) + L(t) + I(t) + V(t) + B(t) + Z(t)}{t} = 0. \tag{8}$$

Furthermore, if $\max\left\{\varpi_{10\,\imath h}, \varpi_{10\,\jmath h}\right\} > \frac{\sigma_1^2+\sigma_2^2+\sigma_3^2+\sigma_4^2+\sigma_5^2+\sigma_6^2}{t}$, *then*

$$\begin{aligned}
&\lim_{t\to\infty} \frac{\int_0^t S(s)dB_1(s)}{t} = 0, \quad \lim_{t\to\infty} \frac{\int_0^t L(s)dB_2(s)}{t} = 0, \quad \lim_{t\to\infty} \frac{\int_0^t I(s)dB_3(s)}{t} = 0,\\
&\lim_{t\to\infty} \frac{\int_0^t B(s)dB_4(s)}{t} = 0, \quad \lim_{t\to\infty} \frac{\int_0^t V(s)dB_5(s)}{t} = 0, \quad \lim_{t\to\infty} \frac{\int_0^t Z(s)dB_6(s)}{t} = 0.
\end{aligned} \tag{9}$$

Thus, the solutions of CHIKV model (4) possess the subsequent features;

$$\begin{aligned}
&\lim_{t\to\infty} \sup S(t) = \frac{\pi}{\varpi_1}, \quad \lim_{t\to\infty} \sup L(t) = 0, \quad \lim_{t\to\infty} \sup I(t) = 0,\\
&\lim_{t\to\infty} \sup B(t) = \frac{\varpi_6}{\delta}, \quad \lim_{t\to\infty} \sup V(t) = 0, \quad \lim_{t\to\infty} \sup Z(t) = \frac{\varpi_8}{\varpi_{10}}.
\end{aligned} \tag{10}$$

Proof: The supporting arguments for this lemma are analogous to those provided for Lemmas 2.1 and 2.2 in [44]; therefore, they are omitted here for brevity in the context of this analysis. □

The previously outlined definitions of mean persistence are particularly noteworthy, as highlighted in [42].

Definition 1: *([45])To establish the property of extinction or persistence, the stochastic model (4) is required to satisfy the following conditions:*

$$\lim_{t\to\infty} \inf \frac{1}{t} \int_0^t \mathbb{W}(\mathsf{s})d\mathsf{s} > 0, \ a.s. \tag{11}$$

The criteria outlined herein are consistent with those detailed in [42], wherein the associated lemmas delineate the requisite conditions for the persistence of infection.

Lemma 2: *(***Strong law***) ([45]) Considering a real-continuous mapping* $\mathbb{S} = \{\mathbb{S}\}_{0\leq t}$*, the local martingale criterion occurs if it disappears as* $t \to 0$ *and*

$$\lim_{t\to\infty}\langle \mathbb{S},\mathbb{S}\rangle_t = \infty,\ a.s. \implies \lim_{t\to\infty}\frac{\Phi_t}{\langle \mathbb{S},\mathbb{S}\rangle_t} = 0,\ a.s.$$
$$\lim_{t\to\infty}\sup\frac{\langle \mathbb{S},\mathbb{S}\rangle_t}{t} < 0,\ a.s. \implies \lim_{t\to\infty}\frac{\mathbb{S}_t}{t} = 0\ a.s. \tag{12}$$

Lemma 3: *([45]) Consider* $\mathbf{h} \in \mathcal{C}([0,\infty)\times\bar{B}(0,\infty))$ *and* $\mathbf{G} \in \mathcal{C}([0,\infty)\times\bar{B}\mathbb{R}) \ni \lim_{t\to\infty}\frac{\mathbf{G}(t)}{t} = 0,\ a.s.$ *if* $t \geq 0$*, then*

$$\log f_2(t) \geq \Gamma_0(t) - \Gamma\int_0^t \mathbf{h}(S)dS + \mathbf{G}(t),\ a.s.$$

Therefore, we have

$$\lim_{t\to\infty}\inf\langle \mathbf{g}(t)\rangle \geq \frac{\Gamma_0}{\Gamma},\ a.s.$$

Here, Γ *and* Γ_0 *indicate positive constants, respectively.*

Definition 2: *(***Approximate optimal control***) ([46]) A set of permissible control strategies* $\{(\mathcal{F}_\eta^\delta, V_\eta^\delta)\}$ *indexed by* $\delta > 0$ *and any member* $(\mathcal{F}_\eta^\delta, V_\eta^\delta)$*, or just* V_η^δ*, within this set is termed as an approximate optimal control if the following condition holds:*

$$|\mathfrak{J}(0,\mathcal{F}_0,V_\eta^\delta) - \mathfrak{J}(0,\mathcal{F}_0)| \leq \epsilon\ (\delta), \tag{13}$$

where

$$\mathfrak{J}(0,\mathcal{F}_0) = \inf_{V_\eta\in\mathbb{V}_{ad}[0,T]}\mathfrak{J}(0,\mathcal{F}_0,V_\eta). \tag{14}$$

The function $\epsilon\ (\delta)$ *satisfies:*

$$\epsilon\ (\delta) \to 0 \quad \text{as} \quad \delta \to 0. \tag{15}$$

If $\exists$ *a fixed* $\mathcal{C} > 0$ *such that:*

$$\epsilon\ (\delta) = \mathcal{C}\delta^p, \tag{16}$$

then V_η^δ *is termed as approximate optimal control of order* δ^p*.*

Definition 3: *(***Generalized gradient in Clarke's sense***) [47] Consider* $\Phi(\cdot) : \Phi \to \mathbb{R}$ *as a locally Lipschitz function on a convex domain* $\Phi \subset \mathbb{R}^n$*. The generalized gradient for Clarke* Ψ *at* $\hat{\mathcal{F}} \in \Phi$ *is stated as:*

$$\partial_{\mathcal{F}}\Psi(\hat{\mathcal{F}}) = \left\{\tilde{\zeta} \in \mathbb{R}^n \mid \tilde{\zeta}\cdot \mathsf{q} \leq \varphi^0(\hat{\mathcal{F}};q), \forall q \in \mathbb{R}^n\right\}, \tag{17}$$

where

$$\Psi^0(\hat{\mathcal{F}};\mathsf{q}) = \limsup_{\substack{\mathcal{F}\to\hat{\mathcal{F}}\\ \mathsf{p}\to 0^+}}\frac{\Phi(\mathcal{F}+\mathsf{pq}) - \Phi(\mathcal{F})}{\mathsf{p}}, \quad \mathcal{F} \in \mathcal{D}, \quad \mathcal{F}+\mathsf{pq} \in \Phi. \tag{18}$$

Lemma 4: *([47]) Suppose that* $\mathsf{a}_1, \mathsf{a}_2, \ldots, \mathsf{a}_n$ *are real-valued functions. Then the sunsequent inequality holds:*

$$|\mathsf{a}_1 + \mathsf{a}_2 + \cdots + \mathsf{a}_n|^m \leq C_m \left(|\mathsf{a}_1|^m + |\mathsf{a}_2|^m + \cdots + |\mathsf{a}_n|^m\right), \tag{19}$$

where $m > 0$ *and*

$$C_m = \begin{cases} 1, & 0 < m \leq 1, \\ n^{m-1}, & m > 1. \end{cases} \tag{20}$$

Lemma 5: *([47]) Suppose that there is a complete metric space* $(\mathbf{A}, d)$ *and a bounded operator* $\mathcal{F}(\cdot) : \mathbf{A} \to \mathbb{R}$ *which is also lower-semicontinuous. If* $\exists q > 0$ *and* $V_q(\cdot) \in_{\mathcal{F}}$ *such that:*

$$\mathcal{F}(V_q(\cdot)) \leq \inf_{V(\cdot) \in_{\mathcal{F}}} \mathcal{F}(V(\cdot)) + q. \tag{21}$$

2.2 Global Positive Solution

To enhance the realism of the CHIKV transmission model, we incorporate a compartment for latently infected cells and introduce stochasticity via a Poisson random measure. The resulting stochastic model (4) serves as a physiological analogue for the population dynamics of CHIKV infection. This model formulation requires the presence of a global, bounded, and non-negative solution. To analyze the well-posedness of the system defined by (4), we adopt the standard assumptions $(\mathbf{A_1})$ and $(\mathbf{A_2})$ stated in Lemma 1. These hypotheses enable us to establish the existence-uniqueness of a global solution. The forthcoming analysis will rigorously demonstrate that, under these assumptions, the stochastic CHIKV model with latently infected cells driven by a Poisson random measure permits a unique global positive solution.

Theorem 2: *Surmise that the stochastic model (4), defined for* $t \geq 0$, *permits a unique solution* $(S(t), L(t), I(t), V(t), B(t), Z(t))$ *corresponding to ICs* $(S(0), L(0), I(0), V(0), B(0), Z(0)) \in \mathbb{R}^6_+$. *Furthermore, the solution stays in* $\mathbb{R}+^6$ *having probability one, means that* $(S(t), L(t), I(t), V(t), B(t), Z(t)) \in \mathbb{R}^6_+ \ \forall\ t \geq 0$, *almost surely.*

Proof: Since the drift and diffusion are guaranteed to be locally Lipschitz by the requirement $(\mathbf{A_1})$, there will be a time t at which the suggested concern will have a locally specific solution in the range $[0, \pi_{\mathfrak{e}})$. The explosion phase is represented here by $\pi_{\mathfrak{e}}$; researchers are directed to [42] for more details. To establish that the outcome is global, it need to be shown that $\pi_{\mathfrak{e}} = \infty$ is adequate. In order to illustrate this, let $\mathbb{K}_0$ be a large enough non-negative real number such that each outcome falls inside the range $[\frac{1}{\mathbb{K}_0}, \mathbb{K}_0]$. As a result, given $\mathbb{K} \geq \mathbb{K}_0$, permit

$$\pi_{\mathbb{K}} = \left\{\inf t \in [0, \pi_{\mathfrak{e}}) : \frac{1}{\mathbb{K}} \geq \min\{\mho\} \quad or \quad \mathbb{K} \leq \max\{\mho\}\right\}, \tag{22}$$

where $\mho = (S(t), L(t), I(t), B(t), V(t), Z(t), (t), I_\Lambda(t))$. Here, $\inf \varnothing = \infty$. Moreover, $\pi_{\mathbb{K}}$ increases as $\mathbb{K} \to \infty$. Suppose that $\pi_{\mathbb{K}}$ possesses a limit of π_∞, It is almost a given that $\pi_\infty \leq \pi_{\mathfrak{e}}$. Alternatively, it is necessary to demonstrate that $\pi_\infty = \infty$. If this supposition is false, then the constant $T > 0$ and Φ lie within $(0, 1)$ such that

$$\mathbf{P}\{\pi_\infty \leq T\} > \Phi. \tag{23}$$

So that, there is a natural number $\mathbb{K}_1 \geq \mathbb{K}_0$, the following holds

$$\varepsilon \leq \mathbf{P}\{T \geq \pi_{\mathbb{K}}\}, \forall \quad \mathbb{K} \geq \mathbb{K}_1. \tag{24}$$

To demonstrate the remaining part of the hypothesis, we proceed by constructing the mapping as follows:

$$\begin{aligned}
d\mathbb{U}(\mho) = {} & L\mathbb{U}(\mho)d\mathrm{t} + \sigma_1(\mathrm{S}-\mathbb{Q})d\mho_1(\mathrm{t}) + \sigma_2(\mathrm{L}-1)d\mho_2(\mathrm{t}) \\
& + \sigma_3(\mathrm{I}-1)d\mho_3(\mathrm{t}) + \sigma_4(\mathrm{B}-1)d\mho_4(\mathrm{t}) + \sigma_5(\mathrm{V}-1)d\mho_5(\mathrm{t}) + \sigma_6(\mathrm{Z}-1)d\mho_6(\mathrm{t}) \\
& + \int_\Phi [\Theta_1(\mho)\mathrm{S} - \mathcal{Q}\log(\Theta_1(\Psi)+1)]\,\bar{\aleph}(d\mathrm{t}, d\Psi) + \int_\Phi [\Theta_2(\mho)\mathrm{L} - \log(\Theta_2(\Psi)+1)]\,\bar{\aleph}(d\mathrm{t}, d\Psi) \\
& + \int_\Phi [\Theta_3(\mho)\mathrm{I} - \log(\Theta_3(\Psi)+1)]\,\bar{\aleph}(d\mathrm{t}, d\Psi) + \int_\Phi [\Theta_4(\mho)\mathrm{B} - \log(\Theta_4(\Psi)+1)]\,\bar{\aleph}(d\mathrm{t}, d\Psi) \\
& + \int_\Phi [\Theta_5(\mho)\mathrm{V} - \log(\Theta_5(\Psi)+1)]\,\bar{\aleph}(d\mathrm{t}, d\Psi) + \int_\Phi [\Theta_6(\mho)\mathrm{Z} - \log(\Theta_6(\Psi)+1)]\,\bar{\aleph}(d\mathrm{t}, d\Psi).
\end{aligned} \tag{25}$$

The aforementioned relationship defines the $L\mathbb{U}$ operator as a mapping from $\mathbb{R}^6+$ to $\mathbb{R}+$. To demonstrate the remaining part of the hypothesis, we proceed by explicitly constructing this mapping as follows:

$$\begin{aligned}
L\mathbb{U} = {} & \left(1-\frac{\mathcal{Q}}{\mathrm{S}}\right)(\pi - \varpi_1\mathrm{S}(\mathrm{t}) - \beta\mathrm{S}(\mathrm{t})\mathrm{V}(\mathrm{t})) + \left(1-\frac{1}{\mathrm{L}}\right) + ((1-\rho)\beta\mathrm{S}(\mathrm{t})\mathrm{V}(\mathrm{t}) - (\Theta+\varphi)\mathrm{L}(\mathrm{t})) \\
& + \left(1-\frac{1}{\mathrm{I}}\right)(\rho\beta\mathrm{S}(\mathrm{t})\mathrm{V}(\mathrm{t}) + \varphi\mathrm{L}(\mathrm{t}) - \varpi_2\mathrm{I}(\mathrm{t}) - \epsilon\mathrm{I}(\mathrm{t})\mathrm{Z}(\mathrm{t})) \\
& + \left(1-\frac{1}{\mathrm{B}}\right)(\varpi_3\mathrm{I}(\mathrm{t}) - \varpi_4\mathrm{V}(\mathrm{t}) - \varpi_5\mathrm{V}(\mathrm{t})\mathrm{B}(\mathrm{t})) \\
& + \left(1-\frac{1}{\mathrm{V}}\right)(\varpi_6 + \varpi_7\mathrm{V}(\mathrm{t})\mathrm{B}(\mathrm{t}) - \delta\mathrm{B}(\mathrm{t})) + \left(1-\frac{\mathcal{Q}}{\mathrm{Z}}\right)(\varpi_8 + \varpi_9\mathrm{I}(\mathrm{t})\mathrm{Z}(\mathrm{t}) - \varpi_{10}\mathrm{Z}(\mathrm{t})) \\
& + \mathcal{Q}\frac{\sigma_1^2}{2} + \frac{\sigma_2^2}{2} + \frac{\sigma_3^2}{2} + \frac{\sigma_4^2}{2} + \frac{\sigma_5^2}{2} + \frac{\sigma_6^2}{2} \\
& + \int_\Phi [\mathcal{Q}\Theta_1(\Psi) - \mathcal{Q}\log(\Theta_1(\Psi)+1)]\,\mathrm{t}(d\Psi) + \int_\Phi [\Theta_2(\Psi) - \log(\Theta_2(\Psi)+1)]\,\mathrm{t}(d\Psi) \\
& + \int_\Phi [\Theta_3(\Psi) - \log(\Theta_3(\Psi)+1)]\,\mathrm{t}(d\Psi) + \int_\Phi [\Theta_4(\Psi) - \log(\Theta_4(\Psi)+1)]\,\mathrm{t}(d\Psi) \\
& + \int_\Phi [\Theta_5(\Psi) - \log(\Theta_5(\Psi)+1)]\,\mathrm{t}(d\Psi) + \int_\Phi [\Theta_6(\Psi) - \log(\Theta_6(\Psi)+1)]\,\mathrm{t}(d\Psi) \\
& \le \pi + \varpi_1\mathbb{Q} + \Theta + \varphi + \varpi_2 + \varpi_6 - \varpi_7 + \varpi_4 + \varpi_{10} + \mathcal{Q}\frac{\sigma_1^2}{2} + \frac{\sigma_2^2}{2} + \frac{\sigma_3^2}{2} + \frac{\sigma_4^2}{2} + \frac{\sigma_5^2}{2} + \frac{\sigma_6^2}{2} \\
& + \int_\Phi [\mathcal{Q}\Theta_1(\Psi) - \mathcal{Q}\log(\Theta_1(\Psi)+1)]\,\mathrm{t}(d\Psi) + \int_\Phi [\Theta_2(\Psi) - \log(\Theta_2(\Psi)+1)]\,\mathrm{t}(d\Psi) \\
& + \int_\Phi [\Theta_3(\Psi) - \log(\Theta_3(\Psi)+1)]\,\mathrm{t}(d\Psi) + \int_\Phi [\Theta_4(\Psi) - \log(\Theta_4(\Psi)+1)]\,\mathrm{t}(d\Psi) \\
& + \int_\Phi [\Theta_5(\Psi) - \log(\Theta_5(\Psi)+1)]\,\mathrm{t}(d\Psi) + \int_\Phi [\Theta_6(\Psi) - \log(\Theta_6(\Psi)+1)]\,\mathrm{t}(d\Psi) \\
& \le \pi + \varpi_1\mathbb{Q} + \Theta + \varphi + \varpi_2 + \varpi_6 - \varpi_7 + \varpi_4 + \varpi_{10} + \mathcal{Q}\frac{\sigma_1^2}{2} + \frac{\sigma_2^2}{2} + \frac{\sigma_3^2}{2} + \frac{\sigma_4^2}{2} + \frac{\sigma_5^2}{2} + \frac{\sigma_6^2}{2} \\
& + \int_\Phi [\mathcal{Q}\Theta_1(\Psi) - \mathcal{Q}\log(\Theta_1(\Psi)+1)]\,\mathrm{t}(d\Psi) + \int_\Phi [\Theta_2(\Psi) - \log(\Theta_2(\Psi)+1)]\,\mathrm{t}(d\Psi) \\
& + \int_\Phi [\Theta_3(\Psi) - \log(\Theta_3(\Psi)+1)]\,\mathrm{t}(d\Psi) + \int_\Phi [\Theta_4(\Psi) - \log(\Theta_4(\Psi)+1)]\,\mathrm{t}(d\Psi) \\
& + \int_\Phi [\Theta_5(\Psi) - \log(\Theta_5(\Psi)+1)]\,\mathrm{t}(d\Psi) + \int_\Phi [\Theta_6(\Psi) - \log(\Theta_6(\Psi)+1)]\,\mathrm{t}(d\Psi).
\end{aligned}$$

Furthermore, (22) ensures the inequality $S + L + I + B + Z + V \leq 1$, thus

$$\begin{aligned}
L\mathbb{U} \leq\ & \pi + \varpi_1\mathbb{Q} + \Theta + \varphi + \varpi_2 + \varpi_6 - \varpi_7 + \varpi_4 + \varpi_{10} \\
& + \frac{\mathcal{Q}\sigma_1^2 + \sigma_2^2 + \sigma_3^2 + \sigma_4^2 + \sigma_5^2 + \sigma_6^2}{2} + \int_\Phi [\mathcal{Q}\Theta_1(\Psi)S - \mathcal{Q}\log(\Theta_1(\Psi)+1)]\, t(d\Psi) \\
& + \int_\Phi [\Theta_2(\Psi)L - \log(\Theta_2(\Psi)+1)]\, t(d\Psi) + \int_\Phi [\Theta_3(\Psi)I - \log(\Theta_3(\Psi)+1)]\, t(d\Psi) \\
& \int_\Phi [\Theta_4(\Psi)B - \log(\Theta_4(\Psi)+1)]\, t(d\Psi) + \int_\Phi [\Theta_5(\Psi)V - \log(\Theta_5(\Psi)+1)]\, t(d\Psi) \\
& \int_\Phi [\mathcal{Q}\Theta_6(\Psi)Z - \mathcal{Q}\log(\Theta_6(\Psi)+1)]\, t(d\Psi) = O.
\end{aligned}$$

For a non-negative O and an automatons fixed (S, L, I, B, V, Z), we arrive at the following:

$$\begin{aligned}
\mathcal{U}(\mho) \leq\ & dt + \sigma_1(S-1)d\mathbb{B}_1(t) + \sigma_2(L-1)d\mathbb{B}_2(t) + \sigma_3(I-1)d\mathbb{B}_3(t) \\
& + \sigma_4(V-1)d\mathbb{B}_4(t) + \sigma_5(B-1)d\mathbb{B}_5(t) + \sigma_6(Z-1)d\mathbb{B}_6(t).
\end{aligned} \tag{26}$$

By evaluating the integral of both sides of Eq. (26) over the interval from 0 to $T \wedge \pi_{\mathbb{K}}$, the following can be articulated as

$$\begin{aligned}
& \mathbf{E}\mathcal{U}(S(T\wedge\pi_{\mathbb{K}}), L(T\wedge\pi_{\mathbb{K}}), I(T\wedge\pi_{\mathbb{K}}), B(T\wedge\pi_{\mathbb{K}}), V(T\wedge\pi_{\mathbb{K}}), Z(T\wedge\pi_{\mathbb{K}})) \\
& \quad \leq \mathcal{U}(S(0), L(0), I(0), V(0), B(0), Z(0)) + \mathbb{K}T < \infty.
\end{aligned} \tag{27}$$

Fix $\Omega_{\mathbb{K}} = \{\pi_{\mathbb{K}} \leq t\}$ for $\mathbb{K} \geq \mathbb{K}_1$ by (24), $P(\Omega_{\mathbb{K}}) \geq \varepsilon$. Observing each $\varpi_9 \in \Omega_{\mathbb{K}}$, at least one of $S(\pi_{\mathbb{K}}, \varpi_9), L(\pi_{\mathbb{K}}, \varpi_9), I(\pi_{\mathbb{K}}, \varpi_9), V(\pi_{\mathbb{K}}, \varpi_9), H(\pi_{\mathbb{K}}, \varpi_9)$, also $R(\pi_{\mathbb{K}}, \varpi_9)$, which is equal either $\{k$ or $\frac{1}{k}\}$. Consequently, $S(\pi_{\mathbb{K}}, \varpi_9), L(\pi_{\mathbb{K}}, \varpi_9), I(\pi_{\mathbb{K}}, \varpi_9), V(\pi_{\mathbb{K}}, \varpi_9), H(\pi_{\mathbb{K}}, \varpi_9)$ and $R(\pi_{\mathbb{K}}, \varpi_9)$ in no way is less than $\{\mathbb{K} - 1 - \log\mathbb{K}$ or $\frac{1}{\mathbb{K}} - 1 - \log\mathbb{K}\}$.

It follows that

$$\begin{aligned}
& \mathcal{U}(S(\pi_{\mathbb{K}}, \varpi_9), L(\pi_{\mathbb{K}}, \varpi_9), I(\pi_{\mathbb{K}}, \varpi_9), V(\pi_{\mathbb{K}}, \varpi_9), B(\pi_{\mathbb{K}}, \varpi_9), Z(\pi_{\mathbb{K}}, \varpi_9)) + \mathbb{K}T \\
& \quad \geq (\mathbb{K} - 1 - \log\mathbb{K}) \wedge \left(\frac{1}{\mathbb{K}} - 1 + \log\mathbb{K}\right).
\end{aligned} \tag{28}$$

Since $\mathsf{a} \wedge \mathsf{b}$ indicates the smallest value of a and b. In view of (27) and , we get

$$\begin{aligned}
& \mathcal{U}(S(0), L(0), I(0), V(0), B(0), Z(0)) + \mathbb{K}T \geq E\,[I_{\Omega_{\mathbb{K}}}\mathcal{U}(S(\pi_{\mathbb{K}}, \varpi_9), L(\pi_{\mathbb{K}}, \varpi_9), I(\pi_{\mathbb{K}}, \varpi_9), \\
& V(\pi_{\mathbb{K}}, \varpi_9), B(\pi_{\mathbb{K}}, \varpi_9), Z(\pi_{\mathbb{K}}, \varpi_9))] \geq \varepsilon\left[(\mathbb{K} - 1 - \log\mathbb{K}) \wedge \left(\frac{1}{\mathbb{K}} - 1 + \log\mathbb{K}\right)\right] \mapsto \infty\ as\ \mathbb{K} \mapsto \infty.
\end{aligned}$$

This leads to a contradiction, thereby implying that $\pi = \infty$ almost surely. Hence, the proof is complete. □

3 Extinction and Persistence of Disease

In what follows, the criteria for extinction and persistence in the mean are analyzed to better explore the long-term dynamics of the CHIKV system that incorporates inadvertently transmitted viruses and stochastic perturbations controlled by a Poisson random measure. In particular, as time gets closer to infinity, the anticipated outcomes of the resulting constituents are implied to continue to be consistently constrained away from zero by the system's persistence in mean. On the other hand, disappearance describes the situation

in which some compartments, like the transmissible group, asymptotically tend to zero as expected. Using features of the adjusted Poisson integral and stochastic Lyapunov functional components, we obtain sufficient requirements in which the infectious community either dies, disappears, or persists in the mean.

Here, we identify key conditions that favor the eventual eradication of CHIKV within the community. Our primary focus is on the asymptotic behavior of the proposed CHIKV model (4). The analysis begins by formulating a threshold parameter for the system, which serves as a criterion for disease extinction. This threshold provides a quantitative condition under which the infection is expected to die out with high probability. The following result establishes a sufficient criteria for the eradication of the infection in the presence of Poisson random measure:

$$\mathbb{R}_{0L} = \frac{\beta\pi(\rho + (1-\rho)\varpi_3)}{(\varpi_1(\varpi_4 + \varpi_5\frac{\varpi_6}{\delta}))(\varpi_2 + \epsilon\,\frac{\varpi_8}{\varpi_{10}} + \frac{\sigma_3^2}{2}) + \int_\Phi [\Theta_3(\mho) - \log(\Theta_3(x)+1)]\,t(d\Psi)}. \tag{29}$$

Theorem 3: *Assume that there is a stochastic model (4) possesses the solution* $(S(t), L(t), I(t), B(t), V(t), Z(t)) \in \mathbb{R}_+^6$ *having ICs* $(S(0), L(0), I(0), B(0), V(0), Z(0)) \in \mathbb{R}_+^6$. *If* $\mathbb{R}_{0h} < 1$, *then the subsequent characteristics of such a model solution must exist:*

$$\begin{aligned}
&\lim_{t\to\infty}\sup S(t) = \frac{\pi}{\varpi_1}, \quad \lim_{t\to\infty}\sup L(t) = 0, \quad \lim_{t\to\infty}\sup I(t) = 0,\\
&\lim_{t\to\infty}\sup B(t) = \frac{\varpi_6}{\delta}, \quad \lim_{t\to\infty}\sup V(t) = 0, \quad \lim_{t\to\infty}\sup Z(t) = \frac{\varpi_8}{\varpi_{10}}.
\end{aligned} \tag{30}$$

In simple terms, the above result implies that CHIKV will eventually be eradicated from the population with probability one.

Proof: After performing the integration on model (4), the subsequent formulae can simply be generated:

$$\begin{aligned}
\frac{1}{t}(S(t) - S(0)) &= \pi - \varpi_1\langle S(t)\rangle - \beta\langle S(t)V(t)\rangle + \frac{\sigma_1\int_0^t S\,dB_1(t)}{t}\\
&\quad + \frac{1}{t}\int_0^t\left[\int_\Phi [\Theta_1(\mho)S(t^-)]\bar{\aleph}(dt, d\Psi)\right]dt,\\
\frac{1}{t}(L(t) - L(0)) &= (1-\rho)\beta\langle S(t)V(t)\rangle - (\Theta + \varphi)\langle L(t)\rangle + \frac{\sigma_2\int_0^t L\,dB_2(t)}{t}\\
&\quad + \frac{1}{t}\int_0^t\left[\int_\Phi [\Theta_2(\mho)L(t^-)]\bar{\aleph}(dt, d\Psi)\right]dt,\\
\frac{1}{t}(I(t) - I(0)) &= \rho\beta\langle S(t)V(t)\rangle + \varphi\langle L(t)\rangle - \varpi_2\langle I(t)\rangle - \epsilon\,\langle I(t)Z(t)\rangle + \frac{\sigma_3\int_0^t I\,dB_3(t)}{t}\\
&\quad + \frac{1}{t}\int_0^t\left[\int_\Phi [\Theta_3(\mho)I(t^-)]\bar{\aleph}(dt, d\Psi)\right]dt,
\end{aligned}$$

$$\frac{1}{t}(B(t)-B(0)) = \varpi_6 + \varpi_7\langle V(t)B(t)\rangle - \delta\langle B(t)\rangle + \frac{\sigma_4\int_0^t B dB_4(t)}{t} + \frac{1}{t}\int_0^t\left[\int_\Phi[\Theta_4(\mho)B(t^-)]\bar{\aleph}(dt,d\Psi)\right]dt,$$

$$\frac{1}{t}(V(t)-V(0)) = \varpi_3\langle I(t)\rangle - \varpi_4\langle V(t)\rangle - \varpi_5\langle V(t)B(t)\rangle + \frac{\sigma_5\int_0^t V dB_5(t)}{t} + \frac{1}{t}\int_0^t\left[\int_\Phi[\Theta_5(\mho)B(t^-)]\bar{\aleph}(dt,d\Psi)\right]dt,$$

$$\frac{1}{t}(Z(t)-Z(0)) = \varpi_8 + \varpi_9\langle I(t)Z(t)\rangle - \varpi_{10}\langle Z(t)\rangle + \frac{\sigma_6\int_0^t Z dB_6(t)}{t} + \frac{1}{t}\int_0^t\left[\int_\Phi[\Theta_6(\mho)Z(t^-)]\bar{\aleph}(dt,d\Psi)\right]dt. \tag{31}$$

Using the fact of (31), one can easily compute

$$\begin{aligned}\langle L(t)\rangle &= \frac{1}{(\Theta+\varphi)}(1-\rho)\beta S(t)V(t) - \frac{1}{(\Theta+\varphi)}\left(\frac{L(t)-L(0)}{t}\right) + \frac{1}{(\Theta+\varphi)}\left(\frac{\int_0^t \sigma_2 L(t)dB_2(t)}{t}\right) \\ &\quad + \frac{\frac{1}{t}\int_0^t\left[\int_\Phi \Theta_2(L)L(t^-)\bar{\aleph}(dt,d\Psi)\right]dt}{(\Theta+\varphi)}, \\ &= \frac{(1-\rho)\beta}{(\Theta+\varphi)}\langle S(t)V(t)\rangle + \mathsf{M}_L(t),\end{aligned} \tag{32}$$

where

$$\mathsf{M}_L = -\frac{1}{(\Theta+\varphi)}\left(\frac{L(t)-L(0)}{t}\right) + \frac{1}{(\Theta+\varphi)}\left(\frac{\int_0^t \sigma_2 L(t)dB_2(t)}{t}\right) + \frac{\frac{1}{t}\int_0^t\left[\int_\Phi \Theta_2(L)L(t^-)\bar{\aleph}(dt,d\Psi)\right]dt}{(\Theta+\varphi)}. \tag{33}$$

Considering the last formulation of (31), we attain

$$\begin{aligned}\langle Z(t)\rangle &= \frac{\varpi_8}{\varpi_{10}} + \frac{\varpi_9}{\varpi_{10}}\langle I(t)Z(t)\rangle - \frac{1}{\varpi_{10}}\left(\frac{(Z(t)-Z(0))}{t}\right) + \frac{1}{\varpi_{10}}\left(\frac{\sigma_6\int_0^t Z dB_6(t)}{t}\right) \\ &\quad + \frac{\frac{1}{t}\int_0^t\left[\int_\Phi[\Theta_6(\mho)Z(t^-)]\bar{\aleph}(dt,d\Psi)\right]dt}{\varpi_{10}}, \\ &= \frac{\varpi_8}{\varpi_{10}} + \mathsf{M}_Z,\end{aligned} \tag{34}$$

whereas

$$\mathsf{M}_Z = -\frac{1}{\varpi_{10}}\left(\frac{(Z(t)-Z(0))}{t}\right) + \frac{\varpi_9}{\varpi_{10}}\langle I(t)Z(t)\rangle + \frac{1}{\varpi_{10}}\left(\frac{\sigma_6\int_0^t Z dB_6(t)}{t}\right)$$

$$+\frac{\frac{1}{t}\int_0^t\left[\int_\Phi[\Theta_6(\mho)Z(t^-)]\bar{\aleph}(dt,d\Psi)\right]dt}{\varpi_{10}}, \tag{35}$$

implementing Itô's technique to the infected human population, the third equation of (31) simplifies to the following form:

$$d\log I(t)=\left[\rho\beta\frac{S(t)V(t)}{I(t)}+\varphi\frac{L(t)}{I(t)}-\varpi_2-\epsilon\frac{Z(t)I(t)}{I(t)}+\frac{\sigma_3}{2}\right]dt+\sigma_3 dB_3(t)$$
$$-\int_\Phi[\Theta_3(\mho)-\log(\Theta_3(x)+1)]\,t(d\Psi)+\int_\Theta[\log(\Theta_3(\Psi)+1)]\,\bar{\aleph}(dt,d\Psi). \tag{36}$$

Applying integration on (36) over $(0,t)$ and dividing by t provides the subsequent relation:

$$\frac{\log I(t)}{t}\le\left[\rho\beta\frac{S(t)V(t)}{I(t)}+\varphi\frac{\frac{(1-\rho)\beta}{(\Theta+\varphi)}\langle S(t)V(t)\rangle+\mathsf{M}_L(t)}{I(t)}-\varpi_2-\epsilon\frac{\varpi_8}{\varpi_{10}}+\mathsf{M}_Z+\frac{\sigma_3}{2}\right]dt+\sigma_3 dB_3(t)$$
$$-\int_\Phi[\Theta_3(\mho)-\log(\Theta_3(x)+1)]\,t(d\Psi)+\int_\Theta[\log(\Theta_3(\Psi)+1)]\,\bar{\aleph}(dt,d\Psi). \tag{37}$$

By replacing (32) with (37), we find

$$\frac{\log I(t)}{t}\le\left[\rho\beta\frac{S(t)V(t)}{I(t)}+\varphi\frac{\frac{(1-\rho)\beta}{(\Theta+\varphi)}\langle S(t)V(t)\rangle+\mathsf{M}_L(t)}{I(t)}+\frac{\log I(0)}{t}-\varpi_2-\epsilon\frac{\varpi_8}{\varpi_{10}}+\mathsf{M}_Z+\frac{\sigma_3}{2}\right]dt$$
$$+\sigma_3 dB_3(t)-\int_\Phi[\Theta_3(\mho)-\log(\Theta_3(x)+1)]\,t(d\Psi)$$
$$+\int_\Theta[\log(\Theta_3(\Psi)+1)]\,\bar{\aleph}(dt,d\Psi),d\Psi)+\frac{\sigma_3 dB_3(t)}{t}. \tag{38}$$

Furthermore, $\mathsf{M}_\jmath(t)=\frac{a_\jmath}{t}\int_0^t d\mathbb{B}_\jmath t$ for $\jmath=\{1,2,\ldots,6\}$ are the martingale operator disappears for $t=0$. Applying $t\to\infty$ and utilizing Lemma 3, we find

$$\lim_{t\to\infty}\sup\frac{1}{t}\int_0^d\mathsf{M}_\jmath t=0. \tag{39}$$

Whenever $\mathbb{R}_{0h}<1$, (37) generates

$$\lim_{t\to\infty}\sup\frac{\log I(t)}{t}\le\left(\varpi_2+\epsilon\frac{\varpi_8}{\varpi_{10}}+\frac{\sigma_3^2}{2}\right)(\mathbb{R}_{0L}-1)<0,\ a.s. \tag{40}$$

Adopting the same technique, we can prove

$$\lim_{t\to\infty}\langle S(t)\rangle=\frac{\pi}{\varpi_1},a.s,\quad \lim_{t\to\infty}\langle L(t)\rangle=0,\ a.s,\lim_{t\to\infty}\langle B(t)\rangle=\frac{\varpi_6}{\delta},\ a.s$$
$$\lim_{t\to\infty}\langle V(t)\rangle=0,\ a.s\quad \lim_{t\to\infty}\langle Z(t)\rangle=\frac{\varpi_8}{\varpi_{10}}.$$

This yields the intended outcome. □

In what follows, we investigate the long-term viability of CHIKV transmission within the general population, specifically under a stochastic framework that incorporates latently infected cells and jump disturbances modeled by a Poisson random measure. To be more precise, we analyze the conditions under which the infection persists, which is a critical prerequisite for designing effective surveillance and control strategies. Our analysis begins with the concept of persistence in the mean, as outlined in [42].

Theorem 4: *Assume that the stochastic CHKIV model (4) is perceived as persistent within mean if:*

$$\liminf_{t\to\infty}\langle L\rangle \geq \frac{4\left(\sqrt{\mathbb{R}^{s}_{0L}}-1\right)}{\mathcal{Q}_1 t},\ a.s, \tag{41}$$

where

$$\mathcal{Q}_1 = \frac{\pi}{\varpi_1 + \frac{\sigma_1^2}{2} - \int_\Phi [\Theta_1(\Psi) - \log(\Theta_1(\Psi)+1)]t d\Psi} \tag{42}$$

and it ensures that the illness will always occur in the community irrespective of t.

Introducing

$$\mathbb{R}^{s}_{0h} = \frac{t}{\mathbf{x}_1\mathbf{x}_2\mathbf{x}_3^2}. \tag{43}$$

Proof: Assume that there are functions $\mathbf{G}_1$ and $\mathbf{G}_2$ for human and reservoir hosts, respectively, defined as:

$$\mathbf{G}_1 = -\mathcal{Q}_1 \ln S(t) - \mathcal{Q}_2 \ln L(t) - \mathcal{Q}_3 \ln I(t) - \mathcal{Q}_4 \ln V(t), \tag{44}$$

where $\mathcal{Q}_\zeta$ $(\zeta = 1, 2, 3, 4)$ are real terms and will be computed later.

Applying the Itô formulation to relation (44), we get

$$\begin{aligned} d\mathbf{G}_1 = {} & L\mathbf{G}_1 - \mathcal{Q}_1\sigma_1 B_1(t) - \mathcal{Q}_2\sigma_2 B_2(t) - \mathcal{Q}_3\sigma_3 B_3(t) - \mathcal{Q}_4\sigma_4 B_4(t) \\ & - \mathcal{Q}_1 \int_\Phi [\Theta_1(\Psi)S - \log(\Theta_1(\Psi)+1)]\bar{\aleph}(dt, d\Psi) \\ & - \mathcal{Q}_2 \int_\Phi [\Theta_2(\Psi)L - \log(\Theta_2(\Psi)+1)]\bar{\aleph}(dt, d\Psi) \\ & - \mathcal{Q}_3 \int_\Phi [\Theta_3(\Psi)I - \log(\Theta_3(\Psi)+1)]\bar{\aleph}(dt, d\Psi) \\ & - \mathcal{Q}_4 \int_\Phi [\Theta_4(\Psi)V - \log(\Theta_4(\Psi)+1)]\bar{\aleph}(dt, d\Psi), \end{aligned} \tag{45}$$

$$\begin{aligned} L\mathbf{G}_1 = {} & -\mathcal{Q}_1 \ln S(t) - \mathcal{Q}_2 \ln L(t) - \mathcal{Q}_3 \ln I(t) - \mathcal{Q}_4 \ln V(t) \\ = {} & -\frac{\mathcal{Q}_1\pi}{S(t)} - \mathcal{Q}_1\varpi_1 - \mathcal{Q}_1\beta V(t) + \mathcal{Q}_1\left\{\frac{\sigma_1^2}{2} + \int_\Phi [\Theta_1(\Psi) - \log(\Theta_1(\Psi)+1)]t d\Psi\right\} \\ & - \mathcal{Q}_2\frac{(1-\rho)\beta S(t)V(t)}{L(t)} - \mathcal{Q}_2(\Theta+\varphi) + \mathcal{Q}_2\left\{\frac{\sigma_2^2}{2} + \int_\Phi [\Theta_2(\Psi) - \log(\Theta_2(\Psi)+1)]t d\Psi\right\} \\ & - \mathcal{Q}_3\rho\beta\frac{S(t)V(t)}{I(t)} + \mathcal{Q}_3\varphi\frac{L(t)}{I(t)} - \mathcal{Q}_3\varpi_2 - \mathcal{Q}_3\,\epsilon\, Z(t) + \mathcal{Q}_3\left\{\frac{\sigma_3^2}{2} + \int_\Phi [\Theta_3(\Psi) - \log(\Theta_3(\Psi)+1)]t d\Psi\right\}. \\ & - \mathcal{Q}_4\varpi_3\frac{I(t)}{V(t)} - \mathcal{Q}_4\varpi_4 - \mathcal{Q}_4\varpi_5 B(t) + \mathcal{Q}_4\left\{\frac{\sigma_4^2}{2} + \int_\Phi [\Theta_4(\Psi) - \log(\Theta_4(\Psi)+1)]t d\Psi\right\} \end{aligned} \tag{46}$$

$$
\begin{aligned}
&\leq -4\sqrt{\mathcal{Q}_1\mathcal{Q}_2\mathcal{Q}_3\mathcal{Q}_4\pi\beta} - \mathcal{Q}_4\varpi_3\mathrm{I}(\mathrm{t}) + \mathcal{Q}_1\left\{\varpi_1 + \frac{\sigma_1^2}{2} + \int_\Phi[\Theta_1(\Psi) - \log(\Theta_1(\Psi)+1)]\mathrm{t}d\Psi\right\}\\
&+ \mathcal{Q}_2\left\{\Theta + \varphi + \frac{\sigma_2^2}{2} + \int_\Phi[\Theta_2(\Psi) - \log(\Theta_2(\Psi)+1)]\mathrm{t}d\Psi\right\}\\
&+ \mathcal{Q}_3\left\{\varpi_2 + \frac{\sigma_3^2}{2} + \int_\Phi[\Theta_3(\Psi) - \log(\Theta_3(\Psi)+1)]\mathrm{t}d\Psi\right\}\\
&+ \mathcal{Q}_4\left\{\varpi_8 + \frac{\sigma_4^2}{2} + \int_\Phi[\Theta_4(\Psi) - \log(\Theta_4(\Psi)+1)]\mathrm{t}d\Psi\right\}.
\end{aligned}
$$

After simplification, we get

$$
\begin{aligned}
\mathcal{Q}_1 &= \frac{\pi}{\varpi_1 + \frac{\sigma_1^2}{2} - \int_\Phi[\Theta_1(\Psi) - \log(\Theta_1(\Psi)+1)]\mathrm{t}d\Psi},\\
\mathcal{Q}_2 &= \frac{\pi}{\Theta + \Psi + \varpi_{10\mathrm{h}} + \frac{\sigma_2^2}{2} - \int_\Phi[\Theta_2(\Psi) - \log(\Theta_2(\varphi)+1)]\mathrm{t}d\Psi},\\
\mathcal{Q}_3 &= \frac{\pi}{\varpi_2 + \frac{\sigma_3^2}{2} - \int_\Phi[\Theta_3(\Psi) - \log(\Theta_3(\Psi)+1)]\mathrm{t}d\Psi},\\
\mathcal{Q}_4 &= \frac{\pi}{\varpi_8 + \phi + \frac{\sigma_4^2}{2} - \int_\Phi[\Theta_4(\Psi) - \log(\Theta_4(\Psi)+1)]\mathrm{t}d\Psi}.
\end{aligned}
$$

For brevity, assume that

$$
\begin{aligned}
\mho_1 &= \varpi_1 + \frac{\sigma_1^2}{2} - \int_\Phi[\Theta_1(\Psi) - \log(\Theta_1(\Psi)+1)]\mathrm{t}d\Psi,\\
\mho_2 &= \Theta + \varphi + \frac{\sigma_2^2}{2} - \int_\Phi[\Theta_2(\Psi) - \log(\Theta_2(\Psi)+1)]\mathrm{t}d\Psi,\\
\mho_3 &= \varpi_2 + \frac{\sigma_3^2}{2} - \int_\Phi[\Theta_3(\Psi) - \log(\Theta_3(\Psi)+1)]\mathrm{t}d\Psi,\\
\mho_4 &= \varpi_8 + \frac{\sigma_4^2}{2} - \int_\Phi[\Theta_4(\Psi) - \log(\Theta_4(\Psi)+1)]\mathrm{t}d\Psi.
\end{aligned}
$$

Utilizing these $\mho_j$, we have

$$
L\mathbf{G}_1 \leq -4\left[\sqrt{\mathbb{R}_{0\mathrm{h}}^{\mathrm{s}}} - 1\right] + \mathcal{Q}_4\mathbf{m}\mathrm{I}. \tag{47}
$$

Integrating both sides of the stochastic CHIKV model (4) and replacing (47) into (44), we have

$$
\begin{aligned}
&\frac{\mathbf{G}_1(\mathrm{S}(\mathrm{t}),\mathrm{L}(\mathrm{t}),\mathrm{I}(\mathrm{t}),\mathrm{V}(\mathrm{t})) - \mathbf{G}_1(\mathrm{S}(0),\mathrm{L}(0),\mathrm{I}(0),\mathrm{V}(0))}{\mathrm{t}}\\
&= -4\left[\sqrt{\mathbb{R}_{0\mathrm{h}}^{\mathrm{s}}} - 1\right] + \mathcal{Q}_4\mathbf{m}\mathrm{I} - \mathcal{Q}_1\sigma_1\mathrm{B}_1(\mathrm{t}) - \mathcal{Q}_2\sigma_2\mathrm{B}_2(\mathrm{t}) - \mathcal{Q}_3\sigma_3\mathrm{B}_3(\mathrm{t})\\
&- \mathcal{Q}_4\sigma_4\mathrm{B}_4(\mathrm{t}) - \mathcal{Q}_1\int_\Phi[\Theta_1(\Psi)\mathrm{S} - \log(\Theta_1(\Psi)+1)]\bar{\aleph}(d\mathrm{t},d\Psi)\\
&- \mathcal{Q}_2\int_\Phi[\Theta_2(\Psi)\mathrm{L} - \log(\Theta_2(\Psi)+1)]\bar{\aleph}(d\mathrm{t},d\Psi)
\end{aligned}
$$

$$
\begin{aligned}
&- \mathcal{Q}_3 \int_{\Phi} [\Theta_3(\Psi)\mathrm{I} - \log(\Theta_3(\Psi)+1)]\bar{\aleph}(d\mathrm{t}, d\Psi) \\
&- \mathcal{Q}_4 \int_{\Phi} [\Theta_4(\Psi)\mathrm{V} - \log(\Theta_4(\Psi)+1)]\bar{\aleph}(d\mathrm{t}, d\Psi) \\
&\leq -4\left[\sqrt{\mathbb{R}_{0\mathrm{h}}^{\mathrm{s}}} - 1\right] + \mathcal{Q}_4 \mathbf{m}\langle \mathrm{I}\rangle - \wp_1(\mathrm{t}).
\end{aligned} \tag{48}
$$

It follows that

$$
\begin{aligned}
\wp_1(\mathrm{t}) = &\frac{\mathcal{Q}_1 \int_{\Phi} [\Theta_1(\Psi)\mathrm{S} - \log(\Theta_1(\Psi)+1)]\bar{\aleph}(d\mathrm{t}, d\Psi)}{\mathrm{t}} \\
&+ \frac{\mathcal{Q}_2 \int_{\Phi} [\Theta_2(\Psi)\mathrm{L} - \log(\Theta_2(\Psi)+1)]\bar{\aleph}(d\mathrm{t}, d\Psi)}{\mathrm{t}} \\
&+ \frac{\mathcal{Q}_3 \int_{\Phi} [\Theta_3(\Psi)\mathrm{I} - \log(\Theta_3(\Psi)+1)]\bar{\aleph}(d\mathrm{t}, d\Psi)}{\mathrm{t}} \\
&+ \frac{\mathcal{Q}_4 \int_{\Phi} [\Theta_4(\Psi)\mathrm{V} - \log(\Theta_4(\Psi)+1)]\bar{\aleph}(d\mathrm{t}, d\Psi)}{\mathrm{t}}.
\end{aligned} \tag{49}
$$

Applying strong law defined in Lemma 2, we get

$$
\lim_{\mathrm{t}\to\infty} \wp_1(\mathrm{t}) = 0. \tag{50}
$$

By utilizing Lemma 3, the limit inferior of (48) is provided as:

$$
\liminf_{\mathrm{t}\to\infty} \langle \mathrm{I}\rangle \geq \frac{4\left(\sqrt{\mathbb{R}_{0\mathrm{h}}^{\mathrm{s}}} - 1\right)}{\mathcal{Q}_4 \mathbf{m}}. \tag{51}
$$

Likewise, $\liminf_{\mathrm{t}\to\infty} \langle \mathrm{I}\rangle \geq 0$.

These outcomes constitute the demonstration of Theorem 4. □

4 Near Optimal Control

Preventing CHIKV outbreaks presents numerous challenges, particularly when considering complex biological interactions, latent infection phases, environmental variability, and stochastic perturbations induced by Poisson random measures. These sources of uncertainty can substantially alter disease dynamics, potentially leading to unforeseen outbreaks or the resurgence of infections, even in the presence of ongoing treatment and control efforts.

To address these difficulties, researchers have developed near-optimal control strategies that aim to balance the epidemiological goal of minimizing disease prevalence with the economic and logistical constraints associated with interventions such as vaccination, antiviral treatment, and vector control (see [30]). Within this framework, we explore the near-optimality criteria of a stochastic control system modeled by a continuous-time Markov chain, where the evolution of the system is influenced by both continuous fluctuations (e.g., Brownian motion) and discrete, abrupt changes (e.g., Poisson-driven jumps).

This probabilistic modeling approach not only provides a more realistic representation of sudden events—such as mass vaccination campaigns or unexpected environmental changes—but also facilitates the application of stochastic control techniques, particularly through recursive optimization and the Hamilton-Jacobi-Bellman (HJB) framework (see [30]). As a result, it enables the formulation of robust, adaptive intervention policies that perform effectively under uncertainty, offering valuable insights for public health

policy, epidemic mitigation, and strategic planning in the context of CHIKV. The system of SDEs under near-optimal control is defined as

$$
\begin{aligned}
dS_t &= (\pi(\Lambda_t) - \varpi_1(\Lambda_t)S_t - \beta(\Lambda_t)S_tV_t - \varpi_{2k}(\Lambda_t)\omega_tS_t)\,dt \\
&\quad + \kappa_1(\Lambda_t)S_t d\mathbb{B}(t) + \int_L \mathbf{g}(t, \Lambda_{t^-}, S_{t^-}, \omega_{t^-}, \vartheta)\bar{\aleph}_k(dt, d\vartheta), \\
&\quad S_{t_0} = S_0, \\
dL_t &= ((1-\rho(\Lambda_t))\beta(\Lambda_t)S_tV_t - (\Theta(\Lambda_t) + \varphi(\Lambda_t))L_t - \varpi_{2k}(\Lambda_t)\omega_tL_t)\,dt \\
&\quad + \kappa_2(\Lambda_t)L_t d\mathbb{B}(t) + \int_L \mathbf{g}(t, \Lambda_{t^-}, L_{t^-}, \omega_{t^-}, \vartheta)\bar{\aleph}_k(dt, d\vartheta), \\
&\quad L_{t_0} = L_0, \\
dI_t &= (\rho(\Lambda_t)\beta(\Lambda_t)S_tV_t + \varphi(\Lambda_t)L_t - \varpi_2(\Lambda_t)I_t - \epsilon\,(t)I_tZ_t - \varpi_{2k}(\Lambda_t)\omega_tI)\,dt \\
&\quad + \kappa_3(\Lambda_t)I_t d\mathbb{B}(t) + \int_L \mathbf{g}(t, \Lambda_{t^-}, I_{t^-}, \omega_{t^-}, \vartheta)\bar{\aleph}_k(dt, d\vartheta), \\
&\quad V_{t_0} = V_0, \\
dV_t &= (\varpi_3(\Lambda_t)I(t) - \varpi_4(\Lambda_t)\omega_t - \varpi_5(\Lambda_t)\omega_tB_t - \varpi_{2k}(\Lambda_t)\omega_tV)\,dt \\
&\quad + \kappa_4(\Lambda_t)V_t d\mathbb{B}(t) + \int_L \mathbf{g}(t, \Lambda_{t^-}, V_{t^-}, \omega_{t^-}, \vartheta)\bar{\aleph}_k(dt, d\vartheta), \\
&\quad V_{t_0} = V_0, \\
dB_t &= (\varpi_6(\Lambda_t) + \varpi_7(\Lambda_t)\omega_tB_t - \delta(\Lambda_t)B_t - \varpi_{2k}(\Lambda_t)\omega_tB_t)\,dt \\
&\quad + \kappa_5(\Lambda_t)B_t d\mathbb{B}(t) + \int_L \mathbf{g}(t, \Lambda_{t^-}, B_{t^-}, \omega_{t^-}, \vartheta)\bar{\aleph}_k(dt, d\vartheta), \\
&\quad B_{t_0} = B_0, \\
dZ_t &= (\varpi_8(\Lambda_t) + \varpi_9(\Lambda_t)I_tZ_t - \varpi_{10}(\Lambda_t)Z_t - \varpi_{2k}(\Lambda_t)\omega_tZ_t)\,dt \\
&\quad + \kappa_6(\Lambda_t)Z_t d\mathbb{B}(t) + \int_L \mathbf{g}(t, \Lambda_{t^-}, Z_{t^-}, \omega_{t^-}, \vartheta)\bar{\aleph}_k(dt, d\vartheta), \\
&\quad I_{t_0} = I_0.
\end{aligned} \tag{52}
$$

Thanks to Kuang et al. [48], we describe the corresponding objective function as:

$$
\mathfrak{J}(0, \Upsilon_0, \omega_t) = E\left[\int_0^{\widehat{\mathfrak{J}}} \tilde{h}(t, \Lambda_t, \Upsilon_t, \omega_t)dt + \hat{h}(\Lambda_{\widehat{\mathfrak{J}}}, \Upsilon_{\widehat{\mathfrak{J}}})\right], \tag{53}
$$

$$
\begin{aligned}
\tilde{h}(t, \Lambda_t, \Upsilon_t, \omega_t) &= E\left[\int_0^{\widehat{\mathfrak{J}}} \left(C_1S_t + C_2L_t + C_3I_t + C_4V_t + C_5B_t + C_6Z_t + \varpi_{2k}\omega_t^2\right)dt\right], \\
\hat{h}(\Lambda_{\widehat{\mathfrak{J}}}, \Upsilon_{\widehat{\mathfrak{J}}}) &= (0, 0, I_t(\Lambda_t), 0, 0),
\end{aligned} \tag{54}
$$

containing $\tilde{h} : [0, \widehat{\mathfrak{J}}] \times \mathcal{S} \times \mathbb{R}_n \times \mathbb{U}_{ad}[0, \widehat{\mathfrak{J}}] \to \mathbb{R}_n$ and $\hat{h} : \mathcal{S} \times \mathbb{R}^n \to \mathbb{R}$.

Lemma 6: *Imagine $\mathbb{F}$, the predictable κ-field on $\rho \times [0, \widehat{\mathfrak{J}}]$, where $\aleph(t, \vartheta)$ is a $\mathbb{F} \times \mathcal{Z}(Y)$ measurable and fulfills*

$$
E\left[\int_0^{\widehat{\mathfrak{J}}} \int_L |\sigma(t, \vartheta)|^2 \varpi_8(d\vartheta)dt\right] < +\infty, \tag{55}
$$

then $\exists$ *a fixed positive constant* $\mathrm{C} > 0$, *for each* $\mathrm{m} \geq 2$ *that*

$$\mathrm{E}\left\{\sup_{\mathrm{t}\in[0,\widehat{\mathfrak{J}}]} \|\int_0^{\widehat{\mathfrak{J}}}\int_{\mathrm{Y}} \sigma(\mathrm{t},\vartheta)\aleph(d\mathrm{t},d\vartheta)\|^{\mathrm{m}}\right\}$$
$$\leq \mathrm{CE}\left\{\int_0^{\widehat{\mathfrak{J}}}\int_{\mathrm{L}} |\sigma(\mathrm{t},\vartheta)|^{\mathrm{m}}\varpi_8(d\vartheta)d\mathrm{t}\right\}. \tag{56}$$

To support the analysis, we introduce the subsequent assumptions:

($\mathbf{A_1}$): The functions $\sigma = \varpi_7, \xi, \tilde{h}$ are continuously differentiable related to Υ_{t} and $\exists$ a fixed $\mathrm{C} > 0$ such that:

$$\|\sigma(\mathrm{t},\Lambda_{\mathrm{t}},\Upsilon_{\mathrm{t}},\omega_{\mathrm{t}})\| + \sup_{\vartheta\in\mathrm{Y}}\|\mathbf{g}(\mathrm{t},\Lambda_{\mathrm{t}},\Upsilon_{\mathrm{t}},\omega_{\mathrm{t}},\vartheta)\| \leq \mathrm{C}(1+\|\Upsilon_{\mathrm{t}}\|+\|\omega_{\mathrm{t}}\|),$$
$$\|\sigma(\mathrm{t},\Lambda_{\mathrm{t}},\Upsilon_{\mathrm{t}},\omega_{\mathrm{t}}) - \sigma(\mathrm{t},\Lambda_{\mathrm{t}},\tilde{\Upsilon}_{\mathrm{t}},\omega_{\mathrm{t}})\| + \sup_{\vartheta\in\mathrm{Y}}\|\mathbf{g}(\mathrm{t},\Lambda_{\mathrm{t}},\Upsilon_{\mathrm{t}},\omega_{\mathrm{t}},\vartheta) - \mathbf{g}(\mathrm{t},\Lambda_{\mathrm{t}},\tilde{\Upsilon}_{\mathrm{t}},\omega_{\mathrm{t}},\vartheta)\|$$
$$\leq \mathrm{C}|\Upsilon_{\mathrm{t}} - \tilde{\Upsilon}_{\mathrm{t}}|,$$
$$\|\sigma_{\Upsilon}(\mathrm{t},\Lambda_{\mathrm{t}},\Upsilon_{\mathrm{t}},\omega_{\mathrm{t}}) - \sigma_{\Upsilon}(\mathrm{t},\Lambda_{\mathrm{t}},\tilde{\Upsilon}_{\mathrm{t}},\omega_{\mathrm{t}})\| + \sup_{\vartheta\in\mathrm{Y}}\|\mathbf{g}_{\Upsilon}(\mathrm{t},\Lambda_{\mathrm{t}},\Upsilon_{\mathrm{t}},\omega_{\mathrm{t}},\vartheta) - \mathbf{g}_{\Upsilon}(\mathrm{t},\Lambda_{\mathrm{t}},\tilde{\Upsilon}_{\mathrm{t}},\omega_{\mathrm{t}},\vartheta)\|$$
$$\leq \mathrm{C}|\Upsilon_{\mathrm{t}} - \tilde{\Upsilon}_{\mathrm{t}}|.$$

($\mathbf{A_2}$): Ensure that $\hat{h}$ be a convex and continuously differentiable function with regard to Υ_{t} and also bounded by $\mathrm{C}(1+\|\Upsilon_{\mathrm{t}}\|)$, it follows that $\exists$ a constant $\mathrm{C} > 0$ and

$$\|\hat{h}(\Lambda_{\mathrm{t}},\Upsilon_{\mathrm{t}}) - \hat{h}(\Lambda_{\mathrm{t}},\tilde{\Upsilon}_{\mathrm{t}})\| + \|\hat{h}_{\Upsilon}(\Lambda_{\mathrm{t}},\Upsilon_{\mathrm{t}}) - \hat{h}(\Lambda_{\mathrm{t}},\tilde{\Upsilon}_{\mathrm{t}})\| \leq \mathrm{C}\|\Upsilon_{\mathrm{t}},\tilde{\Upsilon}_{\mathrm{t}}\|. \tag{57}$$

($\mathbf{A_3}$): The functions $\sigma = \varpi_7, \xi, \tilde{h}$ are differentiable with regard to V and $\exists$ a constant $\mathrm{C} > 0$ such that:

$$\|\sigma(\mathrm{t},\Lambda_{\mathrm{t}},\Upsilon_{\mathrm{t}},\omega_{\mathrm{t}}) - \sigma(\mathrm{t},\Lambda_{\mathrm{t}},\Upsilon_{\mathrm{t}},\tilde{\mathrm{V}}_{\mathrm{t}})\| + \sup_{\vartheta\in\mathrm{Y}}\|\mathbf{g}(\mathrm{t},\Lambda_{\mathrm{t}},\Upsilon_{\mathrm{t}},\omega_{\mathrm{t}},\vartheta) - \mathbf{g}(\mathrm{t},\Lambda_{\mathrm{t}},\Upsilon_{\mathrm{t}},\tilde{\omega}_{\mathrm{t}},\vartheta)\|$$
$$\leq \mathrm{C}\|\omega_{\mathrm{t}} - \tilde{\omega}_{\mathrm{t}}\|,$$
$$\|\sigma_{\omega}(\mathrm{t},\Lambda_{\mathrm{t}},\Upsilon_{\mathrm{t}},\omega_{\mathrm{t}}) - \sigma_{\omega}(\mathrm{t},\Lambda_{\mathrm{t}},\Upsilon_{\mathrm{t}},\tilde{\omega}_{\mathrm{t}})\| + \sup_{\vartheta\in\mathrm{Y}}\|\mathbf{g}_{\omega}(\mathrm{t},\Lambda_{\mathrm{t}},\Upsilon_{\mathrm{t}},\omega_{\mathrm{t}},\vartheta) - \mathbf{g}_{u}(\mathrm{t},\Lambda_{\mathrm{t}},\Upsilon_{\mathrm{t}},\tilde{\omega}_{\mathrm{t}},\vartheta)\|$$
$$\leq \mathrm{C}\|\omega_{\mathrm{t}} - \tilde{\omega}_{\mathrm{t}}\|. \tag{58}$$

Remark 1: *Under the assertions* $(\mathbf{A}_1)-(\mathbf{A}_3)$, *standard arguments establish that* $\exists$ *a pair of constants* r *and* C *achieving*

$$\mathrm{E}\left\{\sup_{0\leq\mathrm{t}\leq\widehat{\mathfrak{J}}} \|\Upsilon_{\mathrm{t}}\|^{\mathrm{r}}\right\} \leq \mathrm{C}. \tag{59}$$

Remark 2: *For any* $\omega_{\mathrm{t}} \in \mathbb{U}_{\mathrm{ad}}[0,\widehat{\mathfrak{J}}]$, *formulation (52) possesses only one* $\mathcal{F}$ *adapted solution* Υ_{t}. *Thus,* $(\Upsilon_{\mathrm{t}},\omega_{\mathrm{t}})$ *is designated as an admissible pair.*

4.1 Adjoint Equation and Related Outcomes

Adjoint equations and pretreatment assessments are essential for the analysis and solution of optimal control challenges in stochastic mechanisms, especially those that simulate CHIKV evolution, including

inactivated infections and jump dynamics. When processes are affected by stochastic components like Wiener procedures, Poisson random measures, or Markov chains, these methods are essential for determining the factors required for optimality. Adjoint equations, which are frequently expressed as backward SDEs, are essential for describing optimum strategies in the context that the stochastic maximum principle (SMP) offers for these kinds of analysis [30].

Applying jump dynamics through Poisson random effects into CHIKV systems makes it possible for better representation of unexpected alterations in the environment or interventional tactics, including widespread vaccination programs. To investigate fundamental claims, estimations, and categorization of these frameworks, the adjoint formulae obtained within this context are essential. Previous studies have demonstrated their significance (see [30]).

To confirm and strengthen the adjoint equations within the CHIKV model (4), we provide initial findings demonstrating their usefulness and well-posedness. In addition, we present a Hamiltonian function that is specific to our stochastic structure, which sheds light on the changing behavior of the system and makes it easier to derive near-optimal control schemes. In addition to improving our comprehension of infectious processes, this method helps create successful approaches to treatment in the face of ambiguity. Additionally, a Hamiltonian function is introduced for the first time to provide further insights into the dynamics and framework of the problem is stated as:

$$\mathbb{H} : [0, \widehat{\mathfrak{I}}] \times \mathcal{S} \times \mathbf{R}^{\mathsf{n}} \times \mathbb{U}_{\mathrm{ad}}[0, \widehat{\mathfrak{I}}] \times \mathbf{R}^{\mathsf{n}} \times \mathbf{R}^{\mathsf{n}} \times \mathbf{R}^{\mathsf{n}} \to \mathbf{R}, \tag{60}$$

which is Fréchet differentiable space and linear convexity in the Υ_t and ω_t arguments, thus we have

$$\begin{aligned}\mathbb{H}(t, \Lambda_t, \Upsilon_t, \omega_t, f_1(t), f_2(t), \sigma(t, \vartheta)) = {} & \varpi_7^{\top}(t, \Lambda_t, \Upsilon_t, \omega_t) f_1(t) + \xi^{\top}(t, \Lambda_t, \Upsilon_t, \omega_t) f_2(t) \\ & + \int_{\mathrm{Y}} \mathbf{g}^{\top}(t, \Lambda_t, \Upsilon_t, \omega_t, \vartheta) \sigma(t, \vartheta) \varpi_8(d\vartheta) + \tilde{h}(t, \Lambda_t, \Upsilon_t, \omega_t),\end{aligned} \tag{61}$$

where

$$\varpi_7^{\top}(t, \Lambda_t, \Upsilon_t, \omega_t) = \begin{bmatrix} \pi - \varpi_1 S(t) - \beta S(t) V(t) \\ (1-\rho)\beta S(t) V(t) - (\Theta + \varphi) L(t) \\ \rho\beta S(t) V(t) + \varphi L(t) - \varpi_2 I(t) - \epsilon I(t) Z(t) \\ \varpi_3 I(t) - \varpi_4 V(t) - \varpi_5 V(t) B(t) \\ \varpi_6 + \varpi_7 V(t) B(t) - \delta B(t) \\ \varpi_8 + \varpi_9 I(t) Z(t) - \varpi_{10} Z(t) \end{bmatrix},$$

$$\xi^{\top}(t, \Lambda_t, \Upsilon_t, \omega_t) = \begin{bmatrix} \kappa_1(\Lambda_t) S(t) dB(t) \\ \kappa_2(\Lambda_t) L(t) dB(t) \\ \kappa_3(\Lambda_t) I(t) dB(t) \\ \kappa_4(\Lambda_t) V(t) dB(t) \\ \kappa_5(\Lambda_t) B(t) dB(t) \\ \kappa_6(\Lambda_t) Z(t) dB(t) \end{bmatrix}, \quad \tilde{h}(t, \Lambda_t, \Upsilon_t, \omega_t) = \begin{bmatrix} \tilde{h}(t, \Lambda_t, S(t), \omega_t) \\ \tilde{h}(t, \Lambda_t, L(t), \omega_t) \\ \tilde{h}(t, \Lambda_t, I(t), \omega_t) \\ \tilde{h}(t, \Lambda_t, V(t), \omega_t) \\ \tilde{h}(t, \Lambda_t, B(t), \omega_t) \\ \tilde{h}(t, \Lambda_t, Z(t), \omega_t) \end{bmatrix},$$

$$\mathbf{g}^{\top}(t, \Lambda_t, \Upsilon_t, \omega_t) = \begin{bmatrix} \mathbf{g}(t, \Lambda_t, S(t), \omega_t) \\ \mathbf{g}(t, \Lambda_t, L(t), \omega_t) \\ \mathbf{g}(t, \Lambda_t, I(t), \omega_t) \\ \mathbf{g}(t, \Lambda_t, V(t), \omega_t) \\ \mathbf{g}(t, \Lambda_t, B(t), \omega_t) \\ \mathbf{g}(t, \Lambda_t, Z(t), \omega_t) \end{bmatrix}. \tag{62}$$

Let ϖ_7, ρ and $\mathbf{g}$ be functions defined as follows:

- $\varpi_7 : [0, \widehat{\mathfrak{J}}] \times \mathcal{S} \times \mathbf{R}_{\mathsf{n}} \times \mathbb{U}_{\mathrm{ad}}[0, \widehat{\mathfrak{J}}] \to \mathbf{R}_{\mathsf{n}}$,
- $\rho : [0, \widehat{\mathfrak{J}}] \times \mathcal{S} \times \mathbf{R}_{\mathsf{n}} \times \mathbb{U}_{\mathrm{ad}}[0, \widehat{\mathfrak{J}}] \to \mathbf{R}_{\mathsf{n}}$,
- $\mathbf{g} : [0, \widehat{\mathfrak{J}}] \times \mathcal{S} \times \mathbf{R}_{\mathsf{n}} \times \mathbb{U}_{\mathrm{ad}}[0, \widehat{\mathfrak{J}}] \to \mathbf{R}_{\mathsf{n}}$.

Here, the continuous-time Markov chain Λ_t for the state space $\mathcal{S} = \{1, 2, \ldots, \mathsf{N}\}$ and ω_t is the control variable, which takes terms in the feasible control collection $\mathbb{U}_{\mathrm{ad}}[0, \widehat{\mathfrak{J}}]$. For simplicity, the state vector is represented as:

$$\Upsilon(t) = [S_t, L_t, I_t, V_t, B_t, Z_t]^\top . \tag{63}$$

We could also add the subsequent boundary value problems to a backward SDE [48] as it gives a way to derive its first-order adjoint equation. It is more advantageous to portray (52) as

$$d\mathrm{f}_{11}(t) = \begin{cases} -\Big(\pi(\Lambda_t) - \varpi_1(\Lambda_t)S(t) - \beta(\Lambda_t)S(t)V(t) - \varpi_{2k}(\Lambda_t)\omega_t S(t) \\ \quad + \int_Y \dfrac{\partial \mathbf{g}^\top}{\partial S(t)}\sigma(t,\vartheta)\varpi_8(d\vartheta) + \dfrac{\partial \tilde{h}}{\partial S(t)}\Big) dt\mathrm{f}_1(t) \\ +\kappa_1(\Lambda_t)S(t)dB(t)\mathrm{f}_2(t) + \int_Y \sigma(t,\vartheta)\bar{\aleph}(dt, d\vartheta) + \wp(t)d\widetilde{\omega}(t), \\ \mathrm{f}_{11}(\widehat{\mathfrak{J}}) = \nabla_{S(t)}\hat{h}(S(t)_{\widehat{\mathfrak{J}}}, \Lambda_{\widehat{\mathfrak{J}}}), \end{cases}$$

$$d\mathrm{f}_{12}(t) = \begin{cases} -\Big((1-\rho)\beta(\Lambda_t)S_t V(t) - (\Theta(\Lambda_t) + \varphi(\Lambda_t))L_t - \varpi_{2k}(\Lambda_t)\omega_t L(t) \\ \quad + \int_Y \dfrac{\partial \mathbf{g}^\top}{\partial L(t)}\sigma(t,\vartheta)\varpi_8(d\vartheta) + \dfrac{\partial \tilde{h}}{\partial L(t)}\Big) dt\mathrm{f}_1(t) + \kappa_2(\Lambda_t)L(t)dB(t)\mathrm{f}_2(t) \\ + \int_Y \sigma(t,\vartheta)\bar{\aleph}(dt, d\vartheta) + \wp(t)d\widetilde{\omega}(t), \\ \mathrm{f}_{12}(\widehat{\mathfrak{J}}) = \nabla_{L(t)}\hat{h}(L(t)_{\widehat{\mathfrak{J}}}, \Lambda_{\widehat{\mathfrak{J}}}), \end{cases}$$

$$d\mathrm{f}_{13}(t) = \begin{cases} -\Big(\rho(\Lambda_t)\beta(\Lambda_t)S(t)V(t) + \varphi(\Lambda_t)L(t) - \varpi_2(\Lambda_t)I(t) - \epsilon\,(t)I(t)Z(t) \\ \quad -\varpi_{2k}(\Lambda_t)\omega_t I(t) + \int_Y \dfrac{\partial \mathbf{g}^\top}{\partial I_t}\sigma(t,\vartheta)\varpi_8(d\vartheta) + \dfrac{\partial \tilde{h}}{\partial I_t}\Big) dt\mathrm{f}_1(t) \\ +\kappa_3(\Lambda_t)I_t dB(t)\mathrm{f}_2(t) + \int_Y \sigma(t,\vartheta)\bar{\aleph}(dt, d\vartheta) + \wp(t)d\widetilde{\omega}(t), \\ \mathrm{f}_{13}(\widehat{\mathfrak{J}}) = \nabla_{I(t)}\hat{h}(I(t)_{\widehat{\mathfrak{J}}}, \Lambda_{\widehat{\mathfrak{J}}}), \end{cases}$$

$$d\mathrm{f}_{14}(t) = \begin{cases} -\Big(\varpi_3(\Lambda_t)I(t) - \varpi_4(\Lambda_t)\omega(t) - \varpi_5(\Lambda_t)\omega(t)B_t - \varpi_{2k}(\Lambda_t)\omega_t V(t) \\ \quad + \int_Y \dfrac{\partial \mathbf{g}^\top}{\partial V_t}\sigma(t,\vartheta)\varpi_8(d\vartheta) + \dfrac{\partial \tilde{h}}{\partial V_t}\Big) dt\mathrm{f}_1(t) \\ +\kappa_4(\Lambda_t)V_t dB(t)\mathrm{f}_2(t) + \int_Y \sigma(t,\vartheta)\bar{\aleph}(dt, d\vartheta) + \wp(t)d\widetilde{\omega}(t), \\ \mathrm{f}_{14}(\widehat{\mathfrak{J}}) = \nabla_{V(t)}\hat{h}(V(t)_{\widehat{\mathfrak{J}}}, \Lambda_{\widehat{\mathfrak{J}}}), \end{cases}$$

$$d\mathrm{f}_{15}(\mathrm{t}) = \begin{cases} -\Big(\varpi_6(\Lambda_\mathrm{t}) + \varpi_7(\Lambda_\mathrm{t})\omega(\mathrm{t})\mathrm{B}(\mathrm{t}) - \delta(\Lambda_\mathrm{t})\mathrm{B}(\mathrm{t}) - \varpi_{2\mathrm{k}}(\Lambda_\mathrm{t})\omega_\mathrm{t}\mathrm{B}(\mathrm{t}) \\ \quad + \int_\mathrm{Y} \dfrac{\partial \mathbf{g}^\top}{\partial \mathrm{B}(\mathrm{t})}\sigma(\mathrm{t},\vartheta)\varpi_8(d\vartheta) + \dfrac{\partial \tilde{h}}{\partial \mathrm{B}(\mathrm{t})}\Big) d\mathrm{tf}_1(\mathrm{t}) \\ \quad + \kappa_5(\Lambda_\mathrm{t})\mathrm{B}(\mathrm{t})d\mathrm{B}(\mathrm{t})\mathrm{f}_2(\mathrm{t}) + \int_\mathrm{Y} \sigma(\mathrm{t},\vartheta)\bar{\aleph}(d\mathrm{t}, d\vartheta) + \wp(\mathrm{t})d\widetilde{\omega}(\mathrm{t}), \\ \mathrm{f}_{15}(\widehat{\mathfrak{J}}) = \nabla_{\mathrm{B}(\mathrm{t})}\hat{h}(\mathrm{B}(\mathrm{t})_{\widehat{\mathfrak{J}}}, \Lambda_{\widehat{\mathfrak{J}}}), \end{cases}$$

$$d\mathrm{f}_{16}(\mathrm{t}) = \begin{cases} -\Big(\varpi_8(\Lambda_\mathrm{t}) + \varpi_9(\Lambda_\mathrm{t})\mathrm{I}(\mathrm{t})\mathrm{Z}(\mathrm{t}) - \varpi_{10}(\Lambda_\mathrm{t})\mathrm{Z}(\mathrm{t}) - \varpi_{2\mathrm{k}}(\Lambda_\mathrm{t})\omega_\mathrm{t}\mathrm{Z}(\mathrm{t}) \\ \quad + \int_\mathrm{Y} \dfrac{\partial \mathbf{g}^\top}{\partial \mathrm{Z}(\mathrm{t})}\sigma(\mathrm{t},\vartheta)\varpi_8(d\vartheta) + \dfrac{\partial \tilde{h}}{\partial \mathrm{Z}(\mathrm{t})}\Big) d\mathrm{tf}_1(\mathrm{t}) \\ \quad + \kappa_6(\Lambda_\mathrm{t})\mathrm{Z}(\mathrm{t})d\mathrm{B}(\mathrm{t})\mathrm{f}_2(\mathrm{t}) + \int_\mathrm{Y} \sigma(\mathrm{t},\vartheta)\bar{\aleph}(d\mathrm{t}, d\vartheta) + \wp(\mathrm{t})d\widetilde{\omega}(\mathrm{t}), \\ cr \quad \mathrm{f}_{16}(\widehat{\mathfrak{J}}) = \nabla_{\mathrm{Z}(\mathrm{t})}\hat{h}(\mathrm{Z}(\mathrm{t})_{\widehat{\mathfrak{J}}}, \Lambda_{\widehat{\mathfrak{J}}}). \end{cases} \tag{64}$$

By defining the vector $\wp(\mathrm{t}) = [\wp^1(\mathrm{t}), \ldots, \wp^\mathsf{n}(\mathrm{t})]^\top$, where each $\wp^k(\mathrm{t})$ belongs to $\mathbf{R}^{\mathsf{N}\times\mathsf{N}}$, with $k = 1, \ldots, \mathsf{n}$. Additionally, $\nabla_\mathrm{Y}\mathbb{H}$ denotes the gradient of the function $\mathbb{H}$ with respect to Υ_t.

We introduce the following representation for $\wp(\mathrm{t})$:

$$\wp(\mathrm{t})d\widetilde{\omega}(\mathrm{t}) = \left[\textstyle\sum_{k\neq \jmath}\wp^1_{\mathrm{ji}}d\widetilde{\omega}_{\mathrm{ji}}(\mathrm{t}), \ldots, \sum_{k\neq \jmath}\wp^\mathsf{n}_{\mathrm{ji}}d\widetilde{\omega}_{\mathrm{ji}}(\mathrm{t})\right]^\top. \tag{65}$$

The given analysis supports the derivation in [49]. Assuming the validity of assertions $(\mathbf{A_1})$ to $(\mathbf{A_3})$, the presence of singular outcomes for $(\mathrm{f}_1(\mathrm{t}), \mathrm{f}_2(\mathrm{t}), \wp(\mathrm{t}), \sigma(\mathrm{t},\vartheta))$ to the 1st order adjoint system (64) is established in [50]. This may be illustrated as follows. We create two metrics, d and $\tilde{d}$, on the collection $\mathbb{U}_{\mathrm{ad}}[0, \widehat{\mathfrak{J}}]$. in view of two control processes ω_t and $\tilde{\omega}_\mathrm{t}$:

$$d(\omega_\mathrm{t}, \tilde{\omega}_\mathrm{t}) = \tilde{\mathrm{f}}_1\left\{(\mathrm{t}, \mathbf{q}_1) \in [0, \widehat{\mathfrak{J}}] \times \Omega\colon \omega(\mathrm{t}, \mathbf{q}_1) \neq \tilde{\omega}(\mathrm{t}, \mathbf{q}_1)\right\}, \tag{66}$$

$$\tilde{\mathfrak{d}}(\omega_\mathrm{t}, \tilde{\omega}_\mathrm{t}) = \mathrm{E}\int_0^{\widehat{\mathfrak{J}}}\left(1 + \|\mathrm{f}_1{}^\epsilon(\mathrm{t})\| + \|\mathrm{f}_2{}^\epsilon(\mathrm{t})\| + \sup_{\vartheta\epsilon\mathrm{Y}}\|\phi^\epsilon(\mathrm{t},\vartheta)\|\right)\|\omega_\mathrm{t} - \tilde{\omega}_\mathrm{t}\|d\mathrm{t}, \tag{67}$$

where the multiplicative measure of Lebesgue measure f_1 is denoted by $\tilde{\mathrm{f}}_1$.

For a closed convex subset $\mathbb{U}$ of $\mathbf{R}^\mathrm{m}$, it follows that $\mathbb{U}_{\mathrm{ad}}$ comprises a complete metric space concerning to the metrics d and $\tilde{d}$, as established in [51].

Theorem 5: *It is assumed in the event that the assertions* $(\mathbf{A_1})-(\mathbf{A_3})$ *are met. In such a scenario, the Eq. (64) has only one solution* $(\mathrm{f}_1(\mathrm{t}), \mathrm{f}_2(\mathrm{t}), \wp(\mathrm{t}), \sigma(\mathrm{t},\vartheta))$ *satisfying:*

$$\mathrm{E}\left\{\sup_{0\le \mathrm{t}\le\widehat{\mathfrak{J}}}\|\mathrm{f}_1(\mathrm{t})\|^2 + \int_0^{\widehat{\mathfrak{J}}}\left[\|\mathrm{f}_1(\mathrm{t})\|^2 + \|\wp(\mathrm{t})\|^2\mathbf{1}_{\{\Lambda(\mathrm{t}^-)=\jmath\pi_{\mathrm{ij}}\}} + \int_\mathrm{Y}\|\sigma(\mathrm{t},\vartheta)\|^2\mathbf{q}_2(d\varsigma)\right]d\mathrm{t}\right\} \le \mathrm{C}. \tag{68}$$

This theorem is proven using an identical approach to the results established in [50,51], and is therefore omitted for brevity.

Theorem 6: *Given that the assertions* $(\mathbf{A_1})-(\mathbf{A_3})$ *are fulfilled. In this situation, all the optimal strategies* $\omega_t, \tilde{\omega}_t \in \mathbb{U}_{ad}[0,\widehat{\mathfrak{I}}]$ *together with the corresponding solutions* $\Upsilon_t, \tilde{\Upsilon}_t$ *of framework (52), there is a non-negative number* C *for which:*

$$\mathrm{E}\sup_{t\in[0,\widehat{\mathfrak{I}}]}\|\Upsilon_t-\tilde{\Upsilon}_t\|^{2\Psi}\le \mathrm{C}d(\omega_t,\tilde{\omega}_t)^{\Psi\vartheta},\quad \Psi\ge 0,\quad 0<\vartheta<1,\quad \Psi\vartheta<1. \tag{69}$$

Proof: By optimizing and applying integration over $(0,\mathsf{r})$ on systems (52), we have

$$\Upsilon(\mathsf{r})-\Upsilon(0)=\int_0^{\mathsf{r}}\varpi_7(t,\Lambda_t,\Upsilon_t,\omega_t)dt+\int_0^{\mathsf{r}}\xi(t,\Lambda_t,\Upsilon_t,\omega_t)d\mathrm{B}(t)+\int_0^{\mathsf{r}}\int_{\mathrm{Y}}\mathbf{g}(t,\Lambda_t,\Upsilon_t^-,\omega_t^-,\vartheta)\widetilde{\aleph}(dt,d\vartheta). \tag{70}$$

For $\Psi\ge 1$, conclude that

$$\begin{aligned}\mathrm{E}\|\Upsilon_{\mathsf{r}}-\tilde{\Upsilon}_{\mathsf{r}}\|^{2\Psi}\le{}&\mathrm{C}_1\mathrm{E}\left\|\int_0^{\mathsf{r}}\int_{\mathrm{Y}}\left(\mathbf{g}(t,\Lambda_t,\Upsilon_{t^-},\omega_{t^-},\vartheta)-\mathbf{g}(t,\Lambda_t,\tilde{\Upsilon}_{t^-},\tilde{\omega}_{t^-},\vartheta)\right)\tilde{N}(dt,d\vartheta)\right|\Big|^{2\Psi}\\&+\mathrm{C}_1\mathrm{E}\left\|\int_0^{\mathsf{r}}\left(\xi(t,\Lambda_t,\Upsilon_t,\omega_t)-\xi(t,\Lambda_t,\tilde{\Upsilon}_t,\tilde{\omega}_t)\right)d\mathrm{B}(t)\right\|^{2\Psi}\\&+\mathrm{C}_1\mathrm{E}\left\|\int_0^{\mathsf{r}}\left(\varpi_7(t,\Lambda_t,\Upsilon_t,\omega_t)-\varpi_7(t,\Lambda_t,\tilde{\Upsilon}_t,\tilde{\omega}_t)\right)dt\right\|^{2\Psi}.\end{aligned} \tag{71}$$

Using the fact of [52], we get

$$\begin{aligned}\mathrm{E}\sup_{t\in[0,\mathsf{r}]}\|\Upsilon_t-\tilde{\Upsilon}_t\|^{2\Psi}\le{}&\mathrm{C}_2\mathrm{E}\int_0^{\mathsf{r}}\int_{\mathrm{Y}}\left\|\mathbf{g}(t,\Lambda_{t^-},\Upsilon_{t^-},\omega_{t^-},\vartheta)-\mathbf{g}(t,\Lambda_t,\tilde{\Upsilon}_{t^-},\tilde{\omega}_{t^-},\vartheta)\right\|^{2\Psi}\mathbf{q}_2(d\vartheta)dt\\&+\mathrm{C}_2\mathrm{E}\int_0^{\mathsf{r}}\left\|\xi(t,\Lambda_t,\Upsilon_t,\omega_t)-\xi(t,\Lambda_t,\tilde{\Upsilon}_t,\tilde{\omega}_t\right\|^{2\Psi}dt\\&+\mathrm{C}_1\mathrm{E}\left\|\int_0^{\mathsf{r}}\left(\varpi_7(t,\Lambda_t,\Upsilon_t,\omega_t)-\varpi_7(t,\Lambda_t,\tilde{\Upsilon}_t,\tilde{\omega}_t)\right)dt\right\|^{2\Psi}.\end{aligned} \tag{72}$$

As a result of Hölder's inequality and Cauchy-Schwarz, we get:

$$\begin{aligned}\mathrm{E}\sup_{t\in[0,\widehat{\mathfrak{I}}]}\|\Upsilon_t-\tilde{\Upsilon}_t\|^{2\Psi}\le{}&\mathrm{C}_3\mathrm{E}\int_0^{\widehat{\mathfrak{I}}}\int_{\mathrm{Y}}\|\mathbf{g}(t,\Lambda_{t^-},\Upsilon_{t^-},\tilde{\omega}_t,\vartheta)-\mathbf{g}(t,\Lambda_{t^-},\Upsilon_{t^-},\tilde{\omega}_t,\vartheta)\|^{2\Psi}\mathbf{q}_2(d\vartheta)dt\\&+\mathrm{C}_3\mathrm{E}\left\{\int_0^{\widehat{\mathfrak{I}}}\|\varpi_7(t,\Lambda_t,\Upsilon_t,\tilde{\omega}_t)-\varpi_7(t,\Lambda_t,\Upsilon_t,\tilde{\omega}_t)\|^{2\Psi}\mathbf{1}_{\omega_t\neq\tilde{\omega}_t}dt\right\}\\&+\mathrm{C}_3\mathrm{E}\left\{\int_0^{\widehat{\mathfrak{I}}}\|\varpi_7(t,\Lambda_t,\Upsilon_t,\tilde{\omega}_t)-\varpi_7(t,\Lambda_t,\tilde{\Upsilon}_t,\tilde{\omega}_t)\|^{2\Psi}dt\right\}\\&+\mathrm{C}_3\mathrm{E}\left\{\int_0^{\widehat{\mathfrak{I}}}\|\xi(t,\Lambda_t,\Upsilon_t,\omega_t)-\xi(t,\Lambda_t,\tilde{\Upsilon}_t,\tilde{\omega}_t)\|^{2\Psi}dt\right\}.\end{aligned} \tag{73}$$

Utilizing $(\mathbf{A_1})$ and $\frac{1}{\rho\Psi}>1$, Hölder's inequality yields

$$\begin{aligned}&\mathrm{E}\int_0^{\widehat{\mathfrak{I}}}\|\varpi_7(t,\Lambda_t,\Upsilon_t,\omega_t)-\varpi_7(t,\Lambda_t,\Upsilon_t,\tilde{\omega}_t)\|^{2\Psi}\mathbf{1}_{\{\omega_t\neq\tilde{\omega}_t\}}dt\\&\le\mathrm{E}\left\{\int_0^{\widehat{\mathfrak{I}}}\|\varpi_7(t,\Lambda_t,\Upsilon_t,\omega_t)-\varpi_7(t,\Lambda_t,\Upsilon_t,\tilde{\omega}_t)\|^{2\Psi(1-\Psi\rho)}dt\right\}^{1-\Psi\rho}\mathrm{E}\left\{\int_0^{\widehat{\mathfrak{I}}}\mathbf{1}_{\{\omega_t\neq\tilde{\omega}_t\}}dt\right\}^{\Psi\rho}\end{aligned}$$

$$\leq C_4 E\left\{\int_0^{\widehat{\mathfrak{I}}}(1+\|\Upsilon_t\|+\|\omega_t\|+\|\tilde{\omega}_t\|)^{2\Psi(1-\Psi\rho)}dt\right\}^{1-\Psi\rho} E\left\{\int_0^{\widehat{\mathfrak{I}}}\mathbf{1}_{\{\omega_t\neq\tilde{\omega}_t\}}dt\right\}^{\Psi\rho}. \tag{74}$$

In view of (74) and observing Remark 2, we have

$$E\sup_{t\in[0,\widehat{\mathfrak{I}}]}\|\Upsilon_t-\tilde{\Upsilon}_t\|^{2\Psi}\leq C_5\left\{E\int_0^{\widehat{\mathfrak{I}}}\mathbf{1}_{\omega_t\neq\tilde{\omega}_t}dt\right\}^{\Psi\rho}+C_5E\int_0^{\widehat{\mathfrak{I}}}\|\Upsilon_t-\tilde{\Upsilon}_t\|^{2\Psi}dt. \tag{75}$$

Making the use of Bellman-Grönwall inequality, yields

$$E\sup_{t\in[0,\widehat{\mathfrak{I}}]}\|\Upsilon_t-\tilde{\Upsilon}_t\|^{2\Psi}\leq CE\left\{\int_0^{\widehat{\mathfrak{I}}}\mathbf{1}_{\omega_t\neq\tilde{\Upsilon}_t}dt\right\}^{\Psi\rho}=Cd(\Upsilon_t,\tilde{\Upsilon}_t)^{\Psi\rho}. \tag{76}$$

Employing the Cauchy-Schwarz variant, we can conclude that $0\leq\Psi<1$.

$$E\sup_{t\in[0,\widehat{\mathfrak{I}}]}\|\Upsilon_t-\tilde{\Upsilon}_t\|^{2\Psi}\leq\left\{E\sup_{t\in[0,\widehat{\mathfrak{I}}]}\|\Upsilon_t-\tilde{\Upsilon}_t\|^{2}\right\}^{\Psi}\leq\{Cd(\omega_t,\tilde{\omega}_t)^{\rho}\}^{\Psi}=Cd(\omega_t,\tilde{\omega}_t)^{\rho\Psi}. \tag{77}$$

This finalizes the demonstration. □

Theorem 7: *Under the hypotheses* $(\mathbf{A_1})-(\mathbf{A_3})$ *hold. Then, not only for tenable couplets* (ω_t,Υ_t), $(\tilde{\omega}_t,\tilde{\Upsilon}_t)$ *as well as the associated adjoint processes* $(f_1(t),f_2(t),\sigma(t,\vartheta))$ *and* $(\tilde{\wp}_1(t),\tilde{\wp}_2(t),\tilde{\wp}(t),\tilde{\vartheta}(t,\varsigma))$, $\exists$ *constants* $\Psi\in(1,2)$, $\rho\in(0,1)$, $(1+\rho)<2/\Psi$ *and* $C>0$ *ensuring that:*

$$\begin{aligned}E\int_0^{\widehat{\mathfrak{I}}}&\Big(\|f_1-\tilde{f}_1\|^{\Psi}+\|f_2-\tilde{f}_2\|^{\Psi}+\|t-\tilde{t}\|^{\Psi}\mathbf{1}_{\Lambda(t^-)=i}\pi_{ij}\\&+\int_{\Upsilon}\|\vartheta-\tilde{\vartheta}\|^{\Psi}\mathbf{q}_2(d\varsigma)\Big)dt\leq Cd(\omega_t,\tilde{\omega}_t)^{\Psi\rho}.\end{aligned} \tag{78}$$

Proof: By presupposing the following notations to be used in this section.

$$\bar{f}_1=f_1(t)-\tilde{f}_1(t),\quad \bar{f}_2=f_2(t)-\tilde{f}_2(t),\quad \bar{\wp}=\wp(t)-\tilde{\wp}(t),\quad \bar{\vartheta}(t,\varsigma)=\sigma(t,\vartheta)-\tilde{\vartheta}(t,\varsigma). \tag{79}$$

The following backward SDE is then satisfied by $(f_1,f_2,\wp,\vartheta)$:

$$d\bar{f}_1(t)=\begin{cases}-\left[\mathbf{r}_{\Upsilon}^{\top}(t,\Lambda_t,\Upsilon_t,\omega_t)\bar{f}_1+\xi_{\Upsilon}^{\top}(t,\Lambda_t,\Upsilon_t,\omega_t)\bar{f}_2\right]dt\\-\left[\int_{\Upsilon}\mathbf{g}_{\Upsilon}^{\top}(t,\Lambda_{t^-},\Upsilon_{t^-},\omega_{t^-},\varsigma)\bar{\vartheta}(t,\varsigma)\mathbf{q}_2(d\varsigma)+\mathcal{L}(t)\right]dt\\+\bar{f}_2dB(t)+\int_{\Upsilon}\bar{\vartheta}(t,\varsigma)\bar{\aleph}(dt,d\varsigma)+\bar{\wp}d\widetilde{\omega}(t),\end{cases} \tag{80}$$

with the boundary condition:

$$\bar{f}_1(\widehat{\mathfrak{I}})=\hat{h}_{\Upsilon}(\Lambda_{\widehat{\mathfrak{I}}},\Upsilon_{\widehat{\mathfrak{I}}})-\hat{h}_{\Upsilon}(\Lambda_{\widehat{\mathfrak{I}}},\tilde{\Upsilon}_{\widehat{\mathfrak{I}}}). \tag{81}$$

The factor $\mathcal{L}(t)$ is presented as:

$$\mathcal{L}(t) = \begin{cases} \left[\mathbf{r}_{\Upsilon}^{\top}(t, \Lambda_t, \Upsilon_t, \omega_t) - \mathbf{r}_{\Upsilon}^{\top}(t, \Lambda_t, \tilde{\Upsilon}_t, \tilde{\omega}_t)\right] \tilde{f}_1(t) \\ + \left[\xi_{\Upsilon}^{\top}(t, \Lambda_t, \Upsilon_t, \omega_t) - \xi_{\Upsilon}^{\top}(t, \Lambda_t, \tilde{\Upsilon}_t, \tilde{\omega}_t)\right] \tilde{f}_2(t) \\ + \int_{\Upsilon} \left[\mathbf{g}_{\Upsilon}^{\top}(t, \Lambda_{t^-}, \Upsilon_{t^-}, \omega_{t^-}, \varsigma) - \mathbf{g}_{\Upsilon}^{\top}(t, \Lambda_{t^-}, \tilde{\Upsilon}_{t^-}, \tilde{\omega}_{t^-}, \varsigma)\right] \\ \tilde{\vartheta}(t, \varsigma)\mathbf{q}_2(d\varsigma) + \left[\tilde{h}_{\Upsilon}(t, \Lambda_t, \Upsilon_t, \omega_t) - \tilde{h}_{\Upsilon}(t, \Lambda_t, \tilde{\Upsilon}_t, \tilde{\omega}_t)\right]. \end{cases} \tag{82}$$

Additionally, by stating a SDE with $\tilde{\vartheta} = \tilde{\vartheta}(t, \varsigma)$

$$dP(t) = \begin{cases} \left[\mathbf{r}_{\Upsilon}(t, \Lambda_t, \Upsilon_t, \omega_t)\bar{P}(t) + \|\bar{f}_1\|^{\Psi-1}\mathrm{sgn}(\bar{f}_1)\right] dt \\ + \left[\xi_{\Upsilon}(t, \Lambda_t, \Upsilon_t, \omega_t)P(t) + \|\bar{f}_2\|^{\Psi-1}\mathrm{sgn}(\bar{f}_2)\right] dB(t) \\ + \int_{\Upsilon} \left[\mathbf{g}_{\Upsilon}(t, \Lambda_{t^-}, \Upsilon_{t^-}, \omega_{t^-}, \varsigma)P(t) + \|\bar{\vartheta}\|^{\Psi-1}\mathrm{sgn}(\bar{\vartheta})\right] \aleph(dt, d\varsigma) \\ + \|\bar{\wp}\|^{\Psi-1}\mathrm{sgn}(\bar{\wp})d\widetilde{\omega}(t), \\ f_{11}(0) = 0, \end{cases} \tag{83}$$

where $\mathrm{sgn}(\bar{f_{11}}) = (\mathrm{sgn}(\bar{f}_{111}), \mathrm{sgn}(\bar{f}_{112}), \mathrm{sgn}(\bar{f}_{113}), \ldots, \mathrm{sgn}(\bar{f}_{11\mathbf{n}}))^{\top}$ represents the sign function for the vector $\bar{f_{11}}$. On the behalf of the fact that $\mathbf{r}_{\Upsilon}$, ξ_{Υ} and $\mathbf{g}_{\Upsilon}$ are bounded and by the following

$$\begin{aligned} &E\int_0^{\widehat{\mathfrak{J}}} \left[\left\|\|\bar{f_{11}}\|^{\Psi-1}\mathrm{sgn}(\bar{f_{11}})\right\|^2 + \left\|\|\bar{f}_2\|^{\Psi-1}\mathrm{sgn}(\bar{f}_2)\right\|^2 + \left\|\|\bar{\wp}\|^{\Psi-1}\mathrm{sgn}(\bar{\wp})\right\|^2\right] dt \\ &+ E\int_0^{\widehat{\mathfrak{J}}} \int_{\Upsilon} \left\|\|\bar{\vartheta}\|^{\Psi-1}\mathrm{sgn}(\bar{\vartheta})\right\|^2 \mathbf{q}_2(d\varsigma)dt < \infty, \end{aligned} \tag{84}$$

the solution of (83) can be verified by checking the existence-uniqueness of outcome similar to (73), for $\frac{\Psi}{\Psi-1} > 2$, yields

$$\begin{aligned} E\sup_{t\in[0,\widehat{\mathfrak{J}}]} \|P(t)\|^{\frac{\Psi}{\Psi-1}} \leq\ & C_1 E\int_0^{\widehat{\mathfrak{J}}} \int_{\Upsilon} \left\|\mathbf{g}_{\Upsilon}(t, \Lambda_{t^-}, \Upsilon_{t^-}, \omega_{t^-}, \varsigma)P(t) + \|\vartheta\|^{\Psi-1}\mathrm{sgn}(\vartheta)\right\|^{\frac{\Psi}{\Psi-1}} \mathbf{q}_2(d\varsigma)dt \\ &+ C_1 E\int_0^{\widehat{\mathfrak{J}}} \left\|\mathbf{r}_{\Upsilon}(t, \Lambda_t, \Upsilon_t, \omega_t)P(t) + \|\bar{f_{11}}\|^{\Psi-1}\mathrm{sgn}(\bar{f_{11}})\right\|^{\frac{\Psi}{\Psi-1}} dt \\ &+ C_1 E\int_0^{\widehat{\mathfrak{J}}} \left\|\xi_{\Upsilon}(t, \Lambda_t, \Upsilon_t, \omega_t)P(t) + \|\bar{f}_2\|^{\Psi-1}\mathrm{sgn}(\bar{f}_2)\right\|^{\frac{\Psi}{\Psi-1}} dt \\ &+ C_1 E\int_0^{\widehat{\mathfrak{J}}} \left[\|\wp(t)\|^{\Psi-1}\mathrm{sgn}(\wp(t))\right]^{\frac{\Psi}{\Psi-1}} \mathbf{1}_{\Lambda(t^-)=J}\pi_{ij}dt. \end{aligned} \tag{85}$$

Lemma 4 and the boundedness of $\mathbf{r}_{\Upsilon}$, ξ_t and $\mathbf{g}_{\Upsilon}$ may be used to obtain

$$\begin{aligned} E\sup_{t\in[0,\widehat{\mathfrak{J}}]} \|f_{11}(t)\|^{\frac{\Psi}{\Psi-1}} \leq\ & C_2 E\int_0^{\widehat{\mathfrak{J}}} \Big[\|\bar{f}_1\|^{\Psi} + \|\bar{f}_2\|^{\Psi} + \|t\|^{\Psi}\mathbf{1}_{\Lambda(t^-)=J}\pi_{ij} \\ &+ \int_{\Upsilon} \|\vartheta\|^{\Psi}\mathbf{q}_2(d\varsigma)\Big] dt + C_2 E\int_0^{\widehat{\mathfrak{J}}} \|P(t)\|^{\frac{\Psi}{\Psi-1}} dt. \end{aligned} \tag{86}$$

The Bellman-Gronwall variant allows us to write

$$E\sup_{t\in[0,\widehat{\mathfrak{J}}]} \|P(t)\|^{\frac{\Psi}{\Psi-1}} \leq \mathbb{S} := C_3 E\int_0^{\widehat{\mathfrak{J}}} \left[\|\bar{f_{11}}\|^{\Psi} + \|\bar{f}_2\|^{\Psi} + \|\bar{\wp}\|^{\Psi}\mathbf{1}_{\Lambda(t^-)=J}\pi_{ij} + \int_{\Upsilon} \|\vartheta\|^{\Psi}\mathbf{q}_2(d\varsigma)\right] dt. \tag{87}$$

It is follow that

$$
\begin{aligned}
&\mathrm{E}[\bar{\mathrm{f}}_{11}(\widehat{\mathfrak{J}})\mathrm{P}(\widehat{\mathfrak{J}})] \\
&= \mathrm{E}\int_0^{\widehat{\mathfrak{J}}} \bar{\mathrm{f}}_{11}^{\top}\left[(\mathbf{r}_{\Upsilon}(\mathrm{t},\Lambda_{\mathrm{t}},\Upsilon_{\mathrm{t}},\omega_{\mathrm{t}}))\,\mathrm{P}(\mathrm{t}) + \|\mathrm{f}_{11}\|^{\Psi-1}\mathrm{sgn}(\bar{\mathrm{f}}_1)\right]d\mathrm{t} \\
&\quad + \mathrm{E}\int_0^{\widehat{\mathfrak{J}}} -\mathrm{P}^{\top}(\mathrm{t})\left[(\mathbf{r}_{\Upsilon}(\mathrm{t},\Lambda_{\mathrm{t}},\Upsilon_{\mathrm{t}},\omega_{\mathrm{t}}))^{\top}\bar{\mathrm{f}}_{11} + \|\mathrm{f}_{11}\|^{\Psi-1}\mathrm{sgn}(\bar{\mathrm{f}}_{11})\right. \\
&\quad \left.+\xi_{\Upsilon}^{\top}(\mathrm{t},\Lambda_{\mathrm{t}},\Upsilon_{\mathrm{t}},\omega_{\mathrm{t}})\right]d\mathrm{t} + \mathrm{E}\int_0^{\widehat{\mathfrak{J}}} -\mathrm{f}_{11}^{\top}(\mathrm{t})\left[\int_{\Upsilon}\mathbf{g}_{\Upsilon}^{\top}(\mathrm{t},\Lambda_{\mathrm{t}^-},\Upsilon_{\mathrm{t}^-},\omega_{\mathrm{t}^-},\varsigma)\mathbf{q}_2(d\vartheta) + \mathcal{L}(\mathrm{t})\right]d\mathrm{t} \\
&\quad + \mathrm{E}\int_0^{\widehat{\mathfrak{J}}} \mathrm{f}_2^{\top}\left[(\xi(\mathrm{t},\Lambda_{\mathrm{t}},\Upsilon_{\mathrm{t}},\omega_{\mathrm{t}}))\,\mathrm{P}(\mathrm{t}) + \|\mathrm{f}_2\|^{\Psi-1}\mathrm{sgn}(\bar{\mathrm{f}}_2)\right]d\mathrm{t} \\
&\quad + \mathrm{E}\int_0^{\widehat{\mathfrak{J}}}\int_{\Upsilon}\bar{\vartheta}^{\top}(\mathrm{t},\vartheta)\left[\mathbf{g}_{\Upsilon}(\mathrm{t},\Lambda_{\mathrm{t}^-},\Upsilon_{\mathrm{t}^-},\omega_{\mathrm{t}^-},\varsigma)\mathrm{P}(\mathrm{t}) + \|\vartheta\|^{\Psi-1}\mathrm{sgn}(\vartheta)\right]\mathbf{q}_2(d\vartheta)d\mathrm{t} \\
&\quad + \mathrm{E}\int_0^{\widehat{\mathfrak{J}}} \bar{\wp}^{\top}\|\bar{\wp}\|^{\Psi-1}\mathrm{sgn}(\bar{\wp})d\mathrm{t}.
\end{aligned} \tag{88}
$$

It is worth-mentioning that

$$
\begin{aligned}
\mathrm{E}[\bar{\mathrm{f}}_{11}(\widehat{\mathfrak{J}})\mathrm{P}(\widehat{\mathfrak{J}})] &= \mathrm{E}\int_0^{\widehat{\mathfrak{J}}}\left(\bar{\mathrm{f}}_{11}^{\top}\|\bar{\mathrm{f}}_{11}\|^{\Psi-1}\mathrm{sgn}(\bar{\mathrm{f}}_{11}) + \bar{\wp}^{\top}\|\mathrm{t}\|^{\Psi-1}\mathrm{sgn}(\bar{\wp}) + \bar{\mathrm{f}}_2^{\top}\|\bar{\mathrm{f}}_2\|^{\Psi-1}\mathrm{sgn}(\bar{\mathrm{f}}_2)\right)d\mathrm{t} \\
&\quad + \mathrm{E}\int_0^{\widehat{\mathfrak{J}}}\int_{\Upsilon}\vartheta^{\top}\|\vartheta\|^{\Psi-1}\mathrm{sgn}(\vartheta)\mathbf{q}_2(d\vartheta)d\mathrm{t} - \mathrm{E}\int_0^{\widehat{\mathfrak{J}}}\mathrm{P}^{\top}(\mathrm{t})\mathcal{L}(\mathrm{t})d\mathrm{t} \\
&= \mathrm{E}\int_0^{\widehat{\mathfrak{J}}}\left[\|\bar{\mathrm{f}}_{11}\|^{\Psi} + \|\bar{\mathrm{f}}_2\|^{\Psi} + \|\bar{\wp}\|^{\Psi} + \mathbf{1}_{\Lambda(\mathrm{t}^-)=J}\pi_{\mathrm{ij}} + \int_{\Upsilon}\|\vartheta\|^{\Psi}\mathbf{q}_2(d\vartheta)\right]d\mathrm{t} \\
&\quad - \mathrm{E}\int_0^{\widehat{\mathfrak{J}}}\mathrm{P}^{\top}(\mathrm{t})\mathcal{L}(\mathrm{t})d\mathrm{t}.
\end{aligned} \tag{89}
$$

Thus, we have

$$
\begin{aligned}
\mathrm{E}[\bar{\mathrm{f}}_{11}^{\top}(\widehat{\mathfrak{J}})\mathrm{P}(\widehat{\mathfrak{J}})] + \mathrm{E}\int_0^{\widehat{\mathfrak{J}}}\mathrm{P}^{\top}(\mathrm{t})\mathcal{L}(\mathrm{t})d\mathrm{t} &\le \mathrm{E}\left[\int_0^{\widehat{\mathfrak{J}}}\|\mathcal{L}(\mathrm{t})\|^{\Psi}d\mathrm{t}\right]^{\frac{1}{\Psi}}\mathrm{E}\left[\int_0^{\widehat{\mathfrak{J}}}\|\mathrm{P}(\mathrm{t})\|^{\frac{\Psi}{\Psi-1}}d\mathrm{t}\right]^{1-\frac{1}{\Psi}} \\
&\quad + \mathrm{E}\left[\hat{h}_{\Upsilon}(\Lambda_{\widehat{\mathfrak{J}}},\Upsilon_{\widehat{\mathfrak{J}}}) - \hat{h}_{\Upsilon}(\Lambda_{\widehat{\mathfrak{J}}},\tilde{\Upsilon}_{\widehat{\mathfrak{J}}})\right]^{\top}\mathrm{P}(\widehat{\mathfrak{J}}).
\end{aligned} \tag{90}
$$

Consequently, we have

$$
\begin{aligned}
\mathrm{E}[\bar{\mathrm{P}}^{\top}(\widehat{\mathfrak{J}})\mathrm{f}_1(\widehat{\mathfrak{J}})] + \mathrm{E}\int_0^{\widehat{\mathfrak{J}}}\mathrm{f}_1^{\top}(\mathrm{t})\mathcal{L}(\mathrm{t})d\mathrm{t} &\le \mathrm{C}_4\mathbb{S}^{\frac{\Psi-1}{\Psi}}\left[\mathrm{E}\left\|\hat{h}_{\Upsilon}(\Lambda_{\widehat{\mathfrak{J}}},\Upsilon_{\widehat{\mathfrak{J}}}) - \hat{h}_{\Upsilon}(\Lambda_{\widehat{\mathfrak{J}}},\tilde{\Upsilon}_{\widehat{\mathfrak{J}}})\right\|^{\Psi}\right]^{\frac{1}{\Psi}} \\
&\quad + \mathrm{C}_4\mathbb{S}^{\frac{\Psi-1}{\Psi}}\mathrm{E}\left[\int_0^{\widehat{\mathfrak{J}}}\|\mathcal{L}(\mathrm{t})\|^{\Psi}d\mathrm{t}\right]^{\frac{1}{\Psi}}.
\end{aligned} \tag{91}
$$

After a straight-forward computation, observe that

$$
\begin{aligned}
\mathrm{E}\left[\bar{\mathrm{f}}_{11}(\widehat{\mathfrak{J}})\bar{\mathrm{P}}(\widehat{\mathfrak{J}})\right] &= \mathrm{E}\int_0^{\widehat{\mathfrak{J}}}\left(\mathrm{f}_{11}^{\top}\|\mathrm{f}_{11}\|^{\Psi-1}\mathrm{sgn}(\mathrm{f}_{11}) + \mathrm{t}^{\top}\|\bar{\wp}\|^{\Psi-1}\mathrm{sgn}(\bar{\wp}) + \mathrm{f}_2^{\top}\|\mathrm{f}_2\|^{\Psi-1}\mathrm{sgn}(\mathrm{f}_2)\right)d\mathrm{t} \\
&\quad + \mathrm{E}\int_0^{\widehat{\mathfrak{J}}}\int_{\Upsilon}\vartheta^{\top}\|\bar{\vartheta}\|^{\Psi-1}\mathrm{sgn}(\bar{\vartheta})\mathbf{q}_2(d\vartheta)d\mathrm{t} - \mathrm{E}\int_0^{\widehat{\mathfrak{J}}}\mathrm{P}^{\top}(\mathrm{t})\mathcal{L}(\mathrm{t})d\mathrm{t}
\end{aligned}
$$

$$= \mathrm{E}\int_0^{\widehat{\mathfrak{J}}}\left[\|\bar{\mathrm{f}_{11}}\|^{\Psi}+\|\bar{\mathrm{f}_2}\|^{\Psi}+\|\bar{\wp}\|^{\Psi}+\mathbf{1}_{\Lambda(\mathrm{t}^-)=J}\pi_J+\int_{\Upsilon}\|\bar{\vartheta}\|^{\Psi}\mathbf{q}_2(d\vartheta)\right]d\mathrm{t}$$
$$-\mathrm{E}\int_0^{\widehat{\mathfrak{J}}}\mathrm{f}_1{}^{\top}(\mathrm{t})\mathcal{L}(\mathrm{t})d\mathrm{t}. \tag{92}$$

Moreover, applying Hölder inequality we have

$$\mathrm{E}\left[\mathrm{f}_{11}^{\top}(\widehat{\mathfrak{J}})\mathrm{P}(\widehat{\mathfrak{J}})\right]+\mathrm{E}\int_0^{\widehat{\mathfrak{J}}}\mathrm{P}^{\top}(\mathrm{t})\mathcal{L}(\mathrm{t})d\mathrm{t}$$
$$\leq \mathrm{E}\left[\left(\int_0^{\widehat{\mathfrak{J}}}\|\mathcal{L}(\mathrm{t})\|^{\Psi}d\mathrm{t}\right)^{\frac{1}{\Psi}}\right]\mathrm{E}\left[\left(\int_0^{\widehat{\mathfrak{J}}}\|\mathrm{f}_1(\mathrm{t})\|^{\Psi}(\Psi-1)d\mathrm{t}\right)^{1-\frac{1}{\Psi}}\right]$$
$$+\mathrm{E}\left[\hat{h}_{\Upsilon}\left(\Lambda_{\widehat{\mathfrak{J}}},\Upsilon_{\widehat{\mathfrak{J}}}\right)-\hat{h}_{\Upsilon}\left(\Lambda_{\widehat{\mathfrak{J}}},\tilde{\Upsilon}_{\widehat{\mathfrak{J}}}\right)\right]^{\top}\mathrm{P}(\widehat{\mathfrak{J}}). \tag{93}$$

Utilizing (87) into (93), we attain:

$$\mathrm{E}\left[\mathrm{f}_{11}^{\top}(\widehat{\mathfrak{J}})\mathrm{P}(\widehat{\mathfrak{J}})\right]+\mathrm{E}\int_0^{\widehat{\mathfrak{J}}}\mathrm{P}^{\top}(\mathrm{t})\mathcal{L}(\mathrm{t})d\mathrm{t}\leq \mathrm{C}_4\mathbb{S}^{\frac{\Psi-1}{\Psi}}\mathrm{E}\left[\|\hat{h}_{\Upsilon}(\Lambda_{\widehat{\mathfrak{J}}},\Upsilon_{\widehat{\mathfrak{J}}})-\hat{h}_{\Upsilon}(\Lambda_{\widehat{\mathfrak{J}}},\tilde{\Upsilon}_{\widehat{\mathfrak{J}}})\|^{\Psi}\right]^{\frac{1}{\Psi}}$$
$$+\mathrm{C}_4\mathbb{S}^{\frac{\Psi-1}{\Psi}}\mathrm{E}\left[\left(\int_0^{\widehat{\mathfrak{J}}}\|\mathcal{L}(\mathrm{t})\|^{\Psi}d\mathrm{t}\right)^{\frac{1}{\Psi}}\right]. \tag{94}$$

Referring to (94) and observing Remark (59), one can write

$$\mathrm{E}\sup_{\mathrm{t}\in[0,\widehat{\mathfrak{J}}]}\|\Upsilon_{\mathrm{t}}-\tilde{\Upsilon}_{\mathrm{t}}\|^{2\Psi}\leq \mathrm{C}_5\left\{\mathrm{E}\int_0^{\widehat{\mathfrak{J}}}\mathbf{1}_{\omega_{\mathrm{t}}\neq\tilde{\omega}_{\mathrm{t}}}d\mathrm{t}\right\}^{\Psi\rho}+\mathrm{C}_5\mathrm{E}\int_0^{\widehat{\mathfrak{J}}}\|\Upsilon_{\mathrm{t}}-\tilde{\Upsilon}_{\mathrm{t}}\|^{2\Psi}d\mathrm{t}. \tag{95}$$

Combining (87), (92) and (95), we have

$$\mathbb{S}\leq \mathrm{C}_5\mathrm{E}\|\hat{h}_{\Upsilon}(\Lambda_{\widehat{\mathfrak{J}}},\Upsilon_{\widehat{\mathfrak{J}}})-\hat{h}_{\Upsilon}(\Lambda_{\widehat{\mathfrak{J}}},\tilde{\Upsilon}_{\widehat{\mathfrak{J}}})\|^{\Psi}+\mathrm{C}_6\mathrm{E}\int_0^{\widehat{\mathfrak{J}}}\|\mathcal{L}(\mathrm{t})\|^{\Psi}d\mathrm{t}. \tag{96}$$

From $(\mathbf{A_2})$ and Theorem 6, we can get

$$\mathrm{E}\|\hat{h}_{\Upsilon}(\Lambda_{\widehat{\mathfrak{J}}},\Upsilon_{\widehat{\mathfrak{J}}})-\hat{h}_{\Upsilon}(\Lambda_{\widehat{\mathfrak{J}}},\tilde{\Upsilon}_{\widehat{\mathfrak{J}}})\|^{\Psi}\leq \mathrm{C}_7\mathrm{E}\|\Upsilon_{\widehat{\mathfrak{J}}}-\tilde{\Upsilon}_{\widehat{\mathfrak{J}}}\|^{\Psi}$$
$$\leq \mathrm{C}_8 d(\omega_{\mathrm{t}},\tilde{\omega}_{\mathrm{t}})^{\Psi\rho^2}. \tag{97}$$

It follows that

$$\mathrm{E}\int_0^{\widehat{\mathfrak{J}}}\|\mathcal{L}(\mathrm{t})\|^{\Psi}d\mathrm{t}$$
$$\leq \mathrm{C}_9\mathrm{E}\int_0^{\widehat{\mathfrak{J}}}\int_{\Upsilon}\|\mathbf{g}_{\Upsilon}^{\top}(\mathrm{t},\Lambda_{\mathrm{t}},\Upsilon_{\mathrm{t}^-},\omega_{\mathrm{t}^-})-\mathbf{g}_{\Upsilon}^{\top}(\mathrm{t},\Lambda_{\mathrm{t}},\tilde{\Upsilon}_{\mathrm{t}^-},\tilde{\omega}_{\mathrm{t}^-})\|^{\Psi}\|\tilde{\phi}(\mathrm{t},\vartheta)\|^{\Psi}\mathbf{q}_2(d\vartheta)d\mathrm{t}$$
$$+\mathrm{C}_9\mathrm{E}\int_0^{\widehat{\mathfrak{J}}}\|\mathbf{r}_{\Upsilon}^{\top}(\mathrm{t},\Lambda_{\mathrm{t}},\Upsilon_{\mathrm{t}},\omega_{\mathrm{t}})-\mathbf{r}_{\Upsilon}^{\top}(\mathrm{t},\Lambda_{\mathrm{t}},\tilde{\Upsilon}_{\mathrm{t}},\omega_{\mathrm{t}})\|^{\Psi}\|\tilde{\mathrm{f}}_1(\mathrm{t})\|^{\Psi}d\mathrm{t}$$
$$+\mathrm{C}_9\mathrm{E}\int_0^{\widehat{\mathfrak{J}}}\|\xi_{\Upsilon}^{\top}(\mathrm{t},\Lambda_{\mathrm{t}},\Upsilon_{\mathrm{t}},\omega_{\mathrm{t}})-\xi_{\Upsilon}^{\top}(\mathrm{t},\Lambda_{\mathrm{t}},\Upsilon_{\mathrm{t}},\tilde{\omega}_{\mathrm{t}})\|^{\Psi}\|\tilde{\mathrm{f}}_2(\mathrm{t})\|^{\Psi}d\mathrm{t}$$

$$+ C_9 E \int_0^{\widehat{\mathfrak{I}}} \|\xi_\Upsilon^\top(t, \Lambda_t, \Upsilon_t, \tilde{\omega}_t) - \xi_\Upsilon^\top(t, \Lambda_t, \tilde{\Upsilon}_t, \tilde{\omega}_t)\|^\Psi \|\tilde{f}_2(t)\|^\Psi dt$$
$$+ C_9 E \int_0^{\widehat{\mathfrak{I}}} \|\tilde{h}_\Upsilon(t, \Lambda_t, \Upsilon_t, \omega_t) - \tilde{h}_\Upsilon(t, \Lambda_t, \tilde{\Upsilon}_t, \omega_t)\|^\Psi dt$$
$$+ C_9 E \int_0^{\widehat{\mathfrak{I}}} \|\tilde{h}_\Upsilon(t, \Lambda_t, \tilde{\Upsilon}_t, \omega_t) - \tilde{h}_\Upsilon(t, \Lambda_t, \tilde{\Upsilon}_t, \tilde{\omega}_t)\|^\Psi dt. \tag{98}$$

For $\frac{2}{\Psi} > 1$, we can deduce by the Hölder inequality and the assertions $(\mathbf{A_1})-(\mathbf{A_3})$ that

$$\int_0^{\widehat{\mathfrak{I}}} \left\|\xi_\Upsilon^\top(t, \Lambda_t, \Upsilon_t, \omega_t) - \xi_\Upsilon^\top(t, \Lambda_t, \Upsilon_t, \tilde{\omega}_t)\right\|^\Psi \left\|\tilde{f}_2(t)\right\|^\Psi dt$$
$$+ \int_0^{\widehat{\mathfrak{I}}} \left\|\xi_\Upsilon^\top(t, \Lambda_t, \Upsilon_t, \tilde{\omega}_t) - \xi_\Upsilon^\top(t, \Lambda_t, \tilde{\Upsilon}_t, \tilde{\omega}_t)\right\|^\Psi \left\|\tilde{f}_2(t)\right\|^\Psi dt$$
$$\leq C_{10} E \left\{ \left(\int_0^{\widehat{\mathfrak{I}}} \left\|\mathbf{1}_{\omega_{\widehat{\mathfrak{I}}} \neq \tilde{\omega}_t}\right\|^{\frac{2\Psi}{2-\Psi}} dt \right)^{1-\frac{\Psi}{2}} \right\} E \left\{ \left(\int_0^{\widehat{\mathfrak{I}}} \left\|\tilde{f}_2(t)\right\|^2 dt \right)^{\frac{\Psi}{2}} \right\}$$
$$+ C_{10} E \left\{ \left(\int_0^{\widehat{\mathfrak{I}}} \left\|\Upsilon_{\widehat{\mathfrak{I}}} - \tilde{\Upsilon}_t\right\|^{\frac{2\Psi}{2-\Psi}} dt \right)^{1-\frac{\Psi}{2}} \right\} E \left\{ \left(\int_0^{\widehat{\mathfrak{I}}} \left\|\tilde{f}_2(t)\right\|^2 dt \right)^{\frac{\Psi}{2}} \right\}. \tag{99}$$

Thanks to $d(\omega_t, \tilde{\omega}_t) \leq 1$ and $(1+\rho)^\Psi < 2$, we get

$$E \left\{ \left(\int_0^{\widehat{\mathfrak{I}}} \left\|\mathbf{1}_{\omega_t \neq \tilde{\omega}_t}\right\|^{\frac{2\Psi}{2-\Psi}} dt \right)^{1-\frac{\Psi}{2}} \right\} = d(\omega_t, \tilde{\omega}_t)^{1-\frac{\Psi}{2}}$$
$$\leq d(\omega_t, \tilde{\omega}_t)^{\Psi\rho/2}. \tag{100}$$

Furthermore, it is straightforward to verify that $\frac{2\Psi}{2-\Psi} > 2$, therefore by Theorem 6, we have

$$E \left\{ \left(\int_0^{\widehat{\mathfrak{I}}} \left\|\Upsilon_t, \tilde{\Upsilon}_t\right\|^{\frac{2\Psi}{2-\Psi}} dt \right)^{1-\frac{\Psi}{2}} \right\} \leq C_{11} d(\omega_t, \tilde{\omega}_t)^{\Psi\rho/(2-\Psi)}$$
$$\leq C_{11} d(\omega_t, \tilde{\omega}_t)^{\Psi\rho/2}. \tag{101}$$

By implementing Theorem 5 and putting (100) and (101) into (99), we may achieve

$$\int_0^{\widehat{\mathfrak{I}}} \left\{ \left\|\xi_\Upsilon^\top(t, \Lambda_t, \Upsilon_t, \omega_t) - \xi_\Upsilon^\top(t, \Lambda_t, \Upsilon_t, \tilde{\omega}_t)\right\|^\Psi + \left\|\xi_\Upsilon^\top(t, \Lambda_t, \Upsilon_t, \tilde{\omega}_t) - \xi_\Upsilon^\top(t, \Lambda_t, \tilde{\Upsilon}_t, \tilde{\omega}_t)\right\|^\Psi \right\}$$
$$\left\|\tilde{f}_2(t)\right\|^\Psi dt \leq C_{12} d(\omega_t, \tilde{\omega}_t)^{\Psi\rho/2}. \tag{102}$$

Analogously, we have

$$\mathrm{E}\int_0^{\widehat{\mathfrak{J}}} \|\mathcal{L}(\mathrm{t})\|^{\Psi} d\mathrm{t} \leq \mathrm{C}_{13} d(\omega_{\mathrm{t}}, \tilde{\omega}_{\mathrm{t}})^{\Psi\rho/2}. \tag{103}$$

The proof that completes the given work can be derived from combining equations (87), (96), (97) and (103). □

4.2 Sufficiency Criteria of Near-Optimality

To effectively implement countermeasures against CHIKV outbreaks, it is essential to establish sufficient conditions under which surveillance and intervention strategies achieve near-optimality. This becomes particularly important when accounting for the accelerated transmission dynamics caused by an undetected latent phase and the inherent randomness introduced via Poisson random measures. The inclusion of latently infected compartments introduces additional variability into the system, while Poisson jumps are employed to model abrupt and spontaneous events—such as emergency public health campaigns (e.g., mass vaccination or intensified vector control) or sudden infestations.

However, the system dynamics are governed by a set of SDEs driven jointly by Brownian motion and Poisson random measures, with a cost functional designed to minimize both the disease burden and the cost of interventions over a finite time horizon.

These conditions ensure that, even in the presence of random outbreaks (Poisson perturbations) and latent dynamics, a control strategy—while not exactly optimal—remains effectively close to the optimal policy in terms of cost and outcome. Such frameworks are critical for designing robust intervention strategies that account for delays in infection, stochastic shocks, and cost constraints, ultimately enhancing epidemic preparedness and control for CHIKV.

We now turn our attention to presenting one of the key results of this study: a sufficient condition, as expressed in (52), under which the proposed control qualifies as a stochastic near-optimal strategy.

Theorem 8: *Assume that the assertions* $(\mathbf{A_1})-(\mathbf{A_3})$ *hold; for any* $\epsilon > 0$ *and suppose that* $(\Upsilon_{\mathrm{t}}^{\epsilon}, \omega_{\mathrm{t}}^{\epsilon})$ *considered to be same for any admissible pair of* $(\mathrm{f}_{1_1}^{\epsilon}(\mathrm{t}), \mathrm{f}_2{}^{\epsilon}(\mathrm{t}), \sigma^{\epsilon}(\mathrm{t}, \vartheta^{\epsilon}))$ *and the corresponding adjoint equation has a solution such as*

$$\begin{aligned}
&\mathrm{E}\int_0^{\widehat{\mathfrak{J}}} \mathbb{H}(\mathrm{t}, \Lambda_{\mathrm{t}}, \Upsilon_{\mathrm{t}}^{\epsilon}, \omega_{\mathrm{t}}^{\epsilon}, \mathrm{f}_1{}^{\epsilon}(\mathrm{t}), \mathrm{f}_2{}^{\epsilon}(\mathrm{t}), \sigma^{\epsilon}(\mathrm{t}, \vartheta^{\epsilon}))d\mathrm{t} \\
&\leq \inf_{\omega_{\mathrm{t}}\epsilon\mathbb{U}_{\mathrm{ad}}[0,\widehat{\mathfrak{J}}]} \mathrm{E}\int_0^{\widehat{\mathfrak{J}}} \mathbb{H}\left(\mathrm{t}, \Lambda_{\mathrm{t}}, \Upsilon_{\mathrm{t}}^{\epsilon}, \omega_{\mathrm{t}}, \mathrm{f}_{1_1}^{\epsilon}(\mathrm{t}), \mathrm{f}_2{}^{\epsilon}(\mathrm{t}), \sigma^{\epsilon}(\mathrm{t}, \vartheta^{\epsilon})\right) d\mathrm{t} + \epsilon,
\end{aligned} \tag{104}$$

consequently, a positive constant C *exists that satisfies*

$$\mathfrak{J}(0, \Upsilon_0, \omega_{\mathrm{t}}^{\epsilon}) \leq \inf_{\omega_{\mathrm{t}}\epsilon\mathbb{U}_{\mathrm{ad}}[0,\widehat{\mathfrak{J}}]} \mathfrak{J}(0, \Upsilon_0, \omega_{\mathrm{t}}) + \mathrm{C}\,\epsilon^{\frac{1}{2}}\ . \tag{105}$$

Proof: To begin with, we present the following useful result

$$\mathsf{W}(\omega) = \mathbb{H}(\mathrm{t}, \Lambda_{\mathrm{t}}, \Upsilon_{\mathrm{t}}^{\epsilon}, \omega_{\mathrm{t}}^{\epsilon}, \mathrm{f}_1{}^{\epsilon}(\mathrm{t}), \mathrm{f}_2{}^{\epsilon}(\mathrm{t}), \sigma^{\epsilon}(\mathrm{t}, \vartheta^{\epsilon})). \tag{106}$$

It is evident that

$$\mathsf{W}(\omega) - \mathsf{W}(\omega^{\epsilon}) = \int_0^{\widehat{\mathfrak{J}}} \left[\varpi_7^{\mathsf{T}}(\mathrm{t}, \Lambda_{\mathrm{t}}, \Upsilon_{\mathrm{t}}^{\epsilon}, \omega_{\mathrm{t}}) - \varpi_7^{\mathsf{T}}(\mathrm{t}, \Lambda_{\mathrm{t}}, \Upsilon_{\mathrm{t}}^{\epsilon}, \omega_{\mathrm{t}}^{\epsilon})\right] \mathrm{f}_{1_1}^{\epsilon}(\mathrm{t}) d(\mathrm{t})$$

$$+\int_0^{\widehat{\mathfrak{J}}}\left[\xi^\top(t,\Lambda_t,\Upsilon_t^\epsilon,\omega_t)-\xi^\top(t,\Lambda_t,\Upsilon_t^\epsilon,\omega_t^\epsilon)\right]f_2{}^\epsilon(t)d(t)$$
$$+\int_0^{\widehat{\mathfrak{J}}}\int_Y\left[\mathbf{g}^\top(t,\Lambda_t,\Upsilon_t^\epsilon,\omega_t,\vartheta)-\mathbf{g}^\top(t,\Lambda_t,\Upsilon_t^\epsilon,\omega_t^\epsilon,\vartheta)\right]\sigma^\epsilon(t,\vartheta)\mathbf{q}_2(d\vartheta)$$
$$+\int_0^{\widehat{\mathfrak{J}}}\left[\tilde{h}(t,\Lambda_t,\Upsilon_t^\epsilon,\omega_t)-\tilde{h}(t,\Lambda_t,\Upsilon_t^\epsilon,\omega_t^\epsilon)\right]. \tag{107}$$

According to $(\mathbf{A_3})$, we attain

$$\begin{aligned}\mathsf{W}(\omega)-\mathsf{W}(\omega^\epsilon)=&\int_0^{\widehat{\mathfrak{J}}}\|\varpi_7^\top(t,\Lambda_t,\Upsilon_t^\epsilon,\omega_t)-\varpi_7^\top(t,\Lambda_t,\Upsilon_t^\epsilon,\omega_t^\epsilon)\|\|f_1\|^\epsilon(t)d(t)\\&+\int_0^{\widehat{\mathfrak{J}}}\|\xi^\top(t,\Lambda_t,\Upsilon_t^\epsilon,\omega_t)-\xi^\top(t,\Lambda_t,\Upsilon_t^\epsilon,\omega_t^\epsilon)\|\|f_2\|^\epsilon(t)d(t)\\&+\int_0^{\widehat{\mathfrak{J}}}\int_Y\|\mathbf{g}^\top(t,\Lambda_t,\Upsilon_t^\epsilon,\omega_t,\vartheta)-\mathbf{g}^\top(t,\Lambda_t,\Upsilon_t^\epsilon,\omega_t^\epsilon,\vartheta)\|\|\sigma^\epsilon(t,\vartheta)\|\mathbf{q}_2(d\vartheta)\\&+\int_0^{\widehat{\mathfrak{J}}}\|\tilde{h}(t,\Lambda_t,\Upsilon_t^\epsilon,\omega_t)-\tilde{h}(t,\Lambda_t,\Upsilon_t^\epsilon,\omega_t^\epsilon)\|\\&\le CE\int_0^{\widehat{\mathfrak{J}}}\left(1+\|f_{1_1}^\epsilon(t)\|+\|f_2{}^\epsilon(t)\|+\sup_{\vartheta\epsilon Y}\|\sigma^\epsilon(t,\vartheta)\|\right)\|\omega_t-\omega_t^\epsilon\|dt\\&=Cd(\omega_t,\omega_t^\epsilon).\end{aligned} \tag{108}$$

Here, operator W supposed to be a continuous on $\mathbb{U}_{ad}[0,\widehat{\mathfrak{J}}]$ through the metric d. By means of (104) and the Ekeland variational concept [46], a control process $\tilde{\omega}_t^\epsilon$ can be identified. The derived $\tilde{\omega}_t^\epsilon\in\mathbb{U}_{ad}[0,\widehat{\mathfrak{J}}]$ is proven to be adequate

$$d(\tilde{\omega}_t^\epsilon,\omega_t^\epsilon)\le\epsilon^{\frac{1}{2}} \tag{109}$$

and

$$\begin{aligned}&E\int_0^{\widehat{\mathfrak{J}}}\mathbb{H}(t,\Lambda_t,\Upsilon_t^\epsilon,\omega_t^\epsilon,f_{1_1}^\epsilon(t),f_2{}^\epsilon(t),\sigma^\epsilon(t,\vartheta^\epsilon))dt\\&\le\inf_{\omega_t\epsilon\mathbb{U}_{ad}[0,\widehat{\mathfrak{J}}]}E\int_0^{\widehat{\mathfrak{J}}}\mathbb{H}\left(t,\Lambda_t,\Upsilon_t^\epsilon,\omega_t,f_1-1^\epsilon(t),f_2{}^\epsilon(t),\sigma^\epsilon(t,\vartheta^\epsilon)\right)dt+d(\tilde{\omega}_t,\omega_t^\epsilon)\,\epsilon^{\frac{1}{2}}\,.\end{aligned} \tag{110}$$

From this, we deduce that

$$\begin{aligned}&E\int_0^{\widehat{\mathfrak{J}}}\widetilde{\mathbb{H}}(t,\Lambda_t,\Upsilon_t^\epsilon,\tilde{\omega}_t^\epsilon,f_{1_1}^\epsilon(t),f_2{}^\epsilon(t),\sigma^\epsilon(t,\vartheta^\epsilon))dt\\&\le E\int_0^{\widehat{\mathfrak{J}}}\widetilde{\mathbb{H}}\left(t,\Lambda_t,\Upsilon_t^\epsilon,\omega_t,f_{1_1}^\epsilon(t),f_2{}^\epsilon(t),\sigma^\epsilon(t,\vartheta^\epsilon)\right)dt,\end{aligned} \tag{111}$$

where

$$\begin{aligned}&E\int_0^{\widehat{\mathfrak{J}}}\widetilde{\mathbb{H}}(t,\Lambda_t,\Upsilon_t^\epsilon,\tilde{\omega}_t^\epsilon,f_{1_1}^\epsilon(t),f_2{}^\epsilon(t),\sigma^\epsilon(t,\vartheta^\epsilon))dt\\&=E\int_0^{\widehat{\mathfrak{J}}}\mathbb{H}\left(t,\Lambda_t,\Upsilon_t^\epsilon,\omega_t,f_{1_1}^\epsilon(t),f_2{}^\epsilon(t),\sigma^\epsilon(t,\vartheta^\epsilon)\right)dt+Z(t)\|\tilde{\omega}_t^\epsilon,\omega_t^\epsilon\|\end{aligned} \tag{112}$$

and

$$Z(t) = 1 + \|f_{11}^{\epsilon}(t)\| + \|f_2{}^{\epsilon}(t)\| + \sup_{\vartheta \in Y} \|\sigma^{\epsilon}(t, \vartheta)\| \geq 1. \tag{113}$$

Therefore, we have

$$\widetilde{\mathbb{H}}\left(t, \Lambda_t, \Upsilon_t^{\epsilon}, \tilde{\omega}_t^{\epsilon}, f_{11}^{\epsilon}(t), f_2{}^{\epsilon}(t), \sigma^{\epsilon}(t, \vartheta^{\epsilon})\right) = \min_{\omega_{\widehat{\mathfrak{J}}} \in \mathbb{U}_{ad}[0,T]} \widetilde{\mathbb{H}}\left(t, \Lambda_t, \Upsilon_t^{\epsilon}, \omega_t^{\epsilon}, f_{11}^{\epsilon}(t), f_2{}^{\epsilon}(t), \sigma^{\epsilon}(t, \vartheta^{\epsilon})\right). \tag{114}$$

By leveraging the finding from [46] and utilizing the property that the adapted gradient of a sum is contained within the sum of the adapted gradients, it follows that:

$$\begin{aligned} 0 \in \partial_{\omega} \widetilde{\mathbb{H}}\left(t, \Lambda_t, \Upsilon_t^{\epsilon}, \tilde{\omega}_t^{\epsilon}, f_{11}^{\epsilon}(t), f_2{}^{\epsilon}(t), \sigma^{\epsilon}(t, \vartheta^{\epsilon})\right) \subset \partial_{\omega} \mathbb{H}\left(t, \Lambda_t, \Upsilon_t^{\epsilon}, \tilde{\omega}_t^{\epsilon}, f_{11}^{\epsilon}(t), f_2{}^{\epsilon}(t), \sigma^{\epsilon}(t, \vartheta^{\epsilon})\right) \\ + \left[-\epsilon^{\frac{1}{2}} Z^{\epsilon}(t), \epsilon^{\frac{1}{2}} Z^{\epsilon}(t)\right]. \end{aligned} \tag{115}$$

Therefore, it is possible to select $\varpi_{10}(t)$ in such a way that

$$\begin{aligned} &\mathbb{H}_{\omega}\left(t, \Lambda_t, \Upsilon_t^{\epsilon}, \tilde{\omega}_t^{\epsilon}, f_{11}^{\epsilon}(t), f_2{}^{\epsilon}(t), \sigma^{\epsilon}(t, \vartheta^{\epsilon})\right) + \varpi_{10}(t) = 0, \\ &\varpi_{10}(t) \in \left[-\epsilon^{\frac{1}{2}} Z^{\epsilon}(t), \epsilon^{\frac{1}{2}} Z^{\epsilon}(t)\right]. \end{aligned} \tag{116}$$

Furthermore, utilizing the aforesaid formulation and the assertion $(\mathbf{A_3})$, which leads to

$$\begin{aligned} &\|\mathbb{H}_{\omega}\left(t, \Lambda_t, \Upsilon_t^{\epsilon}, \omega_t^{\epsilon}, f_{11}^{\epsilon}(t), f_2{}^{\epsilon}(t), \sigma^{\epsilon}(t, \vartheta^{\epsilon})\right)\| \leq \|\mathbb{H}_{\omega}\left(t, \Lambda_t, \Upsilon_t^{\epsilon}, \tilde{\omega}_t^{\epsilon}, f_{11}^{\epsilon}(t), f_2{}^{\epsilon}(t), \sigma^{\epsilon}(t, \vartheta^{\epsilon})\right)\| \\ &\quad + \|\mathbb{H}_{\omega}\left(t, \Lambda_t, \Upsilon_t^{\epsilon}, \omega_t^{\epsilon}, f_{11}^{\epsilon}(t), f_2{}^{\epsilon}(t), \sigma^{\epsilon}(t, \vartheta^{\epsilon})\right) - \mathbb{H}_{\omega}\left(t, \Lambda_t, \Upsilon_t^{\epsilon}, \tilde{\omega}_t^{\epsilon}, f_{11}^{\epsilon}(t), f_2{}^{\epsilon}(t), \sigma^{\epsilon}(t, \vartheta^{\epsilon})\right)\| \\ &\quad \leq \epsilon^{\frac{1}{2}} \mathsf{z}^{\epsilon}(t) + C\left(1 + \|f_{11}^{\epsilon}(t)\| + \|f_2{}^{\epsilon}(t)\| + \sup_{\vartheta \in Y} \|\phi^{\epsilon}(t, \vartheta)\|\right) \|\omega_t^{\epsilon} - \tilde{\omega}_t^{\epsilon}\|. \end{aligned} \tag{117}$$

Since the operator $\mathbb{H}\left(t, \Lambda_t, \Upsilon_t, \omega_t, f_{11}(t), f_2(t), \sigma(t, \vartheta)\right)$ is convex with respect to Υ_t, ω_t, integrating both sides leads to the conclusion that:

$$\begin{aligned} &\int_0^{\widehat{\mathfrak{J}}} \mathbb{H}\left(t, \Lambda_t, \Upsilon_t^{\epsilon}, \omega_t^{\epsilon}, f_{11}^{\epsilon}(t), f_2{}^{\epsilon}(t), \sigma^{\epsilon}(t, \vartheta^{\epsilon})(t, \vartheta)\right) - \mathbb{H}\left(t, \Lambda_t, \Upsilon_t, \omega_t, f_1 - 1^{\epsilon}(t), f_2{}^{\epsilon}(t), \sigma^{\epsilon}(t, \vartheta)\right) dt \\ &\leq \int_0^{\widehat{\mathfrak{J}}} \mathbb{H}_{\Upsilon}^{\top}\left(t, \Lambda_t, \Upsilon_t^{\epsilon}, \omega_t^{\epsilon}, f_{11}^{\epsilon}(t), f_2{}^{\epsilon}(t), \sigma^{\epsilon}(t, \vartheta^{\epsilon})\right)\left(H_t^{\epsilon} - \Upsilon_t\right) dt \\ &+ \int_0^{\widehat{\mathfrak{J}}} \mathbb{H}_{\Upsilon}^{\top}\left(t, \Lambda_t, \Upsilon_t^{\epsilon}, \omega_t^{\epsilon}, f_{11}^{\epsilon}(t), f_2{}^{\epsilon}(t), \sigma^{\epsilon}(t, \vartheta^{\epsilon})\right)\left(\omega_t^{\epsilon} - \omega_t\right) dt. \end{aligned} \tag{118}$$

Taking the expectation on both sides of (118) and merging (109) and (117), we attain

$$\begin{aligned} &E \int_0^{\widehat{\mathfrak{J}}} \mathbb{H}\left(t, \Lambda_t, \Upsilon_t^{\epsilon}, \omega_t^{\epsilon}, f_{11}^{\epsilon}(t), f_2{}^{\epsilon}(t), \sigma^{\epsilon}(t, \vartheta^{\epsilon})(t, \vartheta)\right) - H\left(t, \Lambda_{\widehat{\mathfrak{J}}}, \Upsilon_{\widehat{\mathfrak{J}}}, \omega_{\widehat{\mathfrak{J}}}, f_{11}^{\epsilon}(t), f_2{}^{\epsilon}(t), \phi^{\epsilon}(t, \vartheta)\right) dt \\ &\qquad \leq E \int_0^{\widehat{\mathfrak{J}}} \mathbb{H}_{\Upsilon}^{\top}\left(t, \Lambda_t, \Upsilon_t^{\epsilon}, \omega_t^{\epsilon}, f_{11}^{\epsilon}(t), f_2{}^{\epsilon}(t), \sigma^{\epsilon}(t, \vartheta^{\epsilon})(t, \vartheta)\right)\left(\Upsilon_{\widehat{\mathfrak{J}}}^{\epsilon} - \Upsilon_{\widehat{\mathfrak{J}}}\right) dt + C\,\epsilon^{\frac{1}{2}}. \end{aligned} \tag{119}$$

Due to the convexity of the function $\hat{h}(\Lambda_{\widehat{\mathfrak{J}}}, \Upsilon_{\widehat{\mathfrak{J}}})$, we get

$$E\left[\hat{h}(\Lambda_{\widehat{\mathfrak{J}}}, \Upsilon_{\widehat{\mathfrak{J}}}^{\epsilon}) - \hat{h}(\Lambda_{\widehat{\mathfrak{J}}}, \Upsilon_{\widehat{\mathfrak{J}}})\right] \leq E\left[\hat{h}_{\Upsilon}(\Lambda_{\widehat{\mathfrak{J}}}, \Upsilon_{\widehat{\mathfrak{J}}}^{\epsilon})(\Upsilon_{\widehat{\mathfrak{J}}}^{\epsilon} - \Upsilon_{\widehat{\mathfrak{J}}})\right] = E\left[f_1 - 1^{\epsilon}(t)(\Upsilon_{\widehat{\mathfrak{J}}}^{\epsilon} - \Upsilon_{\widehat{\mathfrak{J}}})\right]. \tag{120}$$

Employing Lemma 3.2 from [46], it is straightforward to get

$$\begin{aligned}\mathrm{E}\left[\mathrm{f}_{11}^{\epsilon}(\mathrm{t})(\Upsilon_{\widehat{\mathfrak{J}}}^{\epsilon}-\Upsilon_{\widehat{\mathfrak{J}}})\right] &= \int_0^{\widehat{\mathfrak{J}}}\int_{\mathrm{Y}}\left[\phi^{\epsilon}(\mathrm{t},\vartheta)\right]^{\top}\left[\mathbf{g}(\mathrm{t},\Lambda_{\widehat{\mathfrak{J}}},\Upsilon_{t-}^{\epsilon},\omega_{\mathrm{t}-}^{\epsilon},\vartheta)-\mathbf{g}(\mathrm{t},\Lambda_{\widehat{\mathfrak{J}}},\Upsilon_{\mathrm{t}-},\omega_{\mathrm{t}-},\vartheta)\right]\mathbf{q}_2(d\vartheta)d\mathrm{t}\\ &+\mathrm{E}\int_0^{\widehat{\mathfrak{J}}}\left[\mathrm{f}_{11}^{\epsilon}(\mathrm{t})\right]^{\top}\left[\varpi_7(\mathrm{t},\Lambda_{\widehat{\mathfrak{J}}},\Upsilon_{\widehat{\mathfrak{J}}}^{\epsilon},\omega_{\mathrm{t}}^{\epsilon})-\varpi_7(\mathrm{t},\Lambda_{\widehat{\mathfrak{J}}},\Upsilon_{\widehat{\mathfrak{J}}},\omega_{\widehat{\mathfrak{J}}})\right]d\mathrm{t}\\ &+\mathrm{E}\int_0^{\widehat{\mathfrak{J}}}\left[\mathrm{f}_2{}^{\epsilon}(\mathrm{t})\right]^{\top}\left[\xi(\mathrm{t},\Lambda_{\widehat{\mathfrak{J}}},\Upsilon_{\widehat{\mathfrak{J}}}^{\epsilon},\omega_{\mathrm{t}}^{\epsilon})-\xi(\mathrm{t},\Lambda_{\widehat{\mathfrak{J}}},\Upsilon_{\widehat{\mathfrak{J}}},\omega_{\widehat{\mathfrak{J}}})\right]d\mathrm{t}.\end{aligned}\tag{121}$$

Consequently, from (119)–(121), we deduce that

$$\mathfrak{J}(0,\Upsilon_0,\omega_{\mathrm{t}}^{\epsilon})\le\mathfrak{J}(0,\Upsilon_0,\omega_{\widehat{\mathfrak{J}}})+\mathrm{C}\epsilon^{\frac{1}{2}}\ .\tag{122}$$

As $\omega_{\widehat{\mathfrak{J}}}$ is arbitrary. This concludes the proof. □

Remark 3: *To establish Theorem 8, the function $H(\cdot)$ must be nearly maximized in its integral form. Furthermore, we can conclude that the ϵ-maximal scenario for the operator $\mathbb{H}(\mathrm{t},\mathbf{r}_{\mathrm{t}},\mathbf{X}_{\mathrm{t}},\omega_{\mathrm{t}},\mathrm{f}_{11}(\mathrm{t}),\mathrm{f}_2(\mathrm{t}),\sigma(\mathrm{t},\vartheta))$ implies near-optimality having an error estimate of order $\epsilon^{\frac{1}{2}}$.*

4.3 Necessary Criterion for Near-Optimal Control

A comprehensive stochastic control strategy is developed by the investigation of the required threshold for near-optimal control of the CHIKV framework (4), which incorporates inadvertent infectious people and is influenced by a Poisson random measure. To precisely represent rapid and unpredictable variations in infectious disease behavior, including unexpected eruptions or interventional impact, this framework employs SDEs featuring jump transitions. In order to minimize a cost criterion that normally weighs operational costs vs. public health objectives, control measures like vaccination or vector elimination are implemented.

Ekeland's variational concept [46] is used to determine the requirements for near-optimality, guaranteeing the presence of nearly optimal controls and permitting a variational evaluation [53]. As a result, a Hamiltonian function is constructed and adjoint mechanisms are introduced, enabling the formulation of a variational inequality. The main finding is that, in comparison to all other permissible controls, the predicted Hamiltonian under a given condition must be almost maximal—within a small error margin—in order for it to be deemed near-optimal. To operate CHIKV effectively and efficiently in the face of unpredictability, this approach offers essential perspectives.

Here, in order to explain the essential assertions of the near-optimal control problem associated with system (52), it follows that any near-optimal control must satisfy a corresponding necessary maximum principle, with an error of order $\epsilon^{\frac{\iota}{2}(1-\frac{\iota}{2})}$ at some intermediate point, where $\iota\in\left[0,\frac{1}{2}\right]$.

Theorem 9: *Assume that $(\Upsilon_{\mathrm{t}}^{\epsilon},\omega_{\mathrm{t}}^{\epsilon})$ denote a valid control pair and let $(\mathrm{f}_{11}^{\epsilon}(\mathrm{t}),\mathrm{f}_2{}^{\epsilon}(\mathrm{t}),\wp^{\epsilon}(\mathrm{t}),\sigma^{\epsilon}(\mathrm{t},\vartheta))$ be the solution to the adjoint equation for some arbitrary $\epsilon>0$. Then $\exists$ constants such that $0<\Psi<1$, $1<\rho<2$ and $(1+\Psi)\rho<2$ having a positive constant $\mathrm{C}>0$ and a parameter ι lies in $\left[0,\frac{1}{2}\right]$, which satisfy the following conditions:*

$$\begin{aligned}-\mathrm{C}\,\epsilon^{\iota^2(1-\iota^2)} &\le \mathrm{E}\int_0^{\widehat{\mathfrak{J}}}\int_{\mathrm{Y}}\left[\phi^{\epsilon}(\mathrm{t},\vartheta)\right]^{\top}\left[\mathbf{g}(\mathrm{t},\omega_{\mathrm{t}},\Upsilon_{\mathrm{t}}^{\epsilon},\omega_{\mathrm{t}},\vartheta)-\mathbf{g}(\mathrm{t},\Lambda_{\mathrm{t}},\Upsilon_{\mathrm{t}}^{\epsilon},\omega_{\mathrm{t}}^{\epsilon},\vartheta)\right]\mathbf{q}_2(d\varpi_1)d\mathrm{t}\\ &+\mathrm{E}\int_0^{\widehat{\mathfrak{J}}}\left[q^{\epsilon}(\mathrm{t})\right]^{\top}\left[\xi(\mathrm{t},\Lambda_{\mathrm{t}},\Upsilon_{\mathrm{t}}^{\epsilon},\omega_{\mathrm{t}})-\xi(\mathrm{t},\Lambda_{\mathrm{t}},\Upsilon_{\mathrm{t}}^{\epsilon},\omega_{\mathrm{t}}^{\epsilon})\right]d\mathrm{t}\end{aligned}$$

$$+ \mathrm{E}\int_0^{\widehat{\mathfrak{J}}} \left[\mathrm{f}_{1_1}^{\epsilon}(\mathrm{t})\right]^{\top}\left[\varpi_7(\mathrm{t},\Lambda_{\mathrm{t}},\Upsilon_{\mathrm{t}}^{\epsilon},\omega_{\mathrm{t}}) - \varpi_7(\mathrm{t},\Lambda_{\mathrm{t}},\Upsilon_{\mathrm{t}}^{\epsilon},\omega_{\mathrm{t}}^{\epsilon})\right] d\mathrm{t}$$
$$+ \mathrm{E}\int_0^{\widehat{\mathfrak{J}}} \tilde{h}(\mathrm{t},\Lambda_{\mathrm{t}},\Upsilon_{\mathrm{t}}^{\epsilon},\omega_{\mathrm{t}}) - \tilde{h}(\mathrm{t},\Lambda_{\mathrm{t}},\Upsilon_{\mathrm{t}}^{\epsilon},\omega_{\mathrm{t}}^{\epsilon})d\mathrm{t}. \tag{123}$$

Proof: Using the Definition 2, the following can be obtained:

$$\mathfrak{J}(0,\Upsilon_0,\omega_{\mathrm{t}}^{\epsilon}) \le \mathfrak{J}(0,\Upsilon_0) + \epsilon\,. \tag{124}$$

Based on Lemma 4, $\exists$ a constant $\Gamma = \frac{\epsilon}{1-\iota^2}$ and $\tilde{\omega}_{\mathrm{t}}^{\epsilon} \in \mathbb{U}_{\mathrm{ad}}[0,\widehat{\mathfrak{J}}]$, so that the following are hold:

$$d(\tilde{\omega}_{\mathrm{t}}^{\epsilon},\omega_{\mathrm{t}}^{\epsilon}) \le \frac{\epsilon}{1-\iota^2},$$
$$\mathfrak{J}(0,\Upsilon_0,\tilde{\omega}_{\mathrm{t}}^{\epsilon}) \le \mathfrak{J}(0,\Upsilon_0,\omega_{\mathrm{t}}) + \epsilon^{\iota^2}\, d(\tilde{\omega}_{\mathrm{t}}^{\epsilon},\omega_{\mathrm{t}}). \tag{125}$$

For practical purposes, we denote:

$$\tilde{\mathfrak{J}}(0,\Upsilon_0,\omega_{\mathrm{t}}) = \mathfrak{J}(0,\Upsilon_0,\omega_{\mathrm{t}}) + \epsilon^{\iota^2}\, d(\tilde{\omega}_{\mathrm{t}}^{\epsilon},\omega_{\mathrm{t}}), \tag{126}$$

which means that:

$$\tilde{\mathfrak{J}}(0,\Upsilon_0,\tilde{\omega}_{\mathrm{t}}^{\epsilon}) \quad \le \quad \tilde{\mathfrak{J}}(0,\Upsilon_0,\omega_{\mathrm{t}}). \tag{127}$$

It is straightforward to demonstrate that $\tilde{\omega}_{\mathrm{t}}^{\epsilon}$ serves as the perfect adjustment for the operator $\tilde{\mathfrak{J}}(0,\Upsilon_0,\omega_{\mathrm{t}})$. For each interval $[\mathrm{t},\bar{\mathrm{t}}+\delta] \subset [0,\widehat{\mathfrak{J}}]$, where $\bar{\mathrm{t}} \in [0,\widehat{\mathfrak{J}})$, we state

$$\omega_{\mathrm{t}}^{\delta} = \tilde{\omega}_{\mathrm{t}}^{\epsilon}\mathbf{1}_{\mathrm{t}\in[0,\widehat{\mathfrak{J}}]\setminus[\mathrm{t},\bar{\mathrm{t}}+\delta]} + \omega_{\mathrm{t}}\mathbf{1}_{\mathrm{t}\in[\mathrm{t},\bar{\mathrm{t}}+\delta]}, \quad \omega_{\mathrm{t}},\tilde{\omega}_{\mathrm{t}}^{\epsilon} \in \mathbb{U}_{\mathrm{ad}}[0,\widehat{\mathfrak{J}}], \tag{128}$$

then, we can fix that $\omega_{\mathrm{t}}^{\delta} \in \mathbb{U}_{\mathrm{ad}}[0,\widehat{\mathfrak{J}}]$. Due to $\tilde{\omega}_{\mathrm{t}}^{\epsilon}$ being optimal control for $\tilde{\mathfrak{J}}(0,\Upsilon_0,\omega_{\mathrm{t}})$, then:

$$\tilde{\mathfrak{J}}(0,\Upsilon_0,\tilde{\omega}_{\mathrm{t}}^{\epsilon}) \quad \le \quad \tilde{\mathfrak{J}}(0,\Upsilon_0,\omega_{\mathrm{t}}^{\delta}). \tag{129}$$

It implies that

$$\tilde{\mathfrak{J}}(0,\Upsilon_0,\tilde{\omega}_{\mathrm{t}}^{\epsilon}) \quad \le \quad \mathfrak{J}(0,\Upsilon_0,\omega_{\mathrm{t}}^{\delta}) + \epsilon^{\iota^2}\, d(\omega_{\mathrm{t}}^{\delta},\tilde{\omega}_{\mathrm{t}}^{\epsilon}). \tag{130}$$

Considering the concept of the control process $\omega_{\mathrm{t}}^{\delta}$ and the metric $\mathfrak{d}$, we have:

$$d(\omega_{\mathrm{t}}^{\delta},\tilde{\omega}_{\mathrm{t}}^{\epsilon}) = \tilde{\mathbb{G}}\left\{(\mathrm{t},\varpi_9) \in [0,\widehat{\mathfrak{J}}] \times \Omega\colon \omega^{\delta}(\mathrm{t},\varpi_9) \ne \tilde{\omega}^{\epsilon}(\mathrm{t},\varpi_9)\right\} \le \delta, \tag{131}$$
$$\mathfrak{J}(0,\Upsilon_0,\omega_{\mathrm{t}}^{\delta}) - \tilde{\mathfrak{J}}(0,\Upsilon_0,\tilde{\omega}_{\mathrm{t}}^{\delta}) \ge -\epsilon\,\iota d(\omega_{\mathrm{t}}^{\delta},\tilde{\omega}_{\mathrm{t}}^{\delta})$$
$$\ge -\epsilon\,\iota\delta. \tag{132}$$

It follows that

$$\mathfrak{J}(0,\Upsilon_0,\omega_{\mathrm{t}}^{\delta}) - \tilde{\mathfrak{J}}(0,\Upsilon_0,\tilde{\omega}_{\mathrm{t}}^{\delta}) = \mathrm{E}\int_0^{\widehat{\mathfrak{J}}}\left[\tilde{h}(\mathrm{t},\Lambda_{\mathrm{t}},\Upsilon_{\mathrm{t}}^{\delta},\omega_{\mathrm{t}}^{\delta}) - \tilde{h}(\mathrm{t},\Lambda_{\mathrm{t}},\tilde{\Upsilon}_{\widehat{\mathfrak{J}}}^{\epsilon},\tilde{\omega}_{\mathrm{t}}^{\delta})\right] d\mathrm{t}$$
$$+ \hat{h}(\Lambda_{\widehat{\mathfrak{J}}},\Upsilon_{\mathrm{t}}^{\delta}) - \hat{h}(\Lambda_{\widehat{\mathfrak{J}}},\tilde{\Upsilon}_{\widehat{\mathfrak{J}}}^{\epsilon})$$
$$\le \mathrm{E}\int_0^{\widehat{\mathfrak{J}}}\left[\tilde{h}(\mathrm{t},\Lambda_{\mathrm{t}},\Upsilon_{\mathrm{t}}^{\delta},\omega_{\mathrm{t}}^{\delta}) - \tilde{h}(\mathrm{t},\Lambda_{\mathrm{t}},\tilde{\Upsilon}_{\widehat{\mathfrak{J}}}^{\epsilon},\omega_{\mathrm{t}}^{\delta})\right] d\mathrm{t}$$

$$
\begin{aligned}
&+ \mathrm{E}\int_{\bar{t}}^{\bar{t}+\delta}\left[\tilde{h}(t,\Lambda_t,\tilde{\Upsilon}^{\epsilon}_{\widehat{\mathfrak{J}}},\omega^{\delta}_t)-\tilde{h}(t,\Lambda_t,\tilde{\Upsilon}^{\epsilon}_{\widehat{\mathfrak{J}}},\tilde{\omega}^{\delta}_t)\right]dt\\
&+ \hat{h}_{\Upsilon}(\Lambda_{\widehat{\mathfrak{J}}},\Upsilon^{\delta}_t)(\Upsilon^{\delta}_t-\tilde{\Upsilon}^{\epsilon}_{\widehat{\mathfrak{J}}}).
\end{aligned}
\tag{133}
$$

Moreover, we have

$$
\begin{aligned}
-\delta\,\epsilon\,\iota \le\ & \mathrm{E}\int_0^{\widehat{\mathfrak{J}}}\left[\tilde{h}(t,\Lambda_t,\Upsilon^{\delta}_t,\omega^{\delta}_t)-\tilde{h}(t,\Lambda_t,\tilde{\Upsilon}^{\epsilon}_{\widehat{\mathfrak{J}}},\omega^{\delta}_t)\right]dt\\
&+ \mathrm{E}\int_{\bar{t}}^{\bar{t}+\delta}\left[\tilde{h}(t,\Lambda_t,\tilde{\Upsilon}^{\epsilon}_{\widehat{\mathfrak{J}}},\omega^{\delta}_t)-\tilde{h}(t,\Lambda_t,\tilde{\Upsilon}^{\epsilon}_{\widehat{\mathfrak{J}}},\tilde{\omega}^{\delta}_t)\right]dt\\
&+ \mathrm{E}\int_0^{\widehat{\mathfrak{J}}}\mathbb{H}^{\top}_{\Upsilon}(t,\Lambda_t,\Upsilon^{\delta}_t,\omega^{\delta}_t,\mathrm{f}_{11}{}^{\delta}(t),\mathrm{f}_2{}^{\delta}(t),\phi^{\delta}(t,\Psi))(\tilde{\Upsilon}^{\epsilon}_{\widehat{\mathfrak{J}}}-\Upsilon^{\delta}_t)dt\\
&+ \mathrm{E}\int_0^{\widehat{\mathfrak{J}}}\mathrm{f}_{11}{}^{\delta}(t)^{\top}\left[\varpi_7(t,\Lambda_t,\Upsilon^{\delta}_t,\omega^{\delta}_t)-\varpi_7(t,\Lambda_t,\tilde{\Upsilon}^{\epsilon}_{\widehat{\mathfrak{J}}},\tilde{\omega}^{\delta}_t)\right]dt\\
&+ \mathrm{E}\int_0^{\widehat{\mathfrak{J}}}\mathrm{f}_2{}^{\delta}(t)^{\top}\left[\xi(t,\Lambda_t,\Upsilon^{\delta}_t,\omega^{\delta}_t)-\xi(t,\Lambda_t,\tilde{\Upsilon}^{\epsilon}_{\widehat{\mathfrak{J}}},\tilde{\omega}^{\delta}_t)\right]dt\\
&+ \mathrm{E}\int_0^{\widehat{\mathfrak{J}}}\int_{\Upsilon}\phi^{\delta}(t,\Psi)^{\top}\left[\mathbf{g}(t,\Lambda_t,\Upsilon^{\delta}_t,\omega^{\delta}_t,\Psi)-\mathbf{g}(t,\Lambda_t,\tilde{\Upsilon}^{\epsilon}_{\widehat{\mathfrak{J}}},\tilde{\omega}^{\delta}_t,\Psi)\right]\mathbf{q}_2(d\Psi)dt.
\end{aligned}
\tag{134}
$$

Consequently, we have

$$
\begin{aligned}
-\epsilon\,\iota \le\ & \mathrm{E}\left[\tilde{h}(t,\Lambda_t,\tilde{\Upsilon}^{\epsilon}_{\widehat{\mathfrak{J}}},\omega_t)-\tilde{h}(t,\Lambda_t,\tilde{\Upsilon}^{\epsilon}_{\widehat{\mathfrak{J}}},\tilde{\omega}^{\delta}_t)\right]\\
&+ \mathrm{E}\left[\tilde{\mathrm{f}}_{11}{}^{\epsilon}(t)^{\top}\left[\varpi_7(t,\Lambda_t,\tilde{\Upsilon}^{\epsilon}_{\widehat{\mathfrak{J}}},\omega_t)-\varpi_7(t,\Lambda_t,\tilde{\Upsilon}^{\epsilon}_{\widehat{\mathfrak{J}}},\tilde{\omega}^{\delta}_t)\right]\right]\\
&+ \mathrm{E}\int_{\Upsilon}\left[\tilde{\phi}^{\epsilon}(t,\Psi)^{\top}\left[\mathbf{g}(t,\Lambda_t,\tilde{\Upsilon}^{\epsilon}_{\widehat{\mathfrak{J}}},\omega_t,\Psi)-\mathbf{g}(t,\Lambda_t,\tilde{\Upsilon}^{\epsilon}_{\widehat{\mathfrak{J}}},\tilde{\omega}^{\delta}_t,\Psi)\right]\mathbf{q}_2(d\Psi)\right]\\
&+ \mathrm{E}\left[\tilde{\mathrm{f}}_2{}^{\epsilon}(t)^{\top}\left[\xi(t,\Lambda_t,\tilde{\Upsilon}^{\epsilon}_{\widehat{\mathfrak{J}}},\omega_t)-\xi(t,\Lambda_t,\tilde{\Upsilon}^{\epsilon}_{\widehat{\mathfrak{J}}},\tilde{\omega}^{\delta}_t)\right]\right].
\end{aligned}
\tag{135}
$$

In view of Theorem 7 and the assertion $(\mathbf{A_1})$, we find

$$
\begin{aligned}
&\mathrm{E}\left\{\int_0^{\widehat{\mathfrak{J}}}\|\tilde{\mathrm{f}}_{11}{}^{\epsilon}(t)-\mathrm{f}_{11}{}^{\epsilon}(t)\|_{\rho}dt\right\}^{\frac{1}{\rho}}\times\mathrm{E}\left\{\int_0^{\widehat{\mathfrak{J}}}\|\mathrm{b}(t,\Lambda_t,\tilde{\Upsilon}^{\epsilon}_t,\omega_t)-\mathrm{b}(t,\Lambda_t,\tilde{\Upsilon}^{\epsilon}_t,\tilde{\omega}^{\epsilon}_t)\|^{\rho-1}_{\rho}dt\right\}^{1-\frac{1}{\rho}}\\
&\le \mathrm{C}\left\{d(\omega^{\epsilon}_t,\tilde{\omega}^{\epsilon}_t)^{\frac{\rho\Psi}{2}}\right\}^{\frac{1}{\rho}}\mathrm{E}\left\{\int_0^{\widehat{\mathfrak{J}}}(1+\|\tilde{\Upsilon}^{\epsilon}_t\|+\|\omega_t\|+\|\tilde{\omega}^{\epsilon}_t\|)^{\rho(\rho-1)}dt\right\}^{1-\frac{1}{\rho}}\\
&\le \mathrm{C}_1 d(\omega^{\epsilon}_t,\tilde{\omega}^{\epsilon}_t)^{\Psi/2}.
\end{aligned}
\tag{136}
$$

On the same way, we can derive from assertion $(\mathbf{A_1})$ and applying Theorem 5 and 6, we have

$$
\begin{aligned}
&\mathrm{E}\left\{\int_0^{\widehat{\mathfrak{J}}}\|\mathrm{f}_{11}{}^{\epsilon}(t)\|^2dt\right\}^{\frac{1}{2}}\mathrm{E}\left\{\int_0^{\widehat{\mathfrak{J}}}\|\mathrm{b}(t,\Lambda_t,\tilde{\Upsilon}^{\epsilon}_t,\omega_t)-\mathrm{b}(t,\Lambda_t,\Upsilon^{\epsilon}_t,\omega_t)\|^2dt\right\}^{\frac{1}{2}}\\
&+\mathrm{E}\left\{\int_0^{\widehat{\mathfrak{J}}}\|\mathrm{f}_{11}{}^{\epsilon}(t)\|^2dt\right\}^{\frac{1}{2}}\mathrm{E}\left\{\int_0^{\widehat{\mathfrak{J}}}\|\mathrm{b}(t,\Lambda_t,\Upsilon^{\epsilon}_t,\tilde{\omega}^{\epsilon}_t)-\mathrm{b}(t,\Lambda_t,\tilde{\Upsilon}^{\epsilon}_t,\tilde{\omega}^{\epsilon}_t)\|^2dt\right\}^{\frac{1}{2}}\\
&\le \mathrm{C}_2 d(\omega^{\epsilon}_t,\tilde{\omega}^{\epsilon}_t)^{\Psi/2}
\end{aligned}
\tag{137}
$$

and

$$
\begin{aligned}
&\mathrm{E}\left\{\int_0^{\widehat{\mathfrak{I}}}\|\mathrm{f}_1-1^{\epsilon}(\mathrm{t})\|^2 d\mathrm{t}\right\}^{\frac{1}{2}}\mathrm{E}\left\{\int_0^{\widehat{\mathfrak{I}}}\|\mathrm{b}(\mathrm{t},\Lambda_{\mathrm{t}},\Upsilon_{\mathrm{t}}^{\epsilon},\omega_{\mathrm{t}}^{\epsilon})-\mathrm{b}(\mathrm{t},\Lambda_{\mathrm{t}},\Upsilon_{\mathrm{t}}^{\epsilon},\tilde{\omega}_{\mathrm{t}}^{\epsilon})\|^2\mathbf{1}_{\omega_{\mathrm{t}}^{\epsilon}\neq\tilde{\omega}_{\mathrm{t}}^{\epsilon}}d\mathrm{t}\right\}^{\frac{1}{2}}\\
&\leq \mathrm{C}_3\left\{\mathrm{E}\left\{\int_0^{\widehat{\mathfrak{I}}}\|\mathrm{b}(\mathrm{t},\Lambda_{\mathrm{t}},\Upsilon_{\mathrm{t}}^{\epsilon},\omega_{\mathrm{t}}^{\epsilon})-\mathrm{b}(\mathrm{t},\Lambda_{\mathrm{t}},\Upsilon_{\mathrm{t}}^{\epsilon},\tilde{\omega}_{\mathrm{t}}^{\epsilon})\|^4 d\mathrm{t}\right\}^{\frac{1}{2}}\mathrm{E}\left\{\int_0^{\widehat{\mathfrak{I}}}\mathbf{1}_{\omega_{\mathrm{t}}^{\epsilon}\neq\tilde{\omega}_{\mathrm{t}}^{\epsilon}}d\mathrm{t}\right\}^{\frac{1}{2}}\right\}^{\frac{1}{2}}\\
&\leq \mathrm{C}_4\mathrm{E}\left\{\int_0^{\widehat{\mathfrak{I}}}(1+\|\omega_{\mathrm{t}}^{\epsilon}\|+\|\Upsilon_{\mathrm{t}}^{\epsilon}\|+\|\tilde{\omega}_{\mathrm{t}}^{\epsilon}\|)^4 d\mathrm{t}\right\}^{\frac{1}{4}}\mathrm{E}\left\{\int_0^{\widehat{\mathfrak{I}}}\mathbf{1}_{\omega_{\mathrm{t}}^{\epsilon}\neq\tilde{\omega}_{\mathrm{t}}^{\epsilon}}d\mathrm{t}\right\}^{\frac{1}{4}}\\
&\leq \mathrm{C}_5 d(\omega_{\mathrm{t}}^{\epsilon},\tilde{\omega}_{\mathrm{t}}^{\epsilon})^{1/4}.
\end{aligned}
\tag{138}
$$

So that, combining (136), (137) and (138), we get

$$
\begin{aligned}
&\mathrm{E}\int_0^{\widehat{\mathfrak{I}}}\left[\tilde{\mathrm{f}}_{1_1}^{\epsilon}(\mathrm{t})\right]^{\top}\left[\mathrm{b}(\mathrm{t},\Lambda_{\mathrm{t}},\tilde{\Upsilon}_{\mathrm{t}}^{\epsilon},\omega_{\mathrm{t}})-\mathrm{b}(\mathrm{t},\Lambda_{\mathrm{t}},\tilde{\Upsilon}_{\mathrm{t}}^{\epsilon},\tilde{\omega}_{\mathrm{t}}^{\epsilon})\right]d\mathrm{t}\\
&-\mathrm{E}\int_0^{\widehat{\mathfrak{I}}}\left[\mathrm{f}_{1_1}^{\epsilon}(\mathrm{t})\right]^{\top}\left[\mathrm{b}(\mathrm{t},\Lambda_{\mathrm{t}},\Upsilon_{\mathrm{t}}^{\epsilon},\omega_{\mathrm{t}})-\mathrm{b}(\mathrm{t},\Lambda_{\mathrm{t}},\Upsilon_{\mathrm{t}}^{\epsilon},\omega_{\mathrm{t}}^{\epsilon})\right]d\mathrm{t}\\
&\leq \mathrm{C}_6 d(\omega_{\mathrm{t}}^{\epsilon},\tilde{\omega}_{\mathrm{t}}^{\epsilon})^{\Psi/2}+\mathrm{C}_5 d(\omega_{\mathrm{t}}^{\epsilon},\tilde{\omega}_{\mathrm{t}}^{\epsilon})^{1/4}.
\end{aligned}
\tag{139}
$$

Observe that $d(\omega_{\mathrm{t}}^{\epsilon},\tilde{\omega}_{\mathrm{t}}^{\epsilon})\leq 1$ and define $\iota=\min\left\{\frac{1}{2},\Psi\right\}$, which means that

$$
\begin{aligned}
&\mathrm{E}\int_0^{\widehat{\mathfrak{I}}}\left[\tilde{\mathrm{f}_{1_1}}^{\epsilon}(\mathrm{t})\right]^{\top}\left[\mathrm{b}(\mathrm{t},\Lambda_{\mathrm{t}},\tilde{\Upsilon}_{\mathrm{t}}^{\epsilon},\omega_{\mathrm{t}})-\mathrm{b}(\mathrm{t},\Lambda_{\mathrm{t}},\tilde{\Upsilon}_{\mathrm{t}}^{\epsilon},\tilde{\omega}_{\mathrm{t}}^{\epsilon})\right]d\mathrm{t}\\
&-\mathrm{E}\int_0^{\widehat{\mathfrak{I}}}\left[\mathrm{f}_{1_1}^{\epsilon}(\mathrm{t})\right]^{\top}\left[\mathrm{b}(\mathrm{t},\Lambda_{\mathrm{t}},\Upsilon_{\mathrm{t}}^{\epsilon},\omega_{\mathrm{t}})-\mathrm{b}(\mathrm{t},\Lambda_{\mathrm{t}},\Upsilon_{\mathrm{t}}^{\epsilon},\omega_{\mathrm{t}}^{\epsilon})\right]d\mathrm{t}\\
&\leq \mathrm{C}_7 d(\omega_{\mathrm{t}}^{\epsilon},\tilde{\omega}_{\mathrm{t}}^{\epsilon})^{\iota/2}.
\end{aligned}
\tag{140}
$$

This completes the proof. □

5 Numerical Experiments

Numerical modeling of CHIKV transmission that incorporates latently infected individuals and Poisson random measures represents a sophisticated approach for understanding the stochastic dynamics of disease spread. In these frameworks, the Poisson random measure accounts for the random occurrence of events—such as sudden outbreaks or control interventions—that influence the dynamics of latent infections.

However, a prominent example is the comprehensive stochastic model developed for CHIKV transmission via *Aedes albopictus*, which effectively captures both outbreak patterns and suppression strategies. This model demonstrates broader applicability across various nations [1], as it integrates multiple factors including virus strain variation, vector control, and geographic containment measures. The inherent randomness of disease transmission is modeled by treating the number of daily human-vector interactions as a Poisson-distributed random variable. To improve computational efficiency, especially when the average interaction rate is high, a normal approximation is employed for simulating daily contacts.

By simulating the spatiotemporal progression of CHIKV, this approach yields valuable insights into the design and evaluation of intervention strategies. Overall, numerical modeling techniques that incorporate

Poisson random measures and other stochastic elements serve as powerful tools for analyzing complex transmission patterns and optimizing control measures under uncertainty.

In order to outline the numerical approach and present the experimental results derived from the implementation of various assertions, a numerical scheme was developed to solve model (4), based on the classical numerical method described in [54]. To efficiently construct the algorithm, we introduced a set of integers, $\mathbb{K} = 0, 1, \ldots, \mathbf{k}$, where $\mathbf{k} \subset \mathbb{Z}$ and $\xi \in \mathsf{s}$. A uniform step size, $\Delta t = \frac{\mathbf{T}}{\mathbf{K}}$, was utilized to discretize the time interval $[0, \mathfrak{I}]$, ensuring accuracy and consistency in the numerical analysis. Moreover, for $\iota \in \{1, \ldots, 6\}$ and $\mathcal{Z}_{\mathsf{K}}^{\mathbf{k}} = S + L + I + V + B + Z$, we define: $\mho_{1\mathbb{Z}}^{\mathsf{in}} \approx \mathcal{W}(t_{n+1}) - \mathcal{W}(t_n) = \sqrt{\mho_1 t}\kappa_{i,n}$, where the latter expression represents the standard Gaussian noise containing mean zero and standard deviation to be one. Furthermore, the impulsive noise with amplitude ω is computed when $\mathsf{s} \equiv (0, +\infty)$ and $\omega(\mathsf{s})$ should be appropriately defined.

$$
\begin{aligned}
S^{\mathbf{m}+1} &= S^{\mathbf{m}} + (\pi - \varpi_1 S(t) - \beta S(t)V(t))\,\Theta t + \sigma_1 S^{\mathbf{m}} dB_{1,\mathbf{m}}(t) \\
&\quad + \frac{\sigma_1^2}{2} S^{\mathbf{m}}(\Theta B_{1,\mathbf{m}}^2 - \Theta t) - \Theta_1(\mho^*) S^{\mathbf{m}} \Theta_{\mathbf{m}}, \\
L^{\mathbf{m}+1} &= L^{\mathbf{m}} + ((1-\rho)\beta S(t)V(t) - (\Theta + \varphi)L(t))\,\Theta(t) + \sigma_2 L^{\mathbf{m}} B_{2,\mathbf{m}}(t) \\
&\quad + \frac{\sigma_2^2}{2} L^{\mathbf{m}}(\Theta B_{2,\mathbf{m}}^2 - \Theta t) - \Theta_1(\mho^*) L^{\mathbf{m}} \Theta_{\mathbf{m}}, \\
I^{\mathbf{m}+1} &= I^{\mathbf{m}} + (\rho\beta S(t)V(t) + \varphi L(t) - \varpi_2 I(t) - \epsilon I(t)Z(t))\,\Theta(t) + \sigma_3 I^{\mathbf{m}} B_{3,\mathbf{m}}(t) \\
&\quad + \frac{\sigma_3^2}{2} I^{\mathbf{m}}(\Theta B_{3,\mathbf{m}}^2 - \Theta t) - \Theta_3(\mho^*) I^{\mathbf{m}} \Theta_{\mathbf{m}}, \\
V^{\mathbf{m}+1} &= V^{\mathbf{m}} + (\varpi_3 I(t) - \varpi_4 V(t) - \varpi_5 V(t)B(t))\,\Theta t + \sigma_4 B^{\mathbf{m}} B_{4,\mathbf{m}}(t) \\
&\quad + \frac{\sigma_4^2}{2} B^{\mathbf{m}}(\Theta B_{4,\mathbf{m}}^2 - \Theta t) - \Theta_4(\mho^*) B^{\mathbf{m}} \Theta_{\mathbf{m}}, \\
B^{\mathbf{m}+1} &= B^{\mathbf{m}} + (\varpi_8 I^{\mathbf{m}} + \pi B^{\mathbf{m}} - \varpi_{10h} V^{\mathbf{m}})\,\Theta t + \sigma_5 S^{\mathbf{m}} dB_{5,\mathbf{m}}(t) \\
&\quad + \frac{\sigma_5^2}{2} V^{\mathbf{m}}(\Theta B_{5,\mathbf{m}}^2 - \Theta t) - \Theta_5(\mho^*) V^{\mathbf{m}} \Theta_{\mathbf{m}}, \\
Z^{\mathbf{m}+1} &= Z^{\mathbf{m}} + (\varpi_8 + \varpi_9 I(t)Z(t) - \varpi_{10} Z(t))\,\Theta t + \sigma_6 Z^{\mathbf{m}} B_{6,\mathbf{m}}(t) \\
&\quad + \frac{\sigma_6^2}{2} Z^{\mathbf{m}}(\Theta B_{6,\mathbf{m}}^2 - \Theta t) - \Theta_6(\mho^*) Z^{\mathbf{m}} \Theta_{\mathbf{m}}.
\end{aligned} \tag{141}
$$

To generate numerical results for the framework (3), the non-negative preserving truncated Euler-Maruyama (PTEM) technique [55] was employed in conjunction with the previously discussed strategies. The PTEM approach has been widely adopted by researchers for analyzing complex physical processes involving stochastic dynamics [56]. This method was selected for its simplicity and robustness in handling jumps induced by Poisson random measures.

For the model (4), specific parameter configurations were required to quantitatively validate the theoretical findings. Two distinct sets of input parameters, summarized in Section 5.1.2, were employed to simulate the system. Such parametric values also include the initial population sizes of individuals. For each parameter grouping, the framework was modeled over the timeframe $[0, 100]$, and the behavior of every component was comprehensively investigated via pictorial depictions.

5.1 Fitting CHIKV Data of Florida State, USA

Here, we use the average per month of CHIKV occurrences documented in Florida, USA, between April 2005 and December 2017 to figure out the unidentified characteristics and ICs of system (2). Inadvertently contaminated individuals are taken into consideration in this investigation. The threshold parameter, $\mathbb{R}_{0L}$, is also computed, along with its mean value and confidence interval.

5.1.1 Data Collection and Assessment

The Florida Department of Health [57] provided us with confirmed case information covering April 2005 and December 2017 to calibrate a mathematical framework describing the propagation evolution of CHIKV in Florida, USA. The total quantity of documented infections, prevalence rates, and demographic profiles by age and geography are among the many details about CHIKV occurrences documented during the virus's inception that are included in this repository. The monthly occurrence of cases reported for every demographic is the primary purpose of this investigation. The overall incidence of CHIKV per 100,000 people in diverse generations from April 2005 and December 2017 is shown in Fig. 2a, which accounts for the contribution of inadvertent contracted infections to the evolution of propagation as

$$\begin{aligned}&\textit{Prevalence of the } \ell \textit{ th demoghraphic}\\&= \frac{\textit{Proportion of freshly identified instances in the } \ell \textit{ th agecateogry}}{\textit{The general demographic of the } \ell \textit{ th age category}} \times 100{,}000. \end{aligned} \tag{142}$$

Table 2 displays the aggregate population of Florida from 2005 to 2019, which was gathered according to the Florida Department of Economic and Demographic Research and the U.S. Census Bureau [58]. Fig. 2b displays the 2010 United States Census information for the state of Florida, which includes age and gender-specific demographic profiles.

The frequency of CHIKV per 100,000 people in every demographic varies seasonally, with notable elevations emerging from the beginning of spring to summertime every year, as seen in Fig. 2a. The general population's estimated monthly CHIKV incidence is 84.2783 cases per 100,000 people. The data shown are age-dependent average recurrence values: 0.2851 for ages 0–5, 0.3288 for ages 6–10, 0.7130 for 11–15, 4.8932 for 16–20, 6.5233 for 21–25, 6.5874 for 26–30, 5.7410 for 31–35, 4.9694 for 36–40, 5.2128 for 41–45, 5.9061 for 46–50, 8.4524 for 51–55, 8.1967 for 56–60, 11.6263 for those 61–65, and 14.8427 for those aged 66 and older (see Table 3). These patterns correspond to the behavior of CHIKV when the host has a latently contaminated lymphocyte component.

Table 2: Population data from 2005 to 2019 (U.S. Census Bureau and Florida office of economic and demographic research) [58]

Year	Entire population	Year	Entire population	Year	Entire population
2005	17,872,000	2010	18,850,000	2015	20,270,000
2006	18,078,000	2011	19,060,000	2016	20,610,000
2007	18,250,000	2012	19,320,000	2017	20,980,000
2008	18,430,000	2013	19,580,000	2018	21,250,000
2009	18,620,000	2014	19,910,000	2019	21,480,000

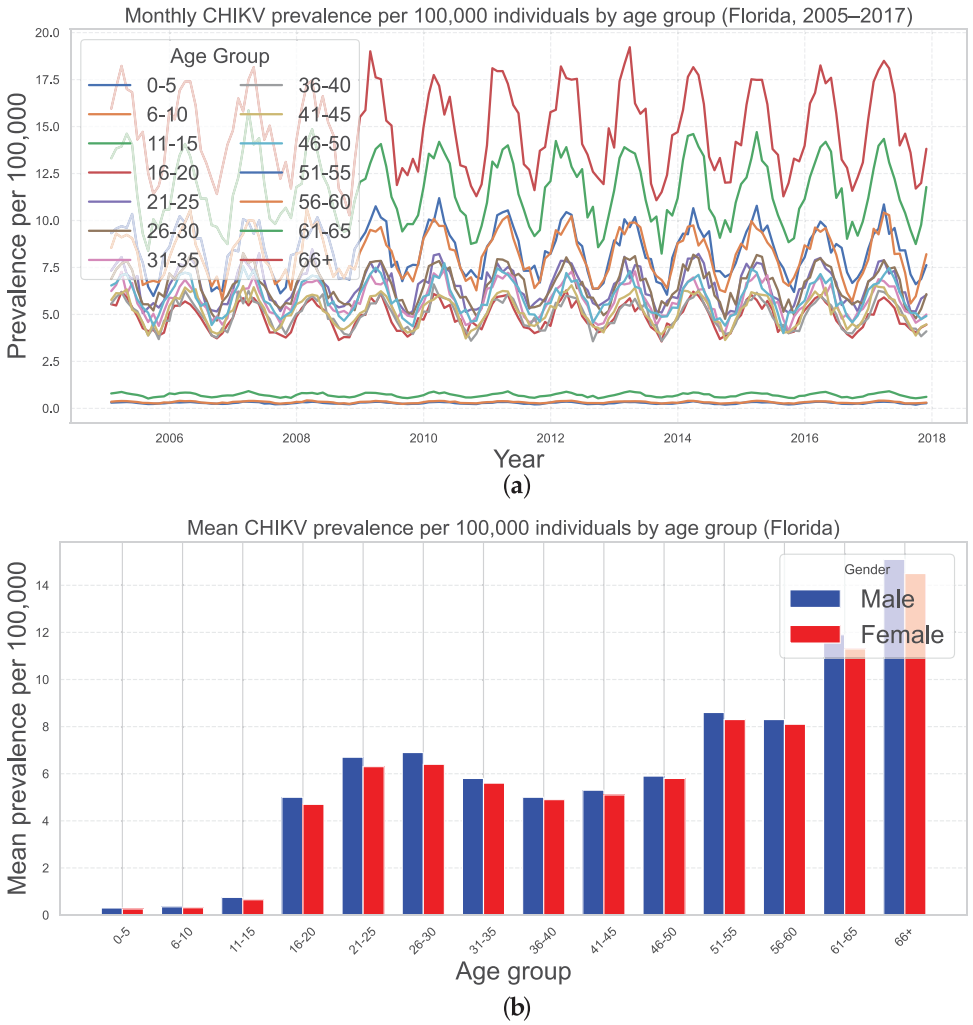

Figure 2: (**a**) Seasonal fluctuation in the prevalence of CHIKV in Florida, USA, across demographics of people per 100,000 people. Integrating an undetected infection phase inside host cells, the findings illustrate CHIKV characteristics. From early spring through summer, heightened predominance is regularly noted. With an overall mean of 84.2783 instances per 100,000 people, age-dependent average monthly prevalence figures are described, varying from 0.2851 (ages 0–5) to 14.8427 (ages 66+). For a complete quantitative decomposition, see Table 3. (**b**) Prevalence of CHIKV in Florida, USA, across demographics of people per 100,000 on a gender basis

Table 3: Monthly incidence of CHIKV per 100,000 people in Florida, USA ([58]), during April 2005 to December 2017. The twenty-fifth and seventy-five percentiles are denoted by lower quartile Q_L and upper quartile Q_U, respectively

Category	Mean ± SD	Min_{val}	Q_L	Median	Q_U	Max_{val}
0–5	0.295 ± 0.215	0.0736	0.1501	0.1923	0.3872	1.021
6–10	0.3401 ± 0.2953	0.0752	0.1357	0.1784	0.4951	1.313
11–15	0.7254 ± 0.3321	0.3902	0.4904	0.5905	0.8313	1.962
16–20	4.9106 ± 1.5402	2.6905	3.7536	4.4409	5.8707	9.902
21–25	6.5233 ± 1.7891	3.1442	4.9817	6.4877	7.9775	10.1162
26–30	6.5874 ± 1.3739	3.2667	5.6593	6.5625	7.3056	10.0414
31–35	5.741 ± 2.0181	3.083	4.2417	5.0779	6.8463	11.5837
36–40	4.9694 ± 1.7879	2.7803	3.8533	4.4234	6.0332	9.3322
41–45	5.2128 ± 1.6104	2.8901	4.0167	4.7214	5.9926	9.7632
46–50	5.9061 ± 1.9095	3.1375	4.3556	5.2637	6.9239	10.2201
51–55	8.4524 ± 2.0461	4.2219	6.2954	7.7816	9.9612	12.4026
56–60	8.1967 ± 1.8844	4.0076	6.1132	7.5837	9.5371	12.1263
61–65	11.6263 ± 2.3485	5.7614	8.9421	10.7893	13.5826	16.9512
66+	14.8427 ± 2.9373	7.3613	11.5487	13.7623	17.1348	20.4321

The age group under fifteen years old has the lowest frequency of CHIKV, while those over 65 had an elevated incidence per 100,000 people. Furthermore, as illustrated in Fig. 3, Pearson's correlation assessment demonstrated a substantial positive association between the demographic variability of CHIKV contaminated people from 2005 to 2017 and the overall incidence of CHIKV per 100,000 individuals. In particular, the correlation coefficient between the mean age of CHIKV-infected people and the occurrence of CHIKV per 100,000 people was higher than 0.85 ($p < 0.01$) over this time frame, indicating that older people are more susceptible to contracting the CHIKV.

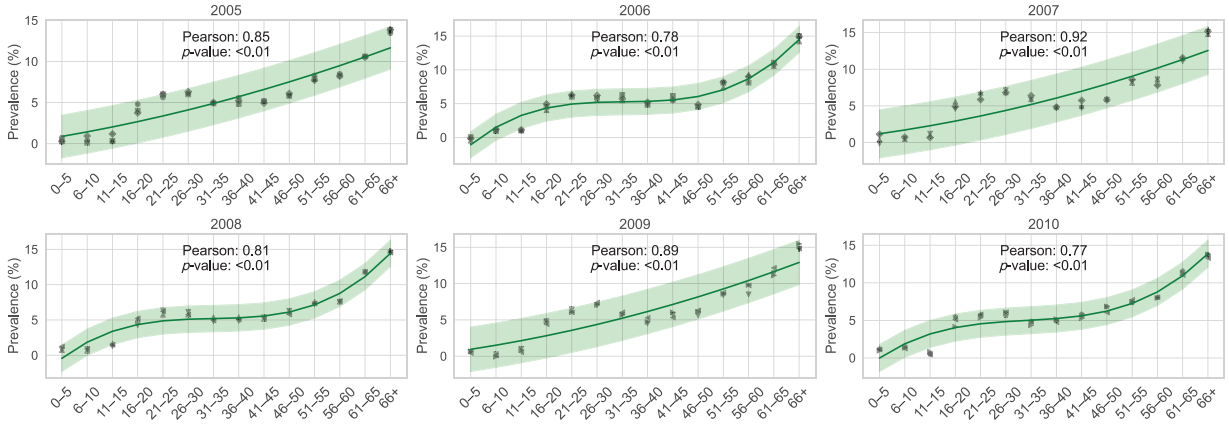

Figure 3: (Continued)

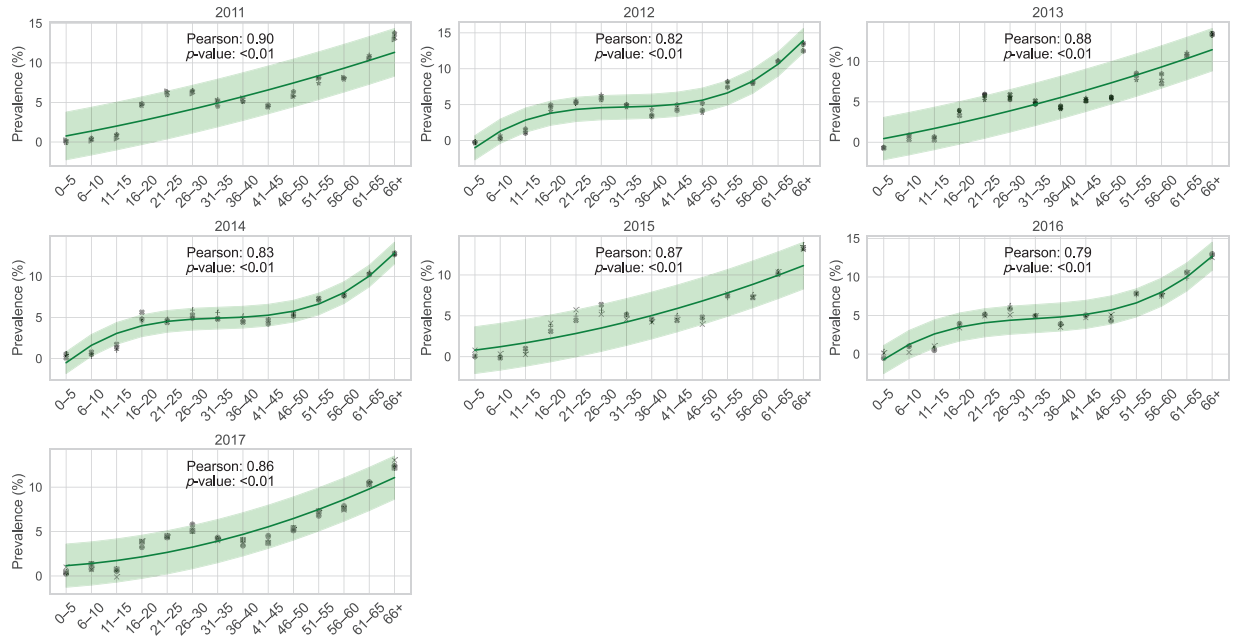

Figure 3: Correlation between age-dependent variations and the prevalence of CHIKV across demographics in Florida, USA, per 100,000 individuals from 2005 to 2017. The prevalence consistently peaks from early spring through summer, with the analysis emphasizing age-specific monthly prevalence, spanning from ages 0–5 to 66 and older

5.1.2 Model Validation and Population Stratification for CHIKV

By analyzing the outcomes of the proposed CHIKV transmission model—which incorporates latently infected cells—against the actual number of confirmed and potential cases, the model's feasibility is validated. This framework simulates the proportion of potentially acquired CHIKV infections in the state of Florida, USA (see [57]). To ensure realistic and comprehensive simulations, the general population is stratified into 14 age groups, ranging from 0–5 years to 66 years and above. This age-structured approach captures heterogeneous susceptibility, contact patterns, and immune responses across different age cohorts, which is particularly relevant for arboviral infections like CHIKV. Subsequently, all parameters and ICs for the system of ODEs (2) governing CHIKV dynamics are estimated. These estimations incorporate both the demographic characteristics of the population and the host immune response, including the latent phase of cellular infection.

(I) To represent demographic behavior, the general population's birth rate, denoted by π_ℓ, is categorized by chronological age and incorporated into the framework. Data-driven obtained from the Florida U.S. Census Bureau [58], it is estimated that individuals under the age of 15 and over the age of 50 contribute minimally to the overall fertility rate. Consequently, the fertility rates for these age groups are set to zero. The nonzero fertility rates are estimated as follows: $\pi_1 = 0.92 \times 10^{-3}$, $\pi_2 = 5.57 \times 10^{-3}$, and $\pi_3 = 6.65 \times 10^{-3}$.

(II) A typical lifespan in the USA is approximately 76 years, data-driven from the U.S. Census Bureau [58]. Accordingly, natural mortality rates (ϖ_{1k1}) are calculated on a monthly basis. For example, for individuals with an average lifespan of 76 years, the monthly natural death rate is given by $\varpi_{11} = \frac{1}{76\times 12}$. Similarly, if a particular demographic group has an average lifespan of 71 years or 66 years, the

corresponding monthly natural death rates are $\varpi_{12} = \frac{1}{71\times12}$ and $\varpi_{13} = \frac{1}{66\times12}$, respectively. These age-specific mortality rates, ϖ_{1k1}, are incorporated into the simulation to accurately reflect generational attrition across different demographic segments.

(III) According to epidemiological research [59], over 10% of individuals who come into contact with CHIKV and harbor a latent cellular infection eventually develop symptoms during their lifetime. Furthermore, it is estimated that within the first two years after infection, approximately 50% of these symptomatic cases—representing about 5% of all infections—progress to a persistent illness [60]. Consequently, we assume a uniform early progression probability across all age groups and set $\beta_\ell = 0.4$ for $1 \le \ell \le 14$.

(IV) Let ρ_ℓ denote the proportion of host cells that are productively infected. The fraction of individuals in age group ℓ who acquire immunity rather than contracting CHIKV upon exposure is represented by $1-\rho_\ell$. According to clinical studies, the effectiveness of the CHIKV vaccine persists for approximately 10 years [61]. Therefore, we assume that significant immunization occurs only within the 0–10 year age range (groups $\ell = 1, 2, 3$), and we set:

$$1-\rho_\ell = \begin{cases} 0.95 & \ell \in [1,3] \\ 0 & \ell \in [4,14]. \end{cases} \tag{143}$$

Thus, vaccination reduces vulnerability to successful infection (i.e., development to nonzero ρ_ℓ) by 95% in the youngest two age categories, but no vaccine-derived immunity is anticipated after age 10.

(V) Here, Θ_ℓ represents the per-cell death probability for cells persistently infected with CHIKV. Exogenous transmission may occur in individuals with latent infections at a rate proportional to Θ_ℓ. The probability of infection for individuals in age group ℓ is denoted by $\beth_\ell$, where $\beth_\ell$ for $1 \le \ell \le 14$. Since persistent infection confers partial protection against reinfection, it follows that $0 < \Theta_\ell < 1$. Based on the estimates provided in [60], we assume a comparable level of immunity across all age groups, with $\Theta_\ell \in [0.15, 0.25]$ for $\ell = 1, \ldots, 14$. While π_ℓ modifies the susceptibility of latently infected individuals to subsequent infection, Θ_ℓ governs the decay rate of the latent compartment in the model formulations.

(VI) The rate at which subconsciously contaminated cells become productively infectious cells is represented by φ_ℓ. Since they only have partial immunity, recovered people can get contaminated again at the rate $\varphi_\ell \beth_\ell$ $(1 \le \ell \le 14)$. Their amount of immunity is thus defined as δ_ℓ, with $0 \le \varphi_\ell \le 1$. We assume a uniform shielding level for any demographic as $\varphi_\ell \in [0.05, 0.25]$, $\ell = 1, \ldots, 14$ taking into account the assumptions of [59]. While $\beth_\ell$ records the receptivity of treated hosts to another infection, φ_ℓ controls the passage from the latent category into an acute infection.

(VII) The ϵ_ℓ is the monthly rate at which CHIKV-latently infected cells reactivate into productive infection in age group ℓ. Based on the age-specific reactivation risks estimated by [62], we have converted their lifetime probabilities into equivalent monthly rates. Thus, the reactivation parameters are given by:

$$\epsilon_\ell = \begin{cases} \left[8.33\times10^{-6}, 1.67\times10^{-5}\right], & \ell \in [1,3], \\ \left[1.50\times10^{-5}, 2.33\times10^{-5}\right], & \ell \in [4,10], \\ \left[1.67\times10^{-5}, 1.60\times10^{-4}\right], & \ell \in [11,13], \\ \left[1.67\times10^{-5}, 3.01\times10^{-4}\right], & \ell = 14. \end{cases} \tag{144}$$

The monthly likelihood that a CHIKV-latent cellular resource could come back into an active infection in all age categories is represented by such ϵ_ℓ levels.

(VIII) We represent by $\varpi_{2\ell}$ the age-dependent likelihood that a vulnerable member of cohort ℓ contracts the virus after coming into touch a potential contagious host, in addition to $\varpi_{2\ell}$ a the per-cell mortality rate of CHIKV-infected cells, which controls the viral transmission period. For the majority of infectious agents influence indirect estimation of $\varpi_{2\ell}$ is typically not possible [4]. Additionally, while large-scale dissemination research (such as in biological representations) can provide insight into the mechanisms of dissemination, they are frequently unsuitable for infectious viruses owing to logistical and righteous limitations ([5]).

We used continuously Morlet wavelet estimation ([63]) to analyze the monthly incidence of cases newly identified in all age categories in order to demonstrate the clear periodicity in CHIKV prevalence. Throughout all 14 communities, the wavelet strength spectrum showed an impressive yearly pattern that was substantial at the 5% level (see Fig. 4a,b). Therefore, we describe $\varpi_{2\ell}$ as an oscillating function that reflects this annual fluctuation, and the cell-death component $\varpi_{2\ell}$ an establishes the duration of infectiousness once lymphocytes acquire effectively infested as $\varpi_{2\ell}(t_1) = \widetilde{\varpi_{2\ell}}\left(1 + \bar{\varpi}_{2\ell}\sin(\pi/6 + \tilde{\phi}_\ell)\right)$, where $\tilde{\phi}_\ell$ is the periodicity of the T-periodic function, $\bar{\varpi}_{2\ell}$ is the intensity of seasonally fluctuations or alternatively the extent of cyclical nature, and $\widetilde{\varpi_{2\ell}}$ is the foundation degree of propagation.

(IX) The total number of people across various age groups is represented as $\mathbb{N}_\ell$, as shown in Table 4, according to data collected in the 2010 demographic surveys released by the Centers for Disease Control and Prevention (CDC), USA [64]. Based on recent projections, approximately 350 million people in the USA have been affected by CHIKV. Therefore, the initial proportion of people with latent infections is calculated as follows:

$$\mathrm{L}_\ell(0) = \frac{300{,}000{,}000 \times \mathbb{N}_\ell}{\sum_{\ell=1}^{14} \mathbb{N}_\ell}, \quad 1 \le \ell \le 14.$$

The initial values for the number of infected individuals $\mathrm{I}_\ell(0)$, virus concentration $\mathrm{V}_\ell(0)$, pathogen concentration $\mathrm{B}_\ell(0)$, and immune factor $\mathrm{Z}_\ell(0)$ are determined by fitting to available epidemiological data. Since adult vaccination programs against CHIKV are currently unavailable or not widely implemented, we assume that $\mathrm{V}_\ell(0) = 0$ for $3 \le \ell \le 4$.

According to center of disease control and prevention [64], 90% of newly detected CHIKV cases receive medical treatment. Therefore, the initial number of treated individuals is assumed to be $\mathrm{Z}_\ell(0) = 0.90 \times \mathrm{I}_\ell(0),\ for\ 1 \le \ell \le 14$.

The initial susceptible population is calculated by subtracting the number of virus concentration, latent, infected, pathogen concentrated, and immune factor from the total population in each age group:

$$\mathrm{S}_\ell(0) = \mathbb{N}_\ell(0) - \mathrm{L}_\ell(0) - \mathrm{I}_\ell(0) - \mathrm{V}_\ell(0) - \mathrm{B}_\ell(0) - \mathrm{Z}_\ell(0),\ (1 \le \ell \le 14). \tag{145}$$

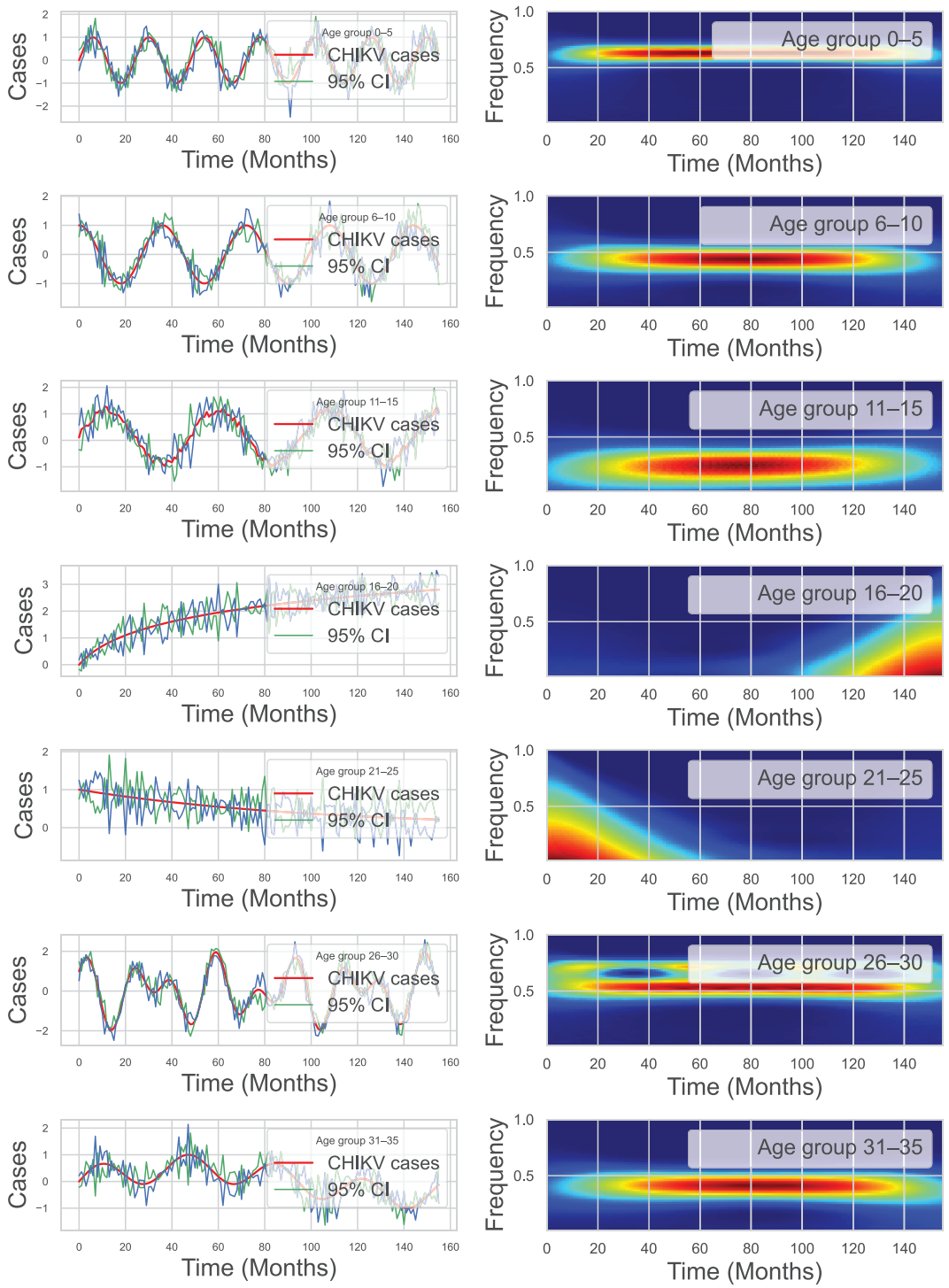

(a)

Figure 4: (Continued)

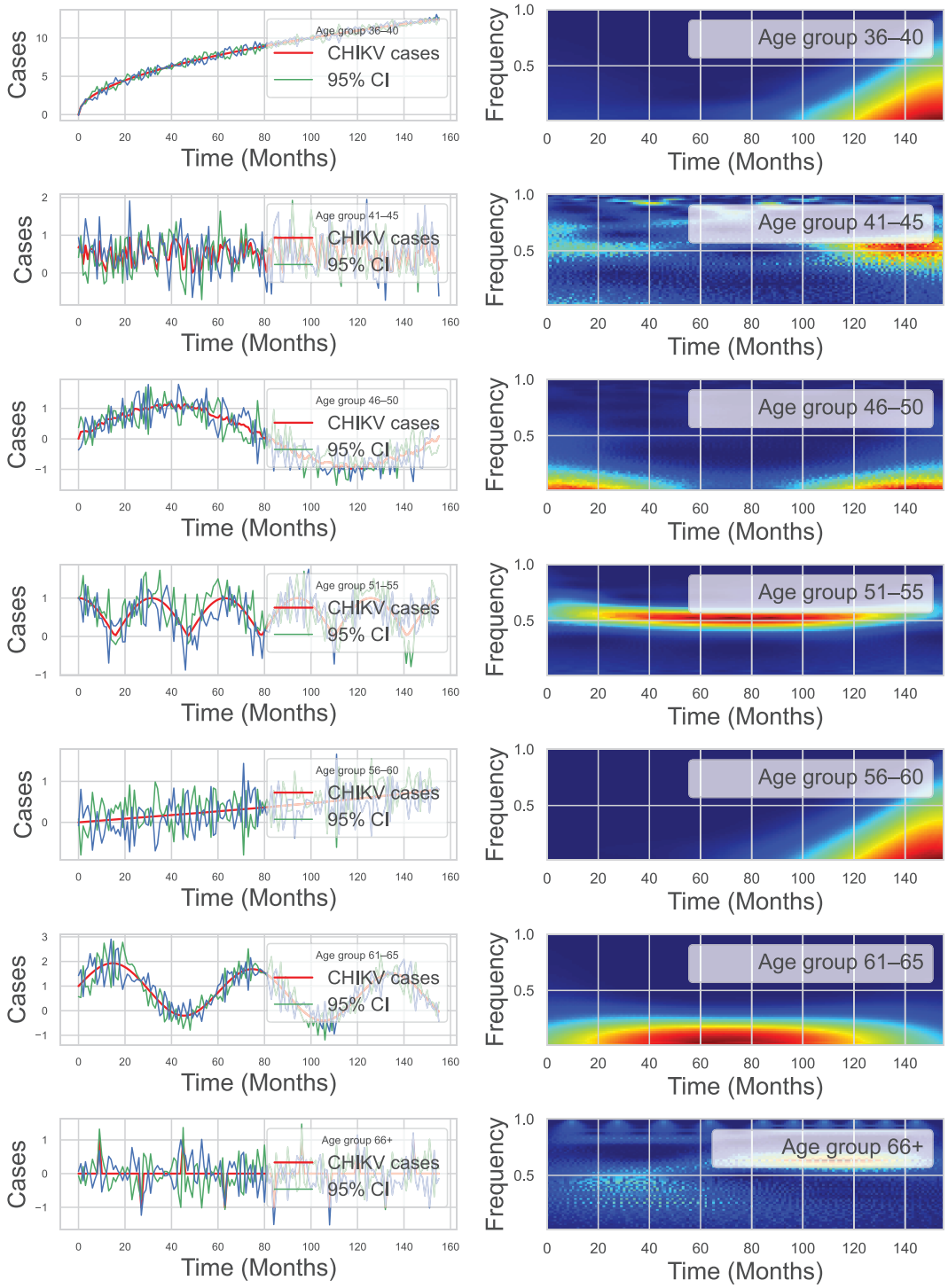

(b)

Figure 4: The wavelet method was applied to analyze the spatiotemporal patterns of monthly new CHIKV cases in Florida, USA, across various age groups from April 2005 to December 2017. The first column displays the corresponding 95% confidence curve (green curve) and the average wavelet spectrum (red line). Additionally, the wavelet spectrum analysis of the monthly reported CHIKV cases time series is presented, with low power values depicted in cyan and blue, intermediate power in orange and yellow, and high power in red. The green line represents the 95% C-I

Table 4: Projected counts of individuals across different age groups (derived from population data for the state of Florida, USA) (see [58])

Category	0–5	5–10	10–15	15–20	20–25	25–30	30–35	35–40
Population	1,200,000	1,150,000	1,180,000	1,300,000	1,450,000	1,300,000	1,250,000	1,400,000
Category	40–45	45–50	50–55	55–60	60–65	65–70	70–75	75–80
Population	1,500,000	1,350,000	1,100,000	1,150,000	950,000	800,000	700,000	600,000

The CHIKV transmission framework with latent infectious cells has been validated through 800,000 repetitions using the MCMC methodology [65], with a burn-in period of 750,000 iterations. We use the recorded monthly prevalence of CHIKV cases as experimental input, considering epidemiological data specific to Florida, USA. These data sets are comparable to those typically used in host-vector interaction studies or more general viral infection modeling approaches. The MCMC procedure captures latent patterns and provides a probabilistic understanding of how well the model fits the observed data, enabling the estimation of unknown parameter values and ICs:

$$\hat{\lambda} = (\hat{\lambda}_1, \ldots, \hat{\lambda}_{\varpi_2}, \ldots, \hat{\lambda}_{\mathrm{B}}), \tag{146}$$

where

$$\hat{\lambda} = \begin{cases} (\varpi_{3\ell}, \varpi_{4\ell}, \varpi_{5\ell}, \varpi_{6\ell}, \varpi_{7\ell}, \varpi_{8\ell}, \varpi_{9\ell}, \varpi_{10\ell}, \delta_\ell, \mathrm{I}_\ell(0), \mathrm{V}_\ell(0), \mathrm{B}_\ell(0)), & \ell \in [1,2] \\ (\varpi_{3\ell}, \varpi_{4\ell}, \varpi_{5\ell}, \varpi_{6\ell}, \varpi_{7\ell}, \varpi_{8\ell}, \varpi_{9\ell}, \varpi_{10\ell}, \delta_\ell, \mathrm{Z}_\ell(0)), & \ell \in [3,12]. \end{cases} \tag{147}$$

Let $\tilde{\mathrm{C}}(t, \hat{\lambda})$, where $1 \le \ell \le 12$, denote the total number of CHIKV-infected individuals (including latently infected) in the ℓth age category. Accordingly, the entire community in the ℓth category, stratified by infection status—including susceptible, latently infected, virus concentration, and immune factors—can be articulated as:

$$\frac{d\tilde{\mathrm{C}}(\mathrm{t}, \hat{\lambda})}{d\mathrm{t}} = \varpi_{4\ell}\varpi_{3\ell}\mathrm{I}_\ell, \quad (1 \le \ell \le \mathrm{B}). \tag{148}$$

Assume that the overall cumulative of infectious people in the ℓth category can be presented as:

$$\tilde{\mathrm{P}}_\ell(\mathrm{t}, \hat{\lambda}) = \varpi_{4\ell}\varpi_{3\ell}\mathrm{I}_\ell, \quad (1 \le \ell \le \mathrm{B}). \tag{149}$$

where $\tilde{\mathrm{P}}_\ell(\mathrm{t}, \hat{\lambda})$ represents the number of new prey individuals (or prey biomass) of the ℓth age group entering the predator-prey interaction, and simulations progress in increments of one month. By collecting $\tilde{\varsigma}$ autonomous sample data from the ℓth demographic, demonstrating the novel prey species or prey biomass observed at the ζth month. The framework was trained using statistics from 2006 to 2015, then it was tested and validated using the dataset from 2016. It is possible to communicate newly collected observational evidence as $\mathrm{G}(\mathrm{t}) = (\mathrm{G}_1(\mathrm{t}), \mathrm{G}_2(\mathrm{t}), \ldots, \mathrm{G}_{\mathrm{B}}(\mathrm{t}))$, where G indicates a $\tilde{\varsigma} \times \mathrm{B}$ matrix. In this case, G stands for the measured biomass or population counts over time for the various ages of the predator and prey species. Suppose a rectangular matrix $\tilde{\varepsilon}$ with $\tilde{\varsigma} \times \mathrm{B}$ follows a matrix-variate probability density function, that is, $\tilde{\varepsilon} \sim \widetilde{\mathrm{N}}(0, \mathrm{I}_{\tilde{\varsigma}}, \sum)$ [66]. Consequently, the following is an expression for the data G:

$$\mathrm{G} = \mathbb{Q} + \tilde{\varepsilon}, \quad \tilde{\varepsilon} \sim \widetilde{\mathrm{N}}\left(0, \mathrm{I}_{\tilde{\varsigma}}, \sum\right), \tag{150}$$

where $\mathbb{Q}$ represents a $\tilde{\varsigma} \times \mathrm{B}$ matrix and $\mathbb{Q}$ indicates the numerical outcomes of over all CHIKV cases of model (2), i.e., $\mathbb{Q} = \left(\tilde{\mathbb{Q}}_1(\mathrm{t}, \hat{\lambda}), \tilde{\mathbb{Q}}_2(\mathrm{t}, \hat{\lambda}), \ldots, \tilde{\mathbb{Q}}_{\mathrm{B}}(\mathrm{t}, \hat{\lambda})\right)$. For convenience, we suppose that during the task, $\sum = diag(\tilde{\beta}_1, \ldots, \tilde{\beta}_{\mathrm{B}})$. Assumed to be an autonomous Gaussian prior characterization is the unidentified component $\hat{\lambda}$ of model (2). Thus, we get

$$\hat{\lambda}_{\mathbb{k}} \sim \widetilde{\mathrm{N}}(\tilde{\Psi}_{\mathbb{k}}, \tilde{\varphi}^2_{\mathbb{k}}), \quad \mathbb{k} = 1, \ldots, \tilde{\mathcal{M}}, \tag{151}$$

where $\tilde{\mathcal{M}}$ represents the quantity of unidentified factors. Additionally, we suppose that the error variance's inverse has a gamma distribution, as formerly stated, having a particular form

$$\tilde{\beta}^{-2}_{\zeta} \sim \Gamma\left(\frac{\mathrm{B}_0}{2}, \frac{\mathrm{B}_0 \mathcal{S}^2_0}{2}\right), \quad \zeta = 1, 2, \ldots, \mathrm{B}, \tag{152}$$

where B_0 and $\tilde{\beta}^2_{\mathcal{S}_0}$ represent the prior mean and precision of variance $\tilde{\beta}^2_{\zeta}$, respectively.

Applying a Gaussian deviation approach, the likelihood function $\mathrm{G}(\mathrm{G}|\hat{\lambda}, \sum)$ for $\tilde{\varsigma}$ autonomous and uniformly dispersed data using (150) is

$$\mathrm{G}(\mathrm{G}|\hat{\lambda}, \sum) = (2\pi)^{-\tilde{\varsigma}\mathrm{B}/2} |\sum|^{-\tilde{\varsigma}/2} \exp\left\{trace\left(\frac{-\sum^{-1} \mathrm{SS}(\hat{\delta})}{2}\right)\right\}, \tag{153}$$

where $\mathrm{SS}(\hat{\lambda}) = (\mathrm{G} - \mathbb{Q})^{\mathbf{T}}(\mathrm{G} - \mathbb{Q})$. For $\zeta = 1, 2, \ldots, \mathrm{B}$, the joint probability distribution of $\tilde{\beta}^2_{\zeta}$ yields

$$\begin{aligned}
&\mathrm{G}(\tilde{\beta}^2_1, \ldots, \tilde{\beta}^2_{\mathrm{B}}|\mathrm{G}, \hat{\lambda}) \propto \mathrm{G}(\mathrm{G}|\tilde{\beta}^2_1, \ldots, \tilde{\beta}^2_{\mathrm{B}}, \hat{\lambda})\mathrm{G}(\tilde{\beta}^2_1, \ldots, \tilde{\beta}^2_{\mathrm{B}}) \\
&= \mathrm{G}(\mathrm{G}|\tilde{\beta}^2_1, \ldots, \tilde{\beta}^2_{\mathrm{B}}, \hat{\lambda}) \prod_{\zeta=1}^{\mathrm{B}} \mathrm{G}(\tilde{\beta}^2_{\zeta}) \\
&= (2\pi)^{-\tilde{\varsigma}\mathrm{B}/2} |\sum|^{-\tilde{\varsigma}/2} \exp\left\{trace\left(\frac{-\sum^{-1} \mathrm{SS}(\hat{\delta})}{2}\right)\right\} \prod_{\zeta=1}^{\mathrm{B}} \frac{\left(\frac{\mathrm{B}_0 \mathcal{S}^2_0}{2}\right)^{\frac{\mathrm{B}_0}{2}}}{\Gamma\left(\frac{\mathrm{B}_0}{2}\right)} (\tilde{\beta}^2_{\zeta})^{-\frac{\mathrm{B}_0}{2}-1} \exp\left(\frac{-\mathrm{B}_0 \mathcal{S}^2_0}{2\tilde{\beta}^2_{\zeta}}\right) \\
&= (2\pi)^{-\tilde{\varsigma}\mathrm{B}/2} |\sum|^{-\tilde{\varsigma}/2} \exp\left\{trace\left(\frac{-\sum^{-1} \mathrm{SS}(\hat{\delta})}{2}\right)\right\} \prod_{\zeta=1}^{\mathrm{B}} \frac{\left(\frac{\mathrm{B}_0 \mathcal{S}^2_0}{2}\right)^{\frac{\mathrm{B}_0}{2}}}{\Gamma\left(\frac{\mathrm{B}_0}{2}\right)} |\sum|^{-\frac{\mathrm{B}_0}{2}-1} \exp\left(\frac{-\sum^{-1} \mathrm{B}_0 \mathcal{S}^2_0}{2}\right) \\
&\propto |\sum|^{-\frac{\tilde{\varsigma}}{2}-\frac{\mathrm{B}_0}{2}-1} \exp\left\{trace\left(\frac{-\sum^{-1} \mathrm{SS}(\hat{\delta})}{2}\right) + trac\left(\frac{-\sum^{-1} \mathrm{B}_0 \mathcal{S}^2_0}{2}\right)\right\}.
\end{aligned} \tag{154}$$

The subsequent expression allows for the computation of the prior sum of squares for the supplied components $\hat{\lambda}$ provided, we consider independent Gaussian prior characterization for them:

$$\mathrm{SS}_{prior}(\hat{\lambda}) = \sum_{\mathbb{k}=1}^{\widetilde{\mathcal{M}}} \left(\frac{\hat{\lambda}_{\mathbb{k}} - \tilde{\Psi}_{\mathbb{k}}}{\tilde{\varphi}_{\mathbb{k}}}\right)^2. \tag{155}$$

It is then possible to describe the posterior distribution of factors $\hat{\lambda}$ in the following manner assuming a specific quantity of dispersion $\tilde{\beta}_{\zeta}$, $(\zeta = 1, 2, \ldots, \mathrm{B})$:

$$
\begin{aligned}
&\mathrm{G}(\hat{\lambda}|\mathrm{G},\textstyle\sum) \propto \mathrm{G}(\mathrm{G}|\hat{\lambda},\textstyle\sum)\mathrm{G}(\hat{\lambda}_1)\mathrm{G}(\hat{\lambda}_2)\ldots\mathrm{G}(\hat{\lambda}_{\widetilde{\mathcal{M}}})\\
&= \mathrm{G}(\mathrm{G}|\hat{\lambda},\textstyle\sum)\prod_{\zeta=1}^{\mathrm{B}}\mathrm{G}(\hat{\lambda}_\zeta)\\
&= (2\pi)^{-\tilde{\zeta}\mathrm{B}/2}|\textstyle\sum|^{-\tilde{\zeta}/2}\exp\left\{trace\left(\frac{-\sum^{-1}\mathrm{SS}(\hat{\delta})}{2}\right)\right\}\prod_{\mathbb{k}=1}^{\widetilde{\mathcal{M}}}\frac{1}{\sqrt{2\pi}\tilde{\varphi}_{\mathbb{k}}}\exp\left\{-\frac{1}{2}\left(\frac{\hat{\lambda}_{\mathbb{k}}-\tilde{\Psi}_{\mathbb{k}}}{\tilde{\varphi}_{\mathbb{k}}}\right)^2\right\}\\
&= (2\pi)^{-\tilde{\zeta}\mathrm{B}/2}|\textstyle\sum|^{-\tilde{\zeta}/2}\exp\left\{trace\left(\frac{-\sum^{-1}\mathrm{SS}(\hat{\delta})}{2}\right)\right\}\prod_{\mathbb{k}=1}^{\widetilde{\mathcal{M}}}\left(\frac{1}{\sqrt{2\pi}}\right)^{\widetilde{\mathcal{M}}}\frac{1}{\tilde{\varphi}_1\tilde{\varphi}_2\ldots\tilde{\varphi}_{\widetilde{\mathcal{M}}}}\exp\left\{-\frac{1}{2}\sum_{\mathbb{k}=1}^{\widetilde{\mathcal{M}}}\left(\frac{\hat{\lambda}_{\mathbb{k}}-\tilde{\Psi}_{\mathbb{k}}}{\tilde{\varphi}_{\mathbb{k}}}\right)^2\right\}\\
&\propto \exp\left\{-\frac{1}{2}\left(trace\left(\sum^{-1}\mathrm{SS}(\hat{\lambda})\right)+\mathrm{SS}_{prior}(\hat{\lambda})\right)\right\}.
\end{aligned}
\tag{156}
$$

The following is a possible expression for the probabilistic ratio required in the Metropolis–Hastings acceptability likelihood:

$$
\frac{\mathrm{G}(\hat{\lambda}_1|\mathrm{G},\sum)}{\mathrm{G}(\hat{\lambda}^2|\mathrm{G},\sum)} = \exp\left\{-\frac{1}{2}\left(\sum^{-1}\mathrm{SS}(\hat{\lambda}^2)-\sum^{-1}\mathrm{SS}(\hat{\lambda}_1)\right)+\frac{1}{2}\left(\mathrm{SS}_{prior}(\hat{\lambda}^2)-\mathrm{SS}_{prior}(\hat{\lambda}_1)\right)\right\}, \tag{157}
$$

where the outcome of creating an additional characteristic set is represented by $\hat{\lambda}^2$ and the quantity of the existing characteristic set is represented by $\hat{\lambda}_1$. Consequently, there is a possibility that the recently introduced unidentified factor value $\hat{\lambda}^2$ will ultimately be approved as

$$
\min\left\{1, \frac{\mathrm{G}(\hat{\lambda}_1|\mathrm{G},\sum)}{\mathrm{I}(\hat{\lambda}^2|\mathrm{G},\sum)}\right\}. \tag{158}
$$

Unidentified characteristics' prior understanding is provided by

$$
\begin{aligned}
&\varpi_{3\ell}\in[0.05,0.95],\quad \varpi_{4\ell}\in[5.5,9.5],\quad \varpi_{5\ell}\in[0.45,1.05],\quad \varpi_{6\ell}\in[0.12,0.68],\quad 1\le\ell\le 12,\\
&\varpi_{7\ell}\in[0.25,0.65],\quad \varpi_{8\ell}\in[0.9,2.2],\quad \varpi_{9\ell}\in[0.015,0.12],\quad \varpi_{10\ell}\in[1.4,2.1],\quad 1\le\ell\le 12,\\
&\delta_{3\ell}\in[1.8,5.2],\quad \mathrm{I}_\ell(0)\in[1\times10^5,2.5\times10^4],\quad 1\le\ell\le 2,\quad \mathrm{V}_\ell(0)\in[5\times10^5,1.1\times10^3],\\
&\mathrm{B}_\ell(0)\in[3.5\times10^8,2.8\times10^7],\quad \mathrm{Z}_\ell(0)\in[3.8\times10^8,2.9\times10^7],\quad 1\le\ell\le 12\\
&\tilde{\beta}_\ell\in[0.0001,0.0002],\quad \hat{\lambda}_\ell\in[0.005,0.010],\quad 1\le\ell\le 3,\\
&\tilde{\beta}_\ell\in[0.00018,0.00028],\quad \hat{\lambda}_\ell\in[0.005,0.007],\quad 4\le\ell\le 9,\\
&\tilde{\beta}_\ell\in[0.00020,0.00193],\quad \hat{\lambda}_\ell\in[0.005,0.016],\quad 9\le\ell\le 11,\\
&\tilde{\beta}_\ell\in[0.00020,0.00365],\quad \hat{\lambda}_\ell\in[0.005,0.025],\quad \ell=12,
\end{aligned}
\tag{159}
$$

and a multivariate normal distribution describes the suggested concentration.

Based on epidemiological field data collected in Florida, USA, and as shown in Fig. 5, we fitted the CHIKV model (2)—which incorporates latency and symptomatic stages of infection—using population-level incidence data stratified by age and infection status. This dataset represents the monthly density of infected individuals (per 100,000 population) across structured compartments, including exposed (latently infected), symptomatic, and immune factor cases. The model was calibrated using the MCMC approach, with the final 10% of 50,000 posterior samples employed for statistical inference and parameter estimation.

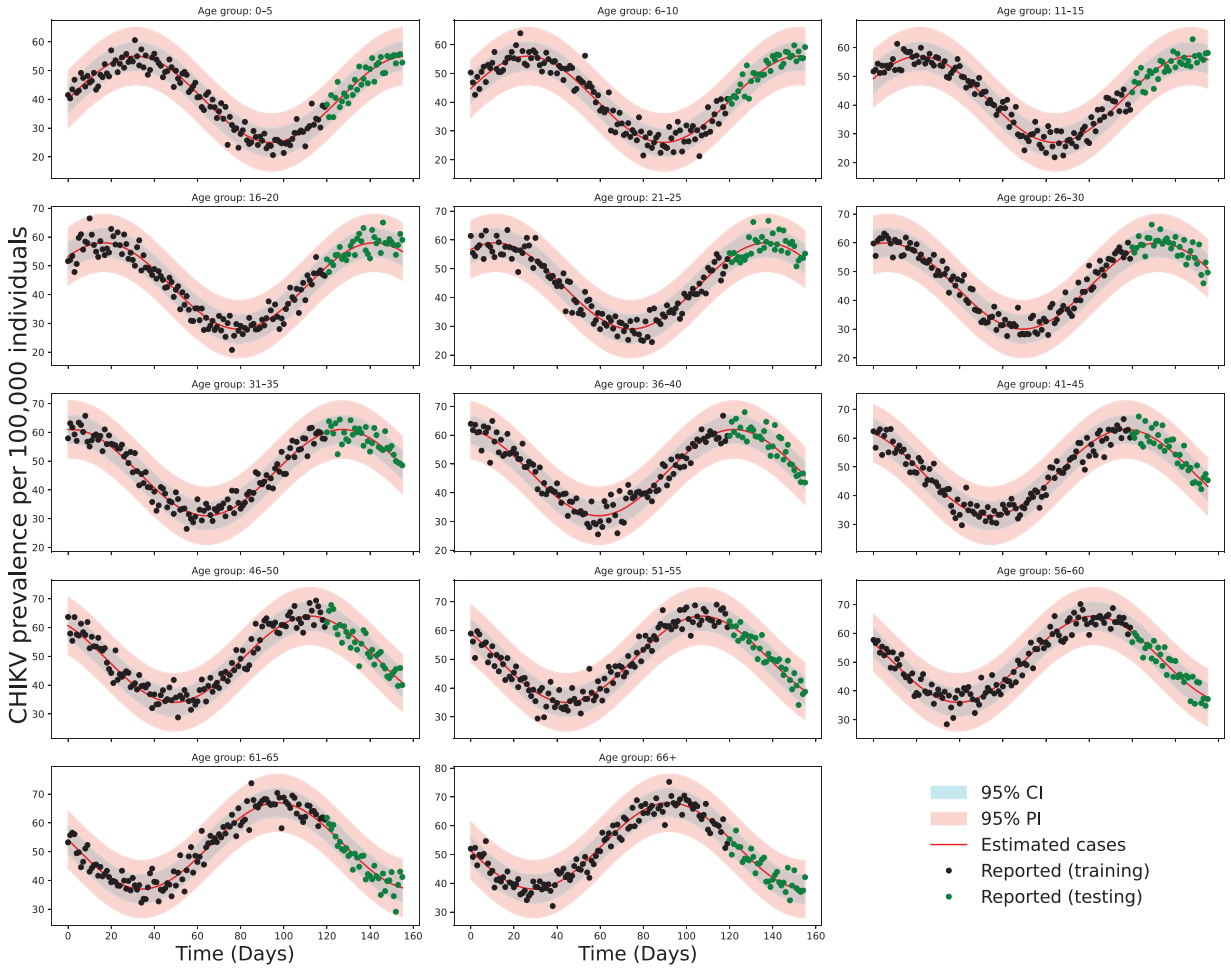

Figure 5: The monthly CHIKV incidence per 100,000 people for various age-factors from April 2005 to December 2017 is shown in the fitting findings. When model (2) is fitted to the measured time series, the simulated trajectories are shown by the solid red lines. The first 120 months of training data are represented by black circles, while the latter 36 months of testing data are represented by green circles. Whereas the light blue shaded area displays the 95% prediction interval (P-I), the magenta shaded area indicates the 95% C-I. A random 10% selection of the previous 50,000 posterior samples was used to generate the final distribution after parameters were inferred using MCMC

Fig. 5 presents the fitted results across age-stratified population classes, showing close agreement between the observed incidence data and the simulated infected population densities. Surface plots for key parameters and ICs of model (2) were generated through MCMC sampling and are displayed in Fig. 6. The constructed model framework demonstrates robust predictive capabilities under the influence of viral transmission dynamics, including latent progression and symptom development. The ratio of our sample size to the free parameters of the model is 28.8:1 > 10:1 [67].

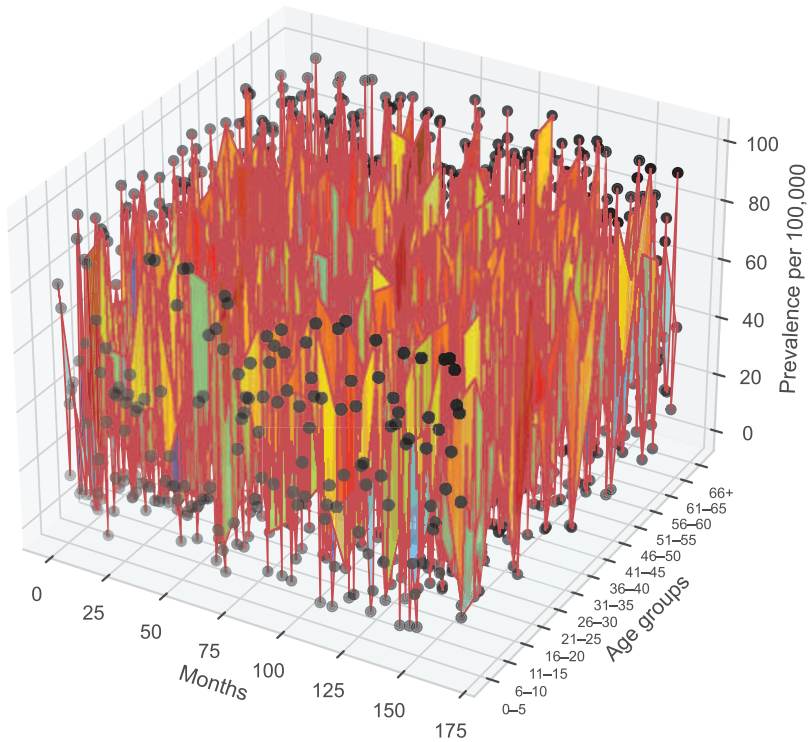

Figure 6: Three-dimensional plot of the predicted outcomes of monthly CHIKV transmission per 100,000 people from April 2005 to December 2017 for various demographic variations. The surface represents the simulated CHIKV prevalence generated from model (2), while black circles correspond to the reported data for each age group over time. CHIKV commonly presents with symptoms such as high fever, severe joint pain, rash, headache, and fatigue, which may vary in severity across different age groups

5.1.3 Contact Matrix for CHIKV Model

Let $\bar{f}_2$ denote the initial contact matrix, shown in Table 4, containing components $\bar{f}_{2\iota\zeta}$ $(\iota, \zeta = 1, 2, \ldots, c)$, where c constitutes the demographic categories in the initial matrix, and ι and ζ index the rows and columns, respectively. An adjusted contact matrix $\mathbf{S} = (Z_{\kappa\ell})$, with $\kappa, \ell = 1, 2, \ldots, r$, is constructed, where r represents the overall demographic categories within simplified framework. Each extended demographic group $\bar{v}$ aggregates a subset of the original groups, namely from $\iota = l_1(\kappa)$ to $\zeta(\kappa)$. The frequency of contact between individuals in age categories ι and ζ is then provided by:

$$\bar{V}_{\iota\ell} = \sum_{\zeta=l_1(\ell)}^{\bar{v}(\ell)} \bar{f}_{2\iota\zeta}. \tag{160}$$

Using Table 4 as a reference, let $\mathbb{N}_\iota$ denote the population size within age group ι. Based on this information, we calculate the interaction rate between age categories κ and ℓ by computing the population-weighted mean of each component, denoted by $\bar{V}$. To address interactions between different generations (i.e., off-diagonal components), we determine the overall interactions from κ to ℓ and from ℓ to κ. Consequently, the total number of interactions between categories κ and ℓ can be written as:

$$\bar{L}_{\kappa\ell} = \sum_{\iota=l_1(\kappa)}^{\bar{v}(\kappa)} \mathbb{N}_\iota \bar{V}_{\iota\ell}, \quad \bar{L}_{\ell\kappa} = \sum_{\iota=l_1(\ell)}^{\bar{v}(\ell)} \mathbb{N}_\iota \bar{\mathbf{W}}_{\iota\kappa} \tag{161}$$

To ensure symmetry between $\bar{\mathrm{L}}_{\kappa\ell}$ and $\bar{\mathrm{L}}_{\ell\kappa}$, we take their average, that is,

$$\mathbf{W}_{\kappa\ell} = \mathbf{W}_{\ell\kappa} = \frac{\bar{\mathrm{L}}_{\kappa\ell} + \bar{\mathrm{L}}_{\ell\kappa}}{2}. \tag{162}$$

In general, the updated contact matrix constituent can be depicted in the form of:

$$\mathrm{s}_{\kappa\ell} = \frac{\mathbf{W}_{\kappa\ell}}{\sum_{\iota=l_1(\kappa)}^{\bar{\mathrm{v}}(\kappa)} \mathbb{N}_\iota}, \quad \mathrm{s}_{\ell\kappa} = \frac{\mathbf{W}_{\ell\kappa}}{\sum_{\iota=l_1(\ell)}^{\bar{\mathrm{v}}(\ell)} \mathbb{N}_\iota}. \tag{163}$$

In this case, $\mathrm{s}_{\kappa\ell}$ represents the monthly interaction rate between a person in the age category κ and others in age grouping ℓ. The diagonal's overall interaction rate is represented by:

$$\mathrm{s}_{\kappa\kappa} = \frac{\sum_{\iota=l_1(\kappa)}^{\bar{\mathrm{v}}(\kappa)} \mathbb{N}_\iota \bar{\mathrm{V}}_{\iota\ell}}{\sum_{\iota=l_1(\kappa)}^{\bar{\mathrm{v}}(\kappa)} \mathbb{N}_\iota}. \tag{164}$$

The contact matrix is essential for studying infections such as CHIKV in epidemic modeling, as it quantifies interactions among different age groups. It captures the frequency of interaction involving susceptible people (columns) and infectious people (rows) across various age categories. Understanding these interactions aids in forecasting disease transmission processes, which are influenced by factors such as community behavior and transportation patterns. The matrix, which can be constructed from demographic data, illustrates how different age groups connect—for example, children interacting more frequently with their families (see Fig. 7). It serves a vital function in designing targeted interventions to curb disease spread, like immunization drives or social distancing strategies. Overall, the contact matrix offers vital insights into epidemic dynamics and helps inform effective public health strategies.

6 Results and Discussion

To analyze the stochastic framework and validate the parameterized model, we conduct numerical simulations of our model (4) in the following section. The objective is to evaluate the effectiveness of coordinated CHIKV prevention and control strategies.

6.1 Sensitivity Analysis

In what follows, the basic reproduction number, $\mathbb{R}_{0\mathrm{I}}$, for the CHIKV model (4) is determined based on the predicted feature estimates and is found to be approximately 1.4978 (95% C-I: 1.4968–1.5823), as illustrated in Fig. 8a,b, respectively. The framework demonstrates consistent robustness since $\mathbb{R}_{0\mathrm{I}} > 1$, indicating that CHIKV will not go extinct in future generations in the absence of additional control measures. This persistent nature suggests that, even with the current control mechanisms, the infection has the potential to continue spreading within the community.

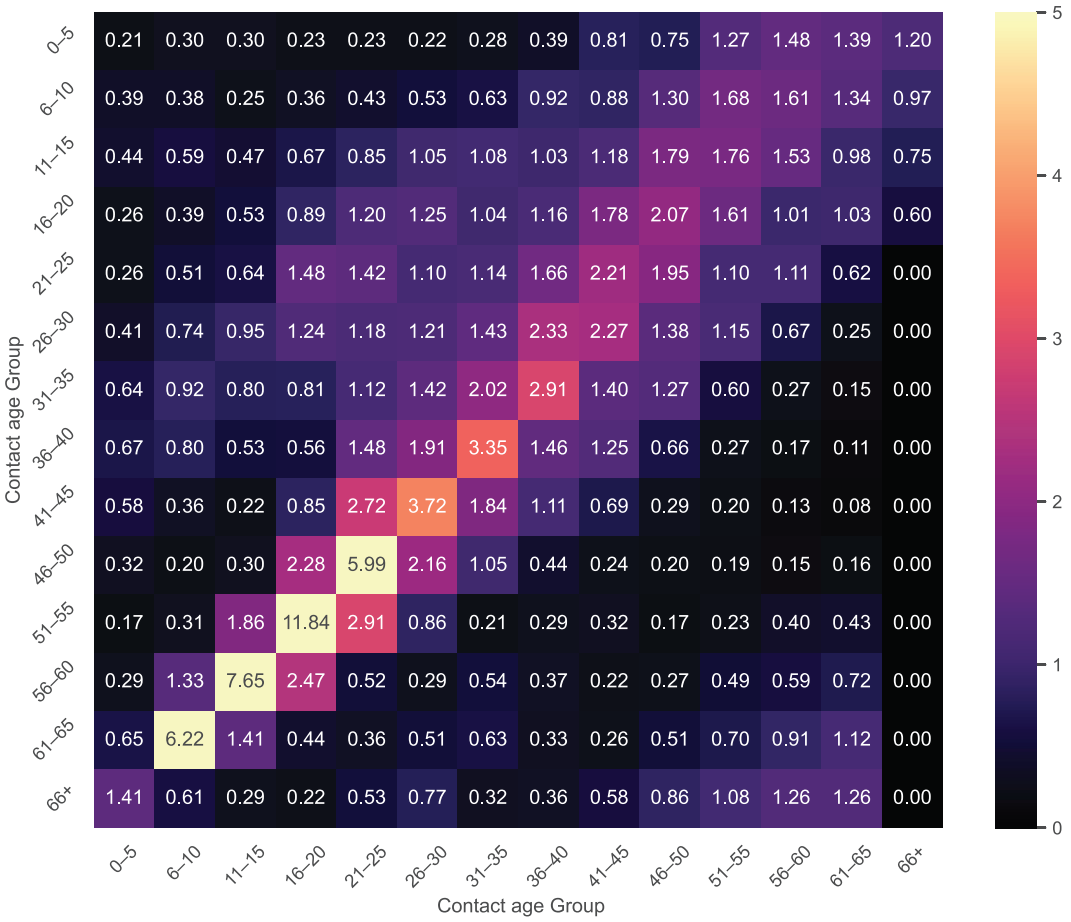

Figure 7: The contact matrix in demographic-structured outbreak models for the propagation of the CHIKV model (2) illustrates how different generations collaborate to forecast transmission and guide focused preventative measures

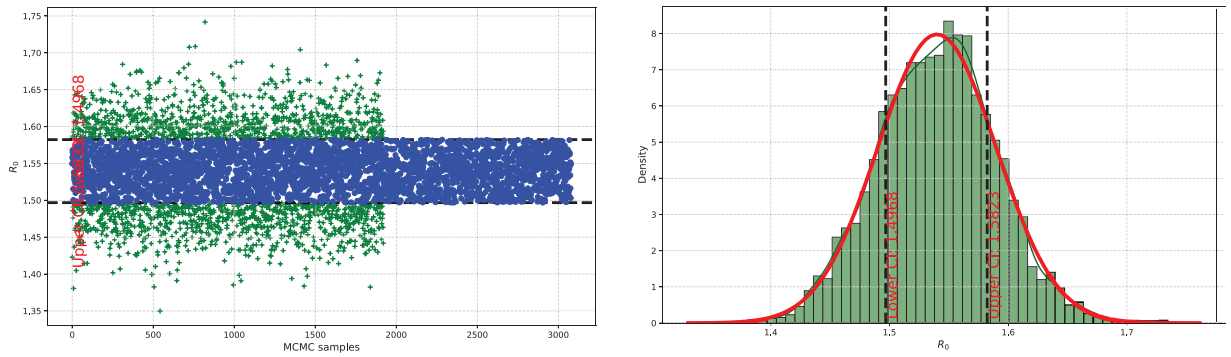

(a) **(b)**

Figure 8: Estimation and distribution of the threshold parameter $\mathbb{R}_{0I}$ for the demographic variability CHIKV system. (**a**) displays the scatter of $\mathbb{R}_{0I}$ values generated from posterior predictive samples. Blue dots represent values within the 95% C-I, red pluses represent values outside the C-I, and horizontal red dashed lines mark the C-I bounds at (1.4968, 1.5823). The estimated mean of $\mathbb{R}_{0I}$ is approximately 1.4978. (**b**) illustrates the frequency distribution of $\mathbb{R}_{0I}$, with a red curve representing its fitted probability density function. Since $\mathbb{R}_{0I} > 1$, the model suggests a sustained potential for CHIKV transmission in the absence of additional interventions. These results highlight the robustness of the modeling framework and support further global sensitivity analysis to identify influential parameters across age groups

Subsequently, we assess the broad dispersion and comparative responsiveness of the parameters incorporated in the CHIKV framework using Latin Hypercube Sampling (LHS) and Partial Rank Correlation Coefficients (PRCCs) (McKay et al. [68]). The aim is to identify the key factors influencing the progression of CHIKV infection. The considered criteria include: $\tilde{\beta}_\ell \in [0.0001, 0.0002]$, $\hat{\lambda}_\ell \in [0.005, 0.010]$,$1 \le \ell \le 3$,$\tilde{\beta}_\ell \in [0.00018, 0.00028]$, $\hat{\lambda}_\ell \in [0.005, 0.007]$, $4 \le \ell \le 9$, $\tilde{\beta}_\ell \in [0.00020, 0.00193]$, $\hat{\lambda}_\ell \in [0.005, 0.016]$, $9 \le \ell \le 11$, $\tilde{\beta}_\ell \in [0.00020, 0.00365]$, $\hat{\lambda}_\ell \in [0.005, 0.025]$, $\ell = 12$. The output field represents the yearly number of newly identified CHIKV cases, and a value for ϖ_ℓ is provided for $3 \le \ell \le 14$. It is assumed that all supplied parameters follow a normal distribution. Table 5 lists the dispersion values for $\tilde{\beta}_\ell$ and $\hat{\lambda}_\ell$. The coefficients of dispersion for ϖ_ℓ are set to 0.2 and 0.02, respectively.

Table 5: Estimated values of unknown parameters in CHIKV model (4)

Parameter	Mean	Std	95% C-I	Geweke
$\hat{\varpi}_1$	3.8567×10^{-4}	4.9342×10^{-5}	$[3.0206 \times 10^{-4}, 4.9682 \times 10^{-4}]$	0.9410
$\hat{\varpi}_2$	9.8420×10^{-6}	7.9210×10^{-6}	$[2.7276 \times 10^{-7}, 3.0271 \times 10^{-5}]$	0.6401
$\hat{\varpi}_3$	1.6482×10^{-4}	6.9981×10^{-5}	$[2.2534 \times 10^{-5}, 2.9514 \times 10^{-4}]$	0.3302
$\hat{\varpi}_4$	0.005212	7.4021×10^{-5}	$[0.005085, 0.005394]$	0.9875
$\hat{\varpi}_5$	0.01029	7.5842×10^{-5}	$[0.01021, 0.01052]$	0.9985
$\hat{\varpi}_6$	0.007482	1.3271×10^{-4}	$[0.007296, 0.007816]$	0.9730
$\hat{\varpi}_7$	0.006553	1.8124×10^{-4}	$[0.006220, 0.006989]$	0.9447
$\hat{\varpi}_8$	0.007612	2.3921×10^{-4}	$[0.007089, 0.008085]$	0.9618
$\hat{\varpi}_9$	0.008445	1.3210×10^{-4}	$[0.008196, 0.008726]$	0.9690
$\hat{\varpi}_{10}$	0.002139	1.1327×10^{-4}	$[0.001918, 0.002409]$	0.9621
$\hat{\varpi}_{11}$	0.003246	1.6032×10^{-4}	$[0.002974, 0.003549]$	0.9749
$\hat{\varpi}_{12}$	0.004698	1.3425×10^{-4}	$[0.004456, 0.004970]$	0.9886
$\hat{\varpi}_{13}$	0.006085	1.7759×10^{-4}	$[0.005757, 0.006455]$	0.9602
$\hat{\varpi}_{14}$	0.006857	2.1022×10^{-4}	$[0.005444, 0.006270]$	0.9867
$\bar{\varpi}_1$	0.9814	0.01167	[0.9579, 0.9990]	0.9989
$\bar{\varpi}_2$	0.9798	0.01522	[0.9417, 0.9994]	0.9947
$\bar{\varpi}_3$	0.3322	0.06411	[0.2188, 0.4400]	0.7406
$\bar{\varpi}_4$	0.5984	0.03301	[0.5522, 0.6703]	0.9358
$\bar{\varpi}_5$	0.2840	0.01501	[0.2539, 0.3096]	0.9941
$\bar{\varpi}_6$	0.5072	0.03521	[0.4431, 0.5771]	0.8495
$\bar{\varpi}_7$	0.3459	0.03019	[0.2848, 0.3982]	0.8510
$\bar{\varpi}_8$	0.2466	0.02877	[0.1910, 0.2997]	0.8334
$\bar{\varpi}_9$	0.5701	0.03487	[0.5203, 0.6286]	0.9461
$\bar{\varpi}_{10}$	0.3051	0.02780	[0.2454, 0.3606]	0.8541
$\bar{\varpi}_{11}$	0.3476	0.04623	[0.2591, 0.4362]	0.8493
$\bar{\varpi}_{12}$	0.4512	0.04110	[0.3783, 0.5281]	0.9058
$\bar{\varpi}_{13}$	0.3944	0.03312	[0.3361, 0.4591]	0.8930
$\bar{\varpi}_{14}$	0.4882	0.03104	[0.4247, 0.5465]	0.9163
β_ℓ ($\ell \in [1, 3]$)	1.0223×10^{-5}	1.4801×10^{-6}	$[8.4012 \times 10^{-6}, 1.4080 \times 10^{-5}]$	0.6212
β_ℓ ($\ell \in [4, 11]$)	1.7465×10^{-5}	2.2323×10^{-6}	$[1.5104 \times 10^{-5}, 2.2824 \times 10^{-5}]$	0.8085
β_ℓ ($\ell \in [12, 13]$)	9.6358×10^{-5}	3.4132×10^{-5}	$[2.9568 \times 10^{-5}, 1.5601 \times 10^{-4}]$	0.5067
β_ℓ ($\ell = 14$)	3.5632×10^{-5}	1.8690×10^{-5}	$[1.7114 \times 10^{-5}, 8.4069 \times 10^{-5}]$	0.9145

(Continued)

Table 5 (continued)

Parameter	Mean	Std	95% C-I	Geweke
λ_ℓ ($\ell \in [1,3]$)	6.8325×10^{-4}	2.8402×10^{-5}	$[6.2436 \times 10^{-4}, 7.3573 \times 10^{-4}]$	0.9241
λ_ℓ ($\ell \in [4,11]$)	5.7568×10^{-4}	8.2364×10^{-6}	$[5.5141 \times 10^{-4}, 5.8311 \times 10^{-4}]$	0.9904

Table 5 presents the sensitivity factors $\varpi_{1\ell}$, $\varpi_{4\ell}$, $\varpi_{5\ell}$, $\varpi_{8\ell}$ and $\varpi_{10\ell}$ in relation to new cases of CHIKV in 2017, specifically using an age-structured model. The results indicate the recurrence rate for recuperated people aged 16 and above (i.e., λ_ℓ for $\ell \in [4,14]$) shows a strong positive correlation with the total number of new cases. In contrast, the re-occurrence rate for previously treated people younger than 16 (that is, λ_ℓ for $\ell \in [1,3]$) does not exhibit a significant correlation including more incidence, highlighting the importance of preventing relapse in persons above 16 years old.

Further analysis reveals that the risk of reinfection in people harboring latent virus (i.e., λ_ℓ for $\ell \in [4,14]$) aged beyond 16 years is more significant compared to those under 16 years (i.e., λ_ℓ for $\ell \in [1,3]$). Additionally, the CHIKV diagnosis rate (i.e., ρ_ℓ for $\ell \in [1,14]$) is negatively and strongly associated for new incidence, suggesting that improving therapeutic strategies to reduce diagnostic delays can substantially lower the incidence of CHIKV.

Lastly, β_ℓ is the rate of transmission from S to V due to CHIVK (i.e., β_ℓ for $\ell \in [4,14]$) aged over 16 years is significant unfavorable relationship between the aggregate amount of instances rising. Notably, the highly negative association was observed between the overall of reported instances and the regular immunization levels of at-risk people above 66 years old, compared to those aged 20 to 26, underlining the effectiveness of targeted vaccination efforts.

6.2 Extinction of Model

To comprehensively examine the critical factors contributing to the extinction of the CHIKV (4) in human populations—as well as those facilitating its long-term persistence—we refer to the threshold condition $\mathbb{R}_{0I} < 1$. This condition represents a biologically significant tipping point, below which the basic reproduction number indicates a sustained decline in infection incidence over time. Theorem 3 was specifically proven under this constraint, providing a rigorous theoretical foundation for the guaranteed eradication of CHIKV with probability one, assuming essential biological and intervention-based criteria are met.

In this context, virus extinction is primarily driven by stochastic perturbations, natural recovery processes, depletion of infectious reservoirs, increased vector mortality, and the implementation of targeted public health interventions. These include vector control strategies, personal prophylactic measures, and improved environmental hygiene. Even in scenarios with an initially high infection burden, these mechanisms act synergistically to disrupt sustained transmission, ultimately leading to the disappearance of the virus from the host population.

To quantitatively analyze and visualize these findings, we developed a stochastic modeling framework based on Example 1, incorporating random fluctuations to account for real-world uncertainty. Fig. 9 presents numerical simulations illustrating the model's dynamic progression toward the disease-free equilibrium, consistent with the behavior predicted by the corresponding deterministic system. The resulting stochastic trajectories visibly converge toward the extinction boundary, reinforcing both the biological plausibility of CHIKV eradication under coordinated control efforts and the predictive validity of the proposed framework.

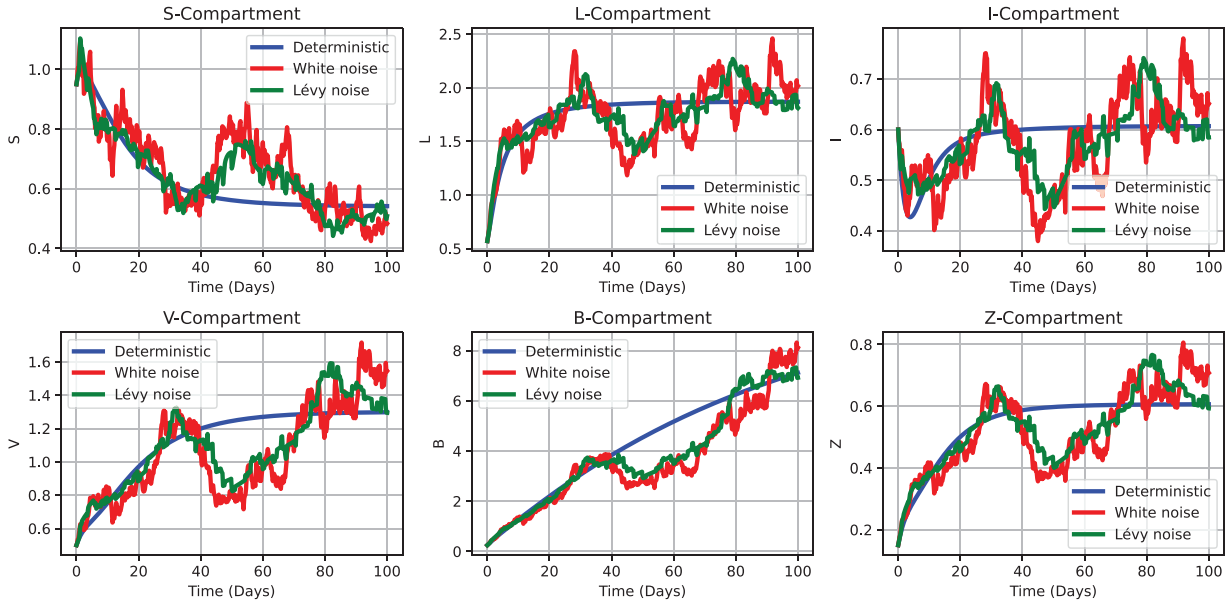

Figure 9: Comparative simulation outcomes of the CHIKV model under deterministic (2), white noise (3), and Lévy noise (4) influences, using the initial parameter values as Test 1 defined in Section 5.1.2. Each subplot depicts the temporal evolution of a distinct compartment—$(S(0), L(0), I(0), V(0), B(0), Z(0))$ = (0.95, 0.57, 0.6, 0.5, 0.25, 0.15) demonstrating convergence to the disease-free equilibrium. This behavior aligns with the theoretical prediction given by Theorem 3, as the basic reproduction number $\mathbb{R}_{0I} = 0.178 < 1$, indicating stochastic extinction and long-term eradication of the infection

Example 1: *In this scenario, the initial parameter values used for Tests 1, 2, and 3 are presented in Section 5.1.2. These values specify the initial conditions for the susceptible, latent, infectious, vector, and two additional compartments, respectively, reflecting a realistic epidemiological setting. Based on these outcomes, we calculate the appropriate threshold factor* $\mathbb{R}_{0I} = 0.178$. *This value satisfies the crucial criterion outlined in Theorem 3, which states that a virus cannot persist in the community for an extended period if* $\mathbb{R}_{0I} < 1$. *Since* $\mathbb{R}_{0I}$ *is smaller than unity, the condition is met. According to the scientific principles of stochastic extinction, this implies that the infection will almost surely disappear over time. Consequently, under this restriction regime, the requirements for CHIKV eradication are fulfilled. As a result, the model's solution pathways asymptotically converge to the disease-free equilibrium. The following formulas describe how each individual component of the framework, representing different demographic categories, converges in probability to its corresponding disease-free state and exhibits asymptotic disintegration behavior:*

$$\lim_{t\to\infty} \sup \frac{\log L(t)}{t} \leq 0, \quad \lim_{t\to\infty} \sup \frac{\log I(t)}{t} \leq 0.$$

Fig. 9 provides statistical evidence for the gradual eradication of the virus in the general population, as confirmed by these changes. Identical behavioral modeling supporting the extinction outcomes, which are considered reliable, is shown in Fig. 10. This situation exemplifies stochastic extinction, where every solution pathway ultimately leads to the complete elimination of the virus. Notably, this convergence trend remains robust under both stochastic and deterministic influences. Furthermore, the impact of stochastic perturbations on disease progression is highlighted by the faster extinction rates observed in trajectories driven by Poisson random measure noise compared to those influenced by normal jump processes (see Fig. 11).

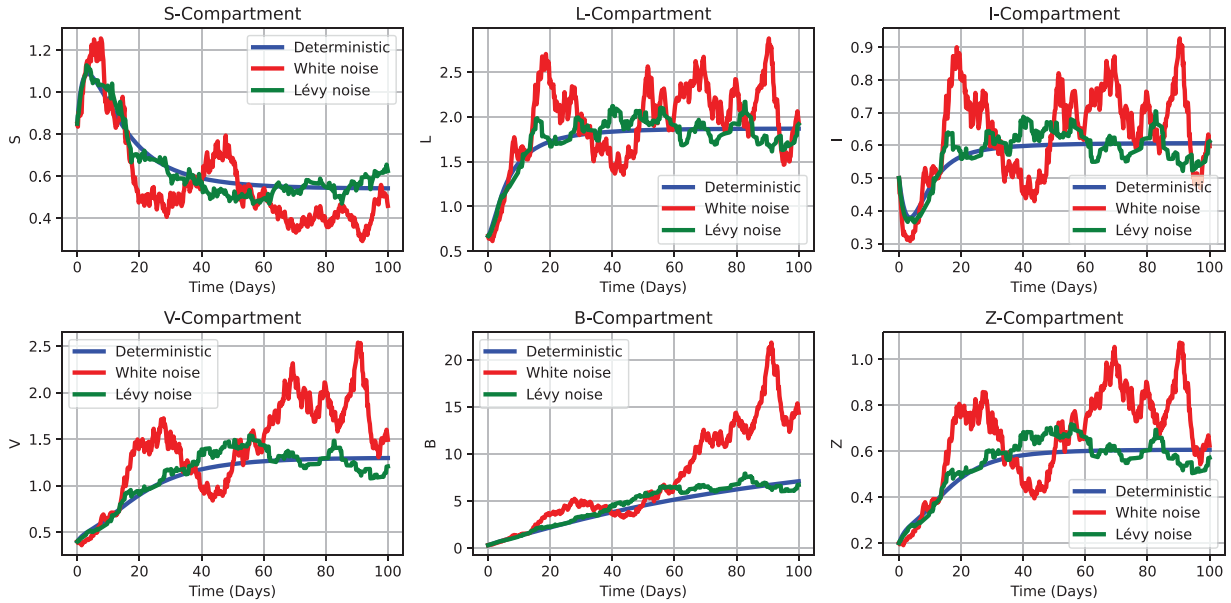

Figure 10: Comparative simulation outcomes of the CHIKV model under deterministic (2), white noise (3), and Lévy noise (4) influences, using the initial parameter values as Test 2 defined in Section 5.1.2. Each subplot depicts the temporal evolution of a distinct compartment—$(S(0), L(0), I(0), V(0), B(0), Z(0))$ = (0.85, 0.67, 0.5, 0.4, 0.3, 0.2) demonstrating convergence to the disease-free equilibrium. This behavior aligns with the theoretical prediction given by Theorem 3, as the basic reproduction number $\mathbb{R}_{0I} = 0.256 < 1$, indicating stochastic extinction and long-term eradication of the infection

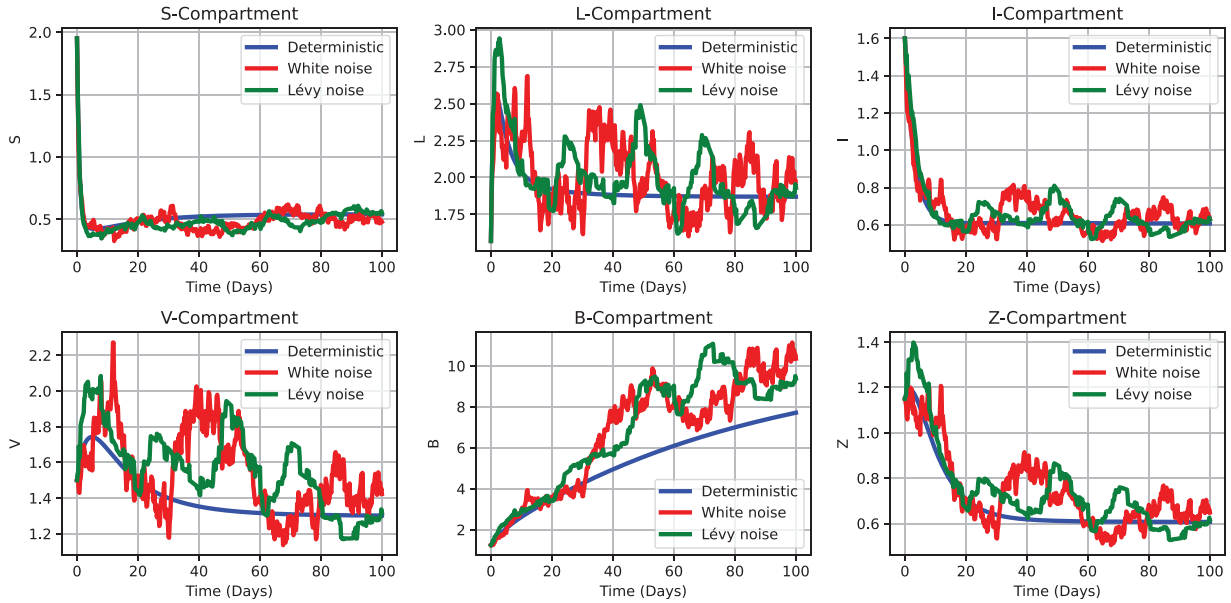

Figure 11: Comparative simulation outcomes of the CHIKV model under deterministic (2), white noise (3), and Lévy noise (4) influences, using the initial parameter values as Test 3 defined in Section 5.1.2. Each subplot depicts the temporal evolution of a distinct compartment—$(S(0), L(0), I(0), V(0), B(0), Z(0))$ = (1.95, 1.57, 1.6, 1.5, 1.25, 1.15) demonstrating convergence to the disease-free equilibrium. This behavior aligns with the theoretical prediction given by Theorem 3, as the basic reproduction number $\mathbb{R}_{0I} = 0.732 < 1$, indicating stochastic extinction and long-term eradication of the infection

6.3 Mean Persistence Based Simulation

Focusing on persistence, this investigation evaluates the robustness of a hypothesis concerning CHIKV patterns within a population. Theorem 4 provides the theoretical foundation for understanding the virus's transmission dynamics, and the results must satisfy its requirements. Section 5.1.2 in Test 2 addresses the case where $\mathbb{R}_{0I} > 1$. Outcomes from deterministic, stochastic, and Lévy-based models are presented in Fig. 12, incorporating elements such as transmission unpredictability and Poisson random measures to demonstrate how stochastic factors influence disease prevalence. These methods account for random processes like migration, birth-death cycles, and the spread of infection. The analysis of epidemic duration, regional impacts, and the effectiveness of control interventions is enhanced through the concept of mean persistence. The deterministic perspective offers insights into population-level consequences and pathogen decline. This approach is crucial for identifying high-risk areas and facilitating targeted interventions such as travel restrictions and the strategic allocation of health resources.

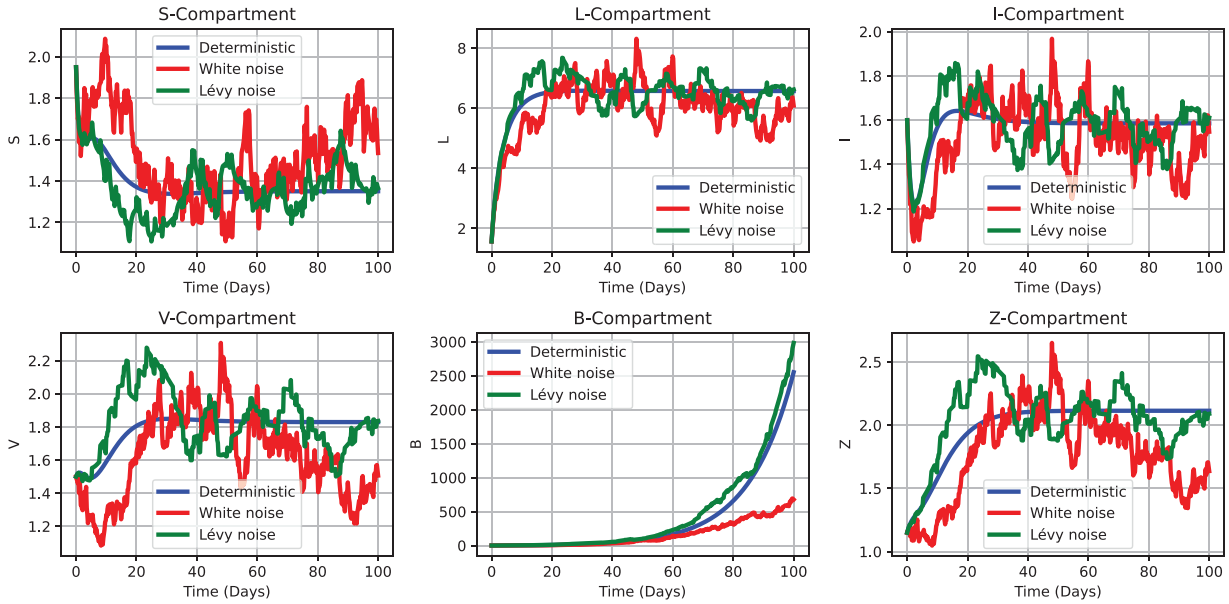

Figure 12: Comparative dynamics of CHIKV transmission under deterministic (2), white noise (3), and Lévy noise (4) frameworks for the case $\mathbb{R}_{0L} > 1$, as discussed in Section 5.1.2. These simulations, corresponding to Theorem 4, explore the persistence and variability of infection patterns in a population. Stochastic influences such as migration, demographic fluctuations, and transmission irregularities are incorporated to reflect real-world uncertainties. The figure highlights how random perturbations affect epidemic persistence, duration, and control strategies, aiding in the identification of high-risk zones and optimization of intervention planning

6.4 Impact of Actively Infected Cells in Concentration (φ)

The concentration of actively infected cells, represented by φ, is pivotal in shaping the dynamics of CHIKV transmission, influencing the system's stability and the infection's spread. Simulations show that reducing φ accelerates CHIKV eradication, emphasizing its importance in disease control. Nonlinear stochastic disturbances, such as Poisson random measures, capture the unpredictable spikes in infection rates caused by external factors like school closures or outbreaks in high-risk settings. These disturbances demonstrate that controlling CHIKV requires more than monitoring the basic reproduction number. CHIKV is regulated by adaptive immunity, and the effectiveness of monoclonal antibody treatments varies (see Fig. 13). The presence of these disturbances highlights the need to consider external, nonlinear

factors in outbreak control. Ultimately, φ determines the intensity and spread of the infection, with higher concentrations leading to more widespread outbreaks. Lowering φ facilitates quicker containment. Understanding φ and incorporating stochastic variability into predictive models is key to effectively managing CHIKV transmission.

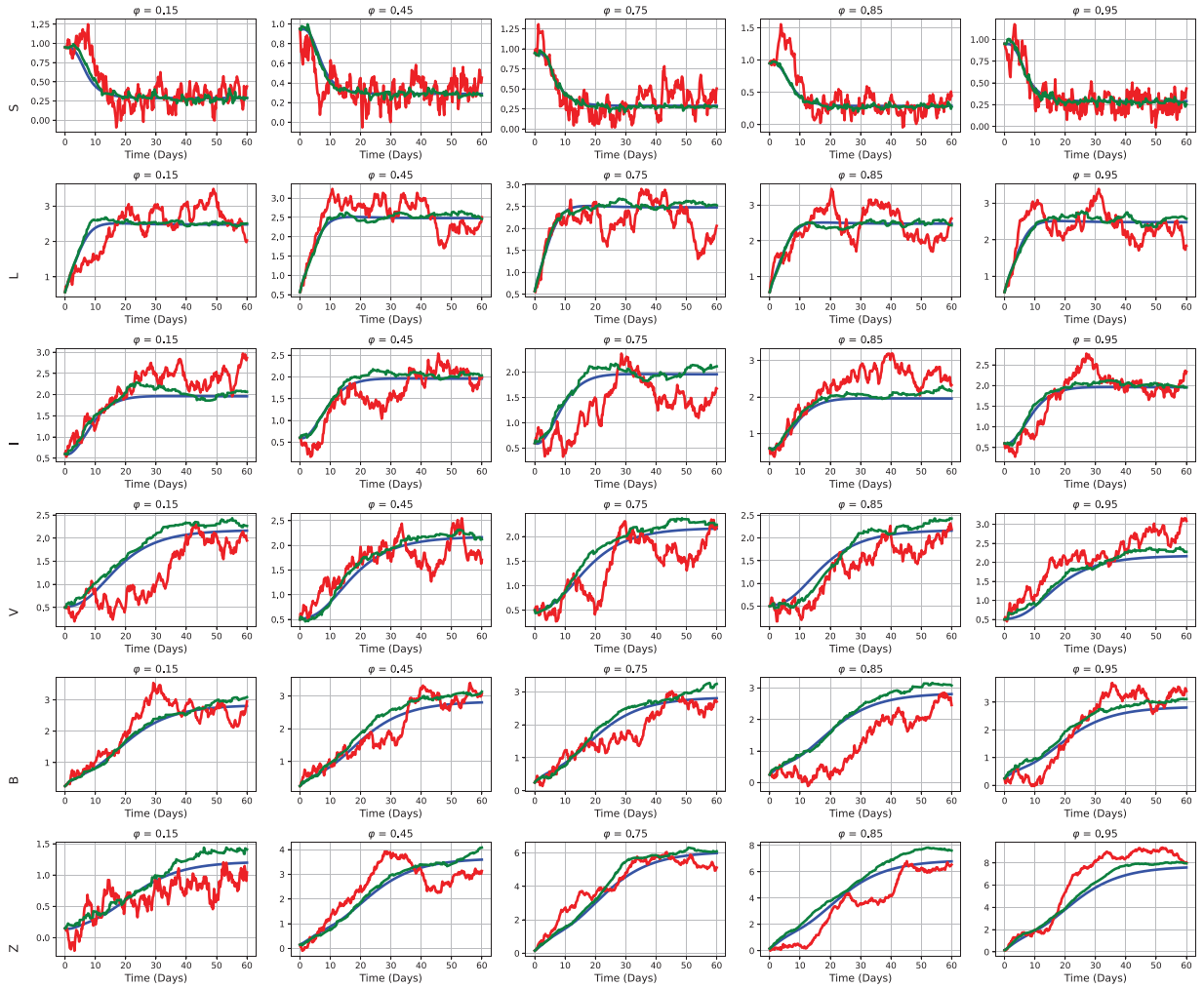

Figure 13: Influence of varying concentrations of actively infected cells φ on the spread and eradication of CHIKV model for deterministic (2), white noise (3) and Lévy noise (4) within a population. Reductions in $\varphi = [0.15, 0.45, 0.75, 0.85, 0.95]$ accelerate the elimination of the infection, emphasizing the importance of controlling infected cell concentrations for effective disease management. The model incorporates nonlinear stochastic disturbances, such as Poisson random measures, to capture unexpected changes in infection rates caused by events like school closures, seasonal fluctuations, and incidents in high-risk settings. These disturbances highlight the need for models that account for external, non-linear factors that influence the transmission of CHIKV

6.5 Impact of ϵ on CHIKV Killing Rate Due to CTL Cells Immune Response

Moreover, the effectiveness of ϵ, representing the cytotoxic T lymphocyte (CTL) cells' immune response, is pivotal in clearing infected cells and, consequently, influencing the CHIKV killing rate. It plays a crucial role in modulating the efficiency of immune responses by controlling how rapidly the immune system targets and eliminates infected cells. As ϵ increases, the immune system's ability to eliminate infected cells improves, leading to a higher viral killing rate and more effective infection control. A higher value of ϵ results in a more

aggressive immune response, which accelerates the clearance of virus-infected cells. This enhanced immune activity reduces the overall virus load, $V(t)$, and contributes to a more rapid decline the infectious people, $I(t)$. As the viral concentration decreases, transmission dynamics are directly affected, resulting in faster infection resolution and a reduced burden on the system. Conversely, a lower value of ϵ weakens the immune response, allowing the virus to persist longer and prolonging the infection's duration, leading to a more severe and sustained epidemic. Simulations indicate that increasing ϵ significantly enhances immune effectiveness, thereby accelerating the elimination of infected individuals and reducing overall epidemic severity. This reinforces the importance of of immune efficiency in controlling the progression and impact of CHIKV outbreaks, emphasizing the significance of the immune response parameters in epidemic management. The dynamic behavior of this process illustrates how adjustments to ϵ can either mitigate or exacerbate the spread of the infection, particularly regarding the hypertrophic effects of CHIKV (see Fig. 14).

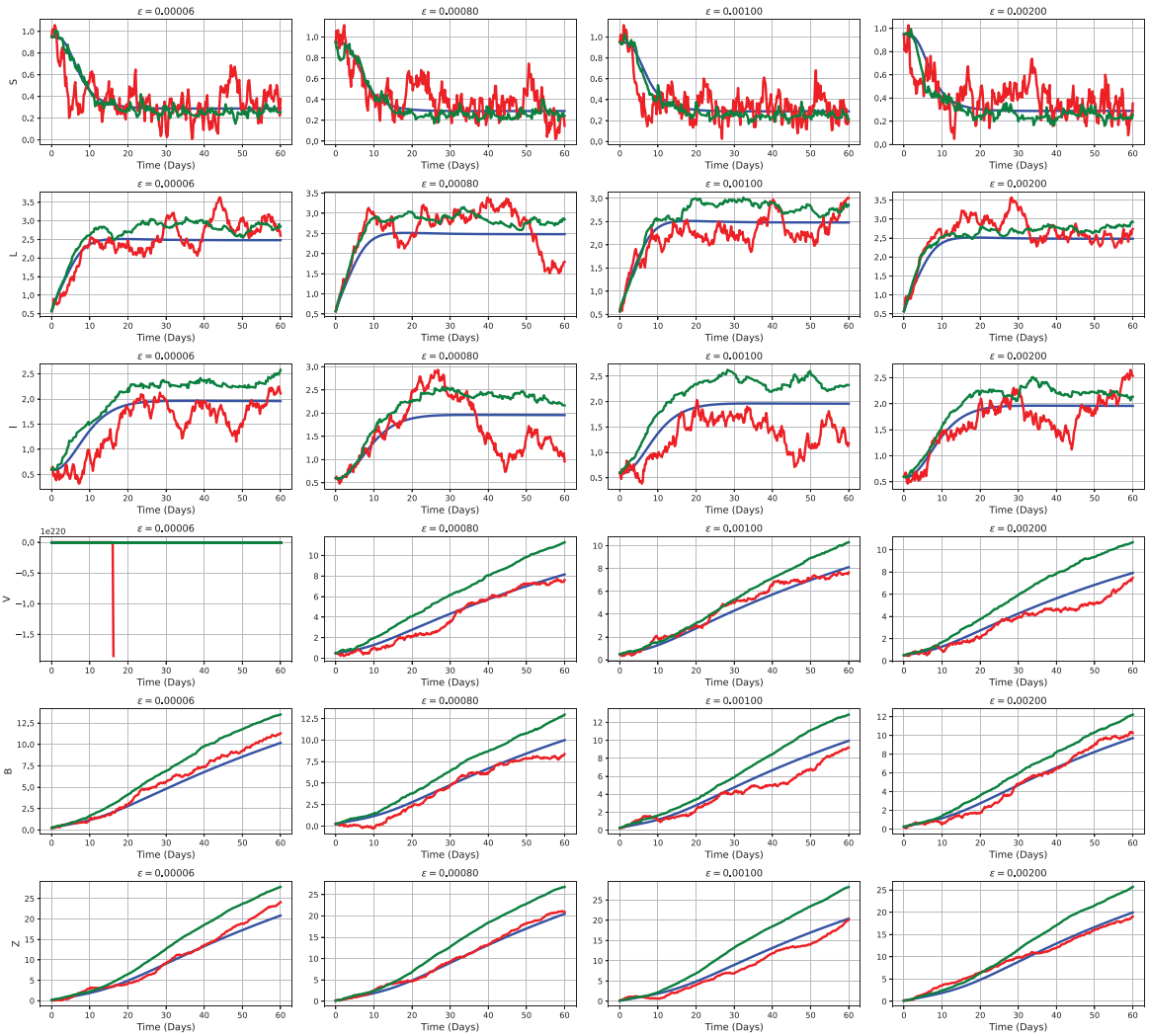

Figure 14: Effectiveness of the CTL cells' immune response, influence the CHIKV killing rate. A higher ϵ accelerates the clearance of infected cells, reduces virus concentration, and leads to a more rapid decline in infected individuals, thereby mitigating the severity and duration of the epidemic. Conversely, a lower ϵ results in a less efficient immune response, prolonging infection and increasing epidemic severity. The figure illustrates the dynamic impact of immune response efficiency on the progression and control of CHIKV outbreaks

6.6 Near Optimal Control Analysis

A stochastic optimal control approach offers a powerful framework for analyzing the dynamics of CHIKV (52) propagation under the influence of continuous control interventions. This method effectively captures the inherent randomness in disease transmission, which may arise from environmental fluctuations, sudden demographic shifts, or unforeseen outbreaks. To accurately represent such stochastic variability, Poisson random measures are employed. These allow the modeling of discrete jump events within the system, reflecting abrupt and irregular changes such as localized infestations or sudden increases in vector populations [50].

The CHIKV model (52) is typically formulated using a compartmental structure that includes the susceptible, latent, and infectious human populations, along with virus concentration, pathogenic load, and immune response compartments. To represent various intervention strategies, a set of time-dependent control functions is introduced, denoted as $\mathrm{u}(\mathrm{t}) = (\mathrm{u}_1(\mathrm{t}), \mathrm{u}_2(\mathrm{t}), \mathrm{u}_3(\mathrm{t}))$. Specifically, $\mathrm{u}_1(\mathrm{t})$ corresponds to vaccination efforts, $\mathrm{u}_2(\mathrm{t})$ captures public health initiatives aimed at reducing exposure through behavioral change and awareness campaigns, and $\mathrm{u}_3(\mathrm{t})$ models vector control measures, such as habitat elimination and insecticide application.

SDEs with jump terms are used to illustrate the system. A Poisson random measure, which introduces unpredictability through discrete, occasional events, governs these jumps. Mathematically, both continuous fluctuations (represented by Brownian motion) and sudden shifts (represented by jumps) affect the evolution of a state variable, such as the pathogenic population $\mathrm{I}(\mathrm{t})$. This leads to the following behavior:

$$d\mathrm{I}(\mathrm{t}) = \digamma_1\left(\mathrm{I}(\mathrm{t}), \mathrm{u}(\mathrm{t})\right) d\mathrm{t} + \sigma_3 \mathrm{I}(\mathrm{t}) d\mathbb{B}_3(\mathrm{t}) + \int_{\Phi} \Theta_3(\Psi)\mathrm{I}(\mathrm{t}^-)\bar{\aleph}(d\mathrm{t}, d\Psi). \tag{165}$$

The deterministic component of the dynamics is represented by $\digamma_1$, the diffusion coefficient for stochastic noise is σ_3, and the jump tendency is captured by the integral component in connection to the compensated Poisson random measure $\bar{\aleph}(d\mathrm{t}, d\Psi)$. The system condition and random parameter Ψ, which could indicate the severity of an outbreak occurrence, are employed by the function Θ_3 to calculate the size of the jumps.

The goal of the control approach is to achieve equilibrium between the economic cost of treatments and the impact of illnesses by minimizing a cost functional over a finite time horizon $\mathbf{T}$. Usually, this is presented as

$$\min_{\mathrm{u}(\mathrm{t})} \mathbb{E}\left[\int_0^{\mathbf{T}} \left(\mathcal{C}_{\mathrm{S}}\mathrm{S}(\mathrm{t}) + \mathcal{C}_{\mathrm{L}}\mathrm{L}(\mathrm{t}) + \mathcal{C}_{\mathrm{I}}\mathrm{I}(\mathrm{t}) + D_1\mathrm{u}_1^2(\mathrm{t}) + D_2\mathrm{u}_2^2(\mathrm{t}) + D_3\mathrm{u}_3^2(\mathrm{t})\right) d\mathrm{t}\right]. \tag{166}$$

The weights $\mathcal{C}_{\mathrm{S}}$, $\mathcal{C}_{\mathrm{L}}$, and $\mathcal{C}_{\mathrm{I}}$ represent the relative importance of reducing transmission, administering treatments, and controlling mosquito populations, respectively, while D_1, D_2, and D_3 penalize the implementation of control measures.

Exact control is often unattainable due to the challenges posed by randomness and jumps. As a result, computational techniques such as adaptive programming, Pontryagin's Maximum Principle in stochastic environments [69], or reinforcement learning-inspired approaches are employed to identify near-optimal control strategies. These methods allow for the dynamic adaptation of control strategies to prevent CHIKV spread, responding to observable situations and jump events.

The following is a detailed algorithm for implementing near-optimal control of the CHIKV epidemic model, governed by a SDE with Poisson random measures. This algorithm utilizes stochastic simulation with control approximation, often through the stochastic maximum principle or dynamic programming

combined with MCMC-based backward-forward sweep methods. The Hamiltonian $\mathcal{H}$ for the controlled process is defined as:

$$\mathcal{H} = \langle \lambda_S, f_S(\mathbf{X}, \mathrm{u}) \rangle + \langle \lambda_L, f_L(\mathbf{X}, \mathrm{u}) \rangle + \langle \lambda_I, f_I(\mathbf{X}, u) \rangle + L(\mathbf{X}, \mathrm{u}), \tag{167}$$

where $\lambda_S, \lambda_L, \lambda_I$ are adjoint variables and $L(\mathbf{X}, \mathrm{u})$ is the running cost functional.

- Initialize control variables $\mathrm{u}^0(\mathrm{t})$ and state variables $\mathbf{X}^0(\mathrm{t})$ over time grid $\mathrm{t} \in [0, T]$.
- For each iteration $k = 1$ to maximum iterations.
- Simulate the state equations $\mathbf{X}^\ell(\mathrm{t})$ using $\mathrm{u}^{\ell-1}(\mathrm{t})$ with Lévy noise via MCMC samples.
- Solve the backward BSDEs for adjoint variables $\lambda^\ell(\mathrm{t})$ using terminal conditions.
- Hamiltonian Minimization: Update control $\mathrm{u}^\ell(\mathrm{t})$ by minimizing $\mathcal{H}(\mathbf{X}^\ell, \lambda^\ell, \mathrm{u})$ pointwise.
- Check for convergence: if $\|\mathrm{u}^\ell - \mathrm{u}^{\ell-1}\| < \mathrm{tol}$,
- Final control u^* and state trajectories $\mathbf{X}^*$.

This formulation allows us to analyze and optimize the trade-off between reducing the number of infections and the expense of applying interventions [50].

6.7 Parameter Selection and Simulation Setup

The weight parameters in the objective functional are set as $\mathcal{C}_S = 0.1$, $\mathcal{C}_L = 0.5$, and $\mathcal{C}_I = 1.0$ to ensure a balanced quantitative evaluation. These values help maintain equilibrium within the disease transmission dynamics while appropriately prioritizing distinct prevention strategies. The simulation is conducted over the time interval $[0, 100]$ days, with initial conditions for each compartment specified in Section 5.1.2. The impact of the control functions $\mathrm{u}_\iota(\mathrm{t})$, for $\iota = 1, 2, 3$, is analyzed in terms of minimizing the objective functional while preserving a biologically feasible and infection-stable system structure. A control intensity of $\mathrm{t}_0 = 2.345$ is selected to enhance vaccination and other prevention efforts without compromising the structural integrity of the model.

This study investigates the impact of time-dependent near-optimal control strategies within a stochastic epidemic model comprising multiple compartments. The interactions among these compartments are shaped by persistent infection dynamics, vaccination interventions, and random disturbances in transmission. To account for external uncertainties—such as environmental variability and individual behavioral changes—a Poisson random measure is incorporated into the model, effectively simulating stochastic fluctuations in disease spread.

The assessment of age-structured near-optimal strategies for mitigating CHIKV recurrence under stochastic influences is facilitated by this framework. It explicitly incorporates age-dependent interactions among susceptible, latent, and infectious individuals within each stratification category. These dynamics are influenced by behavioral patterns, vaccination policies, and external disturbances modeled via a Poisson random measure.

As illustrated in Fig. 15, targeted control measures significantly enhance the stability of the susceptible population $\mathrm{S}(\mathrm{t}, \ell)$, where ℓ denotes the age-structured cohort. In contrast, in the absence of intervention, this compartment experiences substantial declines across all age groups, highlighting the critical role of structured immunization programs and non-pharmaceutical interventions in reducing disease prevalence.

Theorem 5 and Theorem 6 provide theoretical proof of the effectiveness of the suggested control strategy. The adjoint Eq. (64) is well-posed and has a unique solution $(\mathrm{f}_1(\mathrm{t}), \mathrm{f}_2(\mathrm{t}), \wp(\mathrm{t}), \sigma(\mathrm{t}, \vartheta))$ that satisfies the bound given in (68). These theorems are validated under the assumptions of (166) and (167), respectively.

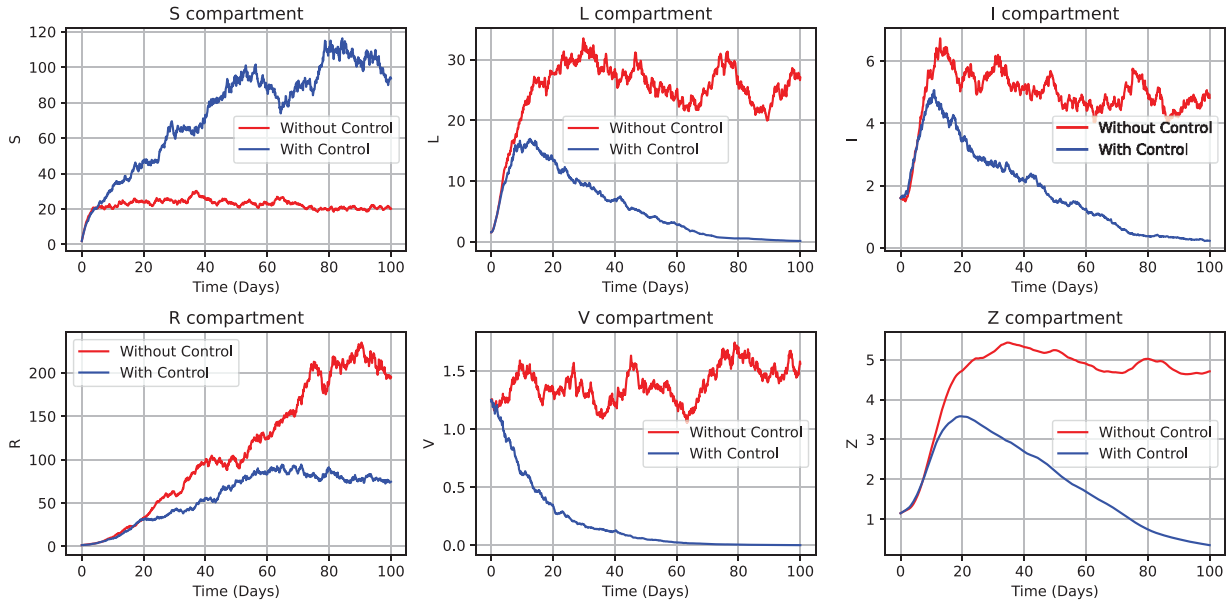

Figure 15: Impact of age-targeted control strategies on the CHIKV model (52). The plot demonstrates that in the presence of optimal interventions, $S(t,\ell)$ remains more stable across age cohorts, as opposed to the significant decline observed without control measures. This supports the analytical findings of Theorems 5 and 6, which ensure the well-posedness and boundedness of the adjoint system (64) under assumptions (166) and (167), reinforcing the efficacy and biological relevance of the proposed near-optimal control framework

These findings ensure the biological authenticity across all age groups by validating the implemented control concentrations over a short time period and confirming the stability of infectious agent dynamics. Furthermore, the model incorporates stratification across age groups, where the disease dynamics for each compartment—susceptible $S(t,\ell)$, latent $L(t,\ell)$, and infectious $I(t,\ell)$—are regulated by time-dependent control variables $u_\iota(t)_{\iota=1}^{3}$ that aim to mitigate disease prevalence while accounting for stochastic effects introduced via Lévy noise and Poisson random measures.

The analysis employs a Hamiltonian framework to construct an adjoint system, coupling the state dynamics with backward stochastic differential equations (BSDEs). The cost functional is defined to balance public health outcomes with control expenditures and is structured as follows:

$$\mathcal{J}(u_1,u_2,u_3) = \mathbb{E}\int_0^{\widehat{\mathfrak{I}}}\left[\mathcal{C}_S\|S(t,\ell)\|^2 + \mathcal{C}_L\|L(t,\ell)\|^2 + \mathcal{C}_I\|I(t,\ell)\|^2 + \sum_{\iota=1}^{3} D_{u_\iota}\|u_\iota(t)\|^2\right]dt.$$

Under the assumptions $(\mathbf{A_1})$–$(\mathbf{A_3})$, Theorem 7 guarantees the existence and uniqueness of a solution to the adjoint system $\mathrm{E}\int_0^{\widehat{\mathfrak{I}}}\left(\|f_1-\tilde{f}_1\|^{\Psi} + \|f_2-\tilde{f}_2\|^{\Psi} + \|t-\tilde{t}\|^{\Psi}\mathbf{1}_{\Lambda(t^-)=i}\pi_{ij} + \int_Y \|\vartheta-\tilde{\vartheta}\|^{\Psi}\varpi_8(d\varsigma)\right)dt \le Cd(\omega_t,\tilde{\omega}_t)^{\Psi\rho}$.This framework enables the evaluation of age-dependent, near-optimal strategies for controlling CHIKV outbreaks. Within each stratification category, it captures the influence of behavioral trends, immunization programs, and stochastic perturbations modeled by Poisson measures.

Tailored control strategies significantly enhance the stability of the susceptible population $S(t,\ell)$, where ℓ denotes the age-structure index, as demonstrated in Fig. 16. In contrast, in the absence of intervention, this compartment experiences marked declines across all age cohorts. These results emphasize the importance of coordinated vaccination and non-pharmaceutical interventions in reducing infection prevalence.

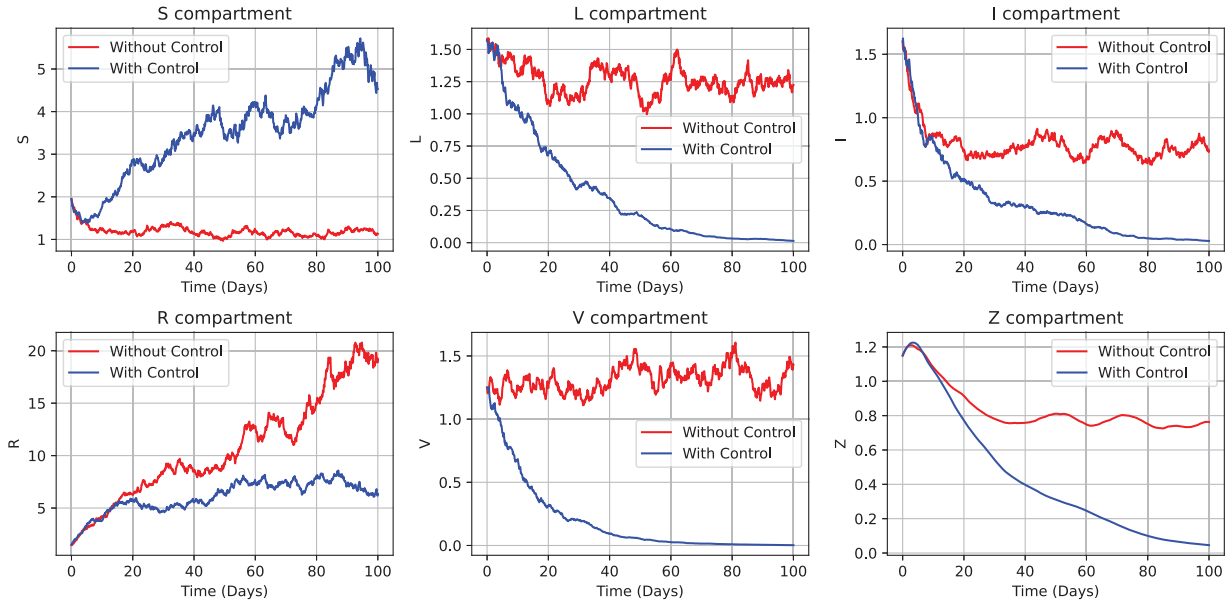

Figure 16: Illustration of the age-structured stochastic CHIKV model (52) dynamics incorporating control variables $u_\iota(t)_{\iota=1}^{3}$ for each epidemiological compartment—susceptible $S(t,\ell)$, latent $L(t,\ell)$, and infectious $I(t,\ell)$—across age groups. The model is driven by stochastic influences, with randomness introduced via Poisson random measures. A Hamiltonian framework couples the forward state dynamics with backward SDEs, leading to a cost functional that quantifies trade-offs between health outcomes and control costs. Theoretical support is provided by Theorem 7, which ensures the existence and uniqueness of solutions under assumptions $(\mathbf{A_1})$–$(\mathbf{A_3})$

Meanwhile, this analysis incorporates time-dependent control functions and Hamiltonian analysis to derive near-optimal intervention strategies. Each compartment, including susceptible $S(t,\ell)$, latent $L(t,\ell)$, and infectious $I(t,\ell)$ individuals, is structured across age classes indexed by ℓ, allowing for a more granular control analysis tailored to population heterogeneity.

The control strategies $u_\iota(t)$ $(\iota = 1,2,3)$ are designed to minimize a weighted cost functional that balances the reduction in disease burden with the cost of implementation provided in (166). Using the Hamiltonian formalism (167), the system dynamics are coupled with the adjoint processes $(f_1(t), f_2(t), \sigma(t,\vartheta))$, and the Hamiltonian $\mathbb{H}$ is defined to reflect the instantaneous cost and dynamics of the system. The sufficiency condition for near-optimality is provided in Theorem 8, which ensures that under assumptions $(\mathbf{A_1})$–$(\mathbf{A_3})$, the control strategy $(\Upsilon_t^\epsilon, \omega_t^\epsilon)$ satisfies (104).

This framework facilitates a rigorous evaluation of age-specific intervention impacts in the presence of stochastic fluctuations, including behavioral variability and environmental noise, modeled through Poisson random measures. The effectiveness of these control strategies is demonstrated in Fig. 17, where the susceptible subpopulation, $S(t,\ell)$, exhibits enhanced stability across age groups under optimal intervention, while it declines significantly in the absence of control measures. This highlights the importance of integrating age-structured and stochastic factors into the design of epidemic control policies.

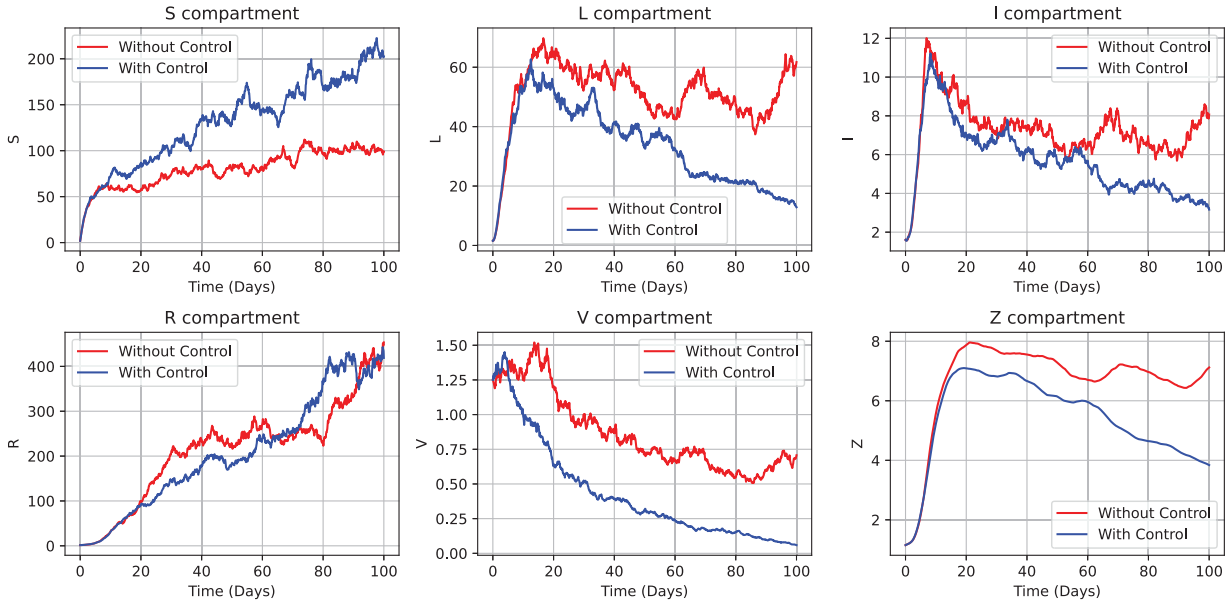

Figure 17: Depiction of the optimal control strategies $u_\iota(t)$ $(\iota = 1, 2, 3)$, which are formulated to minimize the weighted cost functional given in (166) for CHIKV model (52). The cost balances reductions in disease burden across the susceptible $S(t, \ell)$, latent $L(t, \ell)$, and infectious $I(t, \ell)$ compartments with the implementation costs associated with each control. The functional incorporates weight parameters $\mathcal{C}_S$, $\mathcal{C}_L$, $\mathcal{C}_I$, and D_{u_ι} to capture the relative priorities of epidemiological containment and resource expenditure. Utilizing the Hamiltonian framework from (167), the system is dynamically linked with adjoint variables $(f_1(t), f_2(t), \sigma(t, \vartheta))$, and the sufficiency of the control's near-optimality is guaranteed under Theorem 8

Moreover, near-optimal control theory, particularly when formulated through Hamiltonian structures and adjoint equations, has proven robust in epidemiological modeling where exact optimal controls are either infeasible or prohibitively costly. By leveraging the sufficiency and necessary optimality conditions (as derived in Theorem 9), the framework ensures that the proposed control strategy performs closely to an ideal optimal scenario without incurring prohibitive computational or logistical costs. This aligns with the broader stochastic control literature in mathematical epidemiology, which emphasizes trade-offs between intervention costs and epidemic mitigation [70]. Fig. 18 illustrates the decline in the infected class and the stabilization of virus/pathogen compartments under this control regime. These outcomes emphasize the importance of both the timing and intensity of interventions in managing outbreaks, especially under conditions of uncertainty.

Together, these strands of literature validate the formulation of an age-structured stochastic CHIKV model embedded with near-optimal control. This approach provides a mathematically rigorous and empirically grounded framework for designing and analyzing intervention policies in the face of demographic diversity and random perturbations.

The figure illustrates an age-structured model for CHIKV, where the human population is divided into three epidemiological states—susceptible, latent, and infectious—across each age group ℓ. This structure reflects real-world heterogeneity in disease progression, contact patterns, and immune responses across demographic strata. As suggested by Esteva and Vargas [70] and later supported by Agusto et al. [71], such stratification is crucial for modeling age-specific interventions and evaluating their differential impacts.

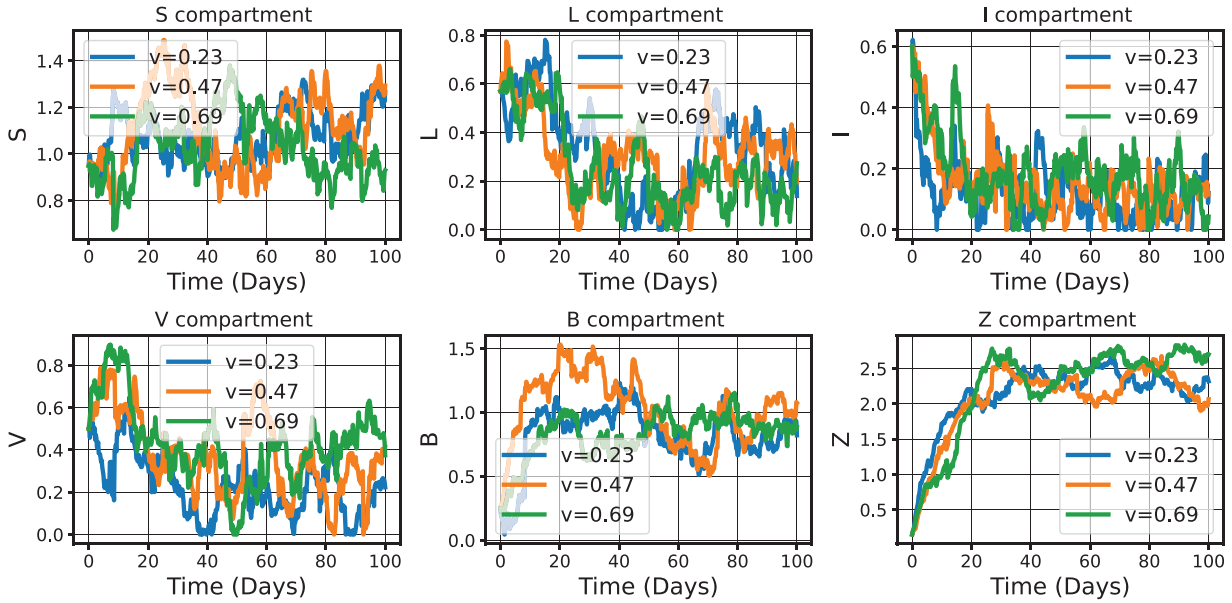

Figure 18: Graphical illustration decline in the infected class and stabilization of virus/pathogen compartments under an age-structured stochastic CHIKV model (52) with near-optimal control. The model incorporates age-specific compartments and stochastic perturbations, such as Lévy noise, to capture abrupt real-world events. Intervention strategies, including age-targeted vaccination and vector control, aim to minimize a cost functional balancing epidemiological outcomes with control efforts describing the necessary criteria of Theorem 9. This approach provides a rigorous and empirically grounded methodology for designing and analyzing intervention policies in the presence of demographic diversity and random fluctuations

Transitions between compartments are governed not only by deterministic epidemiological rates (e.g., transmission, immunization, recovery) but also by stochastic perturbations, which are modeled through a Poisson random measure superimposed with Lévy noise. This framework enables the simulation of abrupt random events, such as climate anomalies, vector density surges, or behavioral changes—phenomena increasingly observed in real epidemics, as highlighted in studies like that of Applebaum [72].

Superimposed on this structure are control arrows representing intervention strategies, denoted by the control process defined in Theorem 9, which satisfies $\rho \in [1, 2)$. These strategies include age-targeted vaccination, vector control, or non-pharmaceutical interventions (e.g., bed nets, awareness campaigns). The controls influence each compartment, reducing susceptibility, delaying exposure, or shortening the infectious period. The objective of these interventions is to minimize a cost functional, balancing epidemiological outcomes (infection prevalence, latency levels) against the cost of control efforts. Inspired by the frameworks of Fleming and Rishel [73] and applied to stochastic epidemic control by Buckwar and Riedler [74], the system leverages near-optimal control theory—a methodology that seeks controls that are close to optimal within a predefined error threshold. Fig. 19 demonstrates not only the interconnectedness of age-specific compartments but also the multi-objective nature of epidemic control under uncertainty. The near-optimal control conditions are governed by a Hamiltonian framework, and necessity conditions (as detailed in theorems like Theorem 9 in this work) are imposed to ensure performance guarantees despite the stochastic noise. In summary, the figure encapsulates a mathematically rigorous and biologically informed framework for designing and analyzing control policies for CHIKV epidemics. It is firmly grounded in the current literature on stochastic differential equations, optimal control theory, and age-structured modeling. Additionally, the control parameters and statistical variations used in the simulation inputs are summarized in Table 6.

Model calibration and validation show strong agreement between theoretical projections and observed epidemic behavior, further supporting the framework's reliability. The close match between synthetic and observed trends confirms that the model accurately captures the nonlinear and stochastic dynamics of CHIKV transmission.

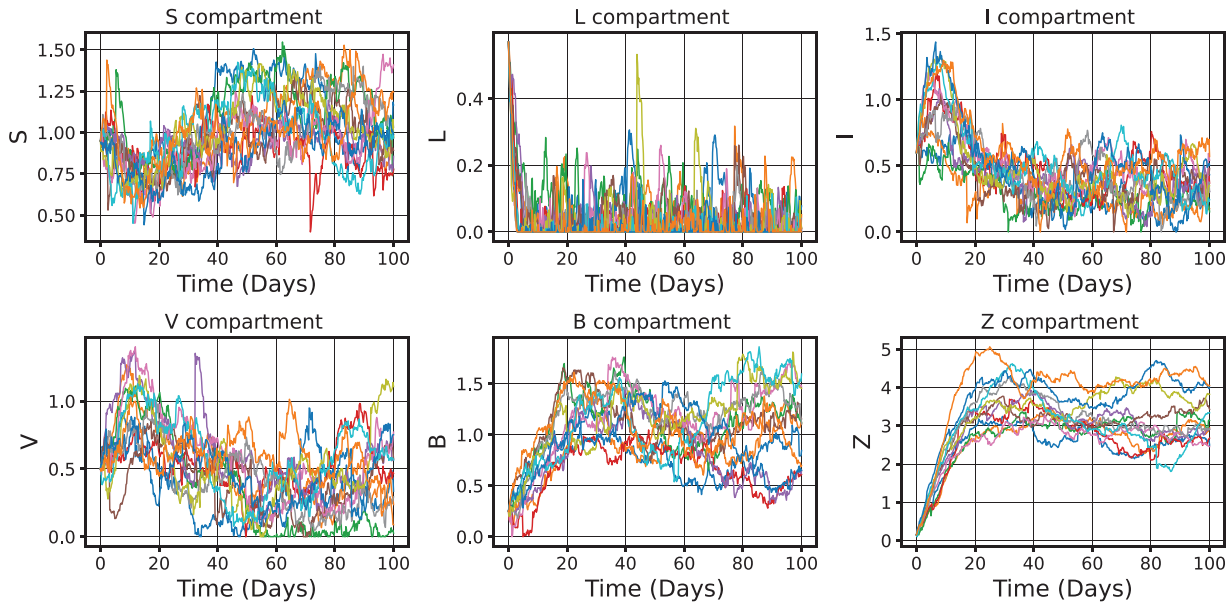

Figure 19: Highlights for the interconnectedness of age-specific compartments and the multi-objective nature of CHIKV epidemic model (52) control under uncertainty. Governed by a Hamiltonian framework, the near-optimal control conditions ensure robustness against stochastic perturbations. The model integrates age structure, stochastic dynamics, and optimal control theory, providing a reliable and biologically informed basis for policy design supported by the argument of Theorem 9, such as $1 < \rho < 2$. Calibration results, summarized in Table 6, demonstrate strong alignment between simulated outcomes and observed epidemic trends

Table 6: Control and model parameters with admissible conditions for the age-structured CHIKV model (52) under Lévy noise

Symbol	Description	Type	Criteria
$u_1(t)$	Vaccination rate of susceptible individuals	Control	$0 \le u_1(t) \le 1$
$u_2(t)$	Quarantine/awareness effort for latent class	Control	$0 \le u_2(t) \le 1$
$u_3(t)$	Treatment intensity for infected individuals	Control	$0 \le u_3(t) \le 1$
β	Virus propagation rate	Model parameter	$\beta > 0$
ϖ_1	Natural mortality rate of susceptible	Model specification	$\varpi_1 \ge 0$
ϖ_2	Death rate due to infection	Model specification	$\varpi_2 \ge 0$
σ_i	Diffusion coefficient (Brownian noise) for i^{th} class	Noise (Brownian)	$\sigma_i \ge 0,\ i = 1, 2, 3, \ldots$
$\Theta_i(\Psi)$	Jump size for i^{th} class (Lévy jump)	Noise (Lévy)	$\Theta_i(\Psi) \in L^2(\Phi, \Psi)$
ϵ	Nonlinear crowding effect in infected class	Model specification	$\epsilon \ge 0$
π	Recruitment/birth rate of susceptibles	Model specification	$\pi \ge 0$
ρ	Proportion progressing to infection directly	Model specification	$0 \le \rho \le 1$
Θ	Progression rate from latent to infectious	Model specification	$\Theta \ge 0$
φ	Activation rate of latent class	Model specification	$\varphi \ge 0$

7 Conclusion

CHIKV, an arthropod-transmitted *alphavirus* of the *Togaviridae* family, remains one of the most significant arthropod-borne viral infections in humans. This study presents a non-autonomous SDE model that incorporates age-structured dynamics and time-dependent prevalence variations to examine the impact of screening and therapeutic strategies on CHIKV spread. By modeling stochastic disruptions through Poisson random measures, the methodology captures sudden and unexpected changes influencing CHIKV transmission. For the Lévy-based model, we derive global positive solutions, ensuring the system's biological feasibility.

The main contributions have been presented as:

- Developed an age-structured stochastic model that integrates demographic, immunization, and therapeutic interventions to more accurately estimate the basic reproduction number ($\mathbb{R}_{0L}$) under stochastic influences.
- Applied MCMC calibration to fit model predictions to monthly CHIKV incidence data (Florida, USA, 2005–2017), estimating undetermined parameters and initial conditions reliably.
- Provided sensitivity assessments across age groups using 95% confidence intervals, prediction intervals, and training-testing validation, offering practical insights into which populations are most at risk.
- Derived near-optimal control strategies using linear constraints and Ekeland's variational principle, enabling precise evaluation of interventions.
- The model can guide public health interventions by identifying age groups with higher CHIKV incidence and evaluating the impact of vaccination and treatment strategies.
- Computed threshold parameter $\mathbb{R}_{0L}$ indicates disease persistence patterns, informing epidemic preparedness and resource allocation.
- Predictions show that individuals over 66 years old have the highest incidence, while those under 16 are least affected, allowing targeted interventions.

Furthermore, future directions include extending the model to multi-variable systems with co-infections and environmental factors, using advanced methods such as deep learning or Kalman filters to improve predictions and validation across regions. The study is limited by assumptions of homogeneous mixing, ignored spatial or vector heterogeneity, and higher computational costs. Despite these, the framework offers valuable insights for CHIKV control and epidemic modeling.

Acknowledgement: The authors would like to thank the Ongoing Research Funding program (ORF-2025-1404), King Saud University, Riyadh, Saudi Arabia.

Funding Statement: Ongoing Research Funding program (ORF-2025-1404), King Saud University, Riyadh, Saudi Arabia.

Author Contributions: The authors confirm contribution to the paper as follows: study conception and design: Maysaa Al-Qurashi, Ayesha Siddiqa; data collection: Shazia Karim, Yu-Ming Chu; analysis, project administration and interpretation of results: Saima Rashid; draft manuscript preparation: Ayesha Siddiqa, Yu-Ming Chu. All authors reviewed the results and approved the final version of the manuscript.

Availability of Data and Materials: Data sharing not applicable to this article as no datasets were generated or analyzed during the current study.

Ethics Approval: Not applicable.

Conflicts of Interest: The authors declare no conflicts of interest to report regarding the present study.

References

1. World Health Organization. Global chikungunya report 2021. Comput Electr Eng. 2021;92:107129.
2. Fritsch H, Giovanetti M, Xavier J, Adelino TER, Fonseca V, de Jesus JG, et al. Retrospective genomic surveillance of chikungunya transmission in Minas Gerais State, Southeast Brazil. Microbiol Spectr. 2022;10(5):e0128522. doi:10.1128/spectrum.01285-22.
3. Cerqueira-Silva T, Pescarini JM, Cardim LL, Leyrat C, Whitaker H, Antunes de Brito CA, et al. Risk of death following chikungunya virus disease in the 100 million Brazilian cohort, 2015–2018: a matched cohort study and self-controlled case series. Lancet Infect Dis. 2024;24:504–13. doi:10.1016/S1473-3099(23)00567-8.
4. Khongwichit S, Chansaenroj J, Chirathaworn C, Poovorawan Y. Chikungunya virus infection: molecular biology, clinical characteristics, and epidemiology in Asian countries. J Biomed Sci. 2021;28(1):84. doi:10.1186/s12929-021-00778-8.
5. Traverse EM, Millsapps EM, Underwood EC, Hopkins HK, Young M, Barr KL. Chikungunya immunopathology as it presents in different organ systems. Viruses. 2022;14(8):1786. doi:10.3390/v14081786.
6. Costa D, Gouveia P, Silva GEB, Neves P, Vajgel G, Cavalcante M, et al. The relationship between chikungunya virus and the kidneys: a scoping review. Rev Med Virol. 2023;33(1):e2357. doi:10.1002/rmv.2357.
7. Brandler S, Ruffié C, Combredet C, Brault J-B, Najburg V, Prevost M-C, et al. A recombinant measles vaccine expressing chikungunya virus-like particles is strongly immunogenic and protects mice from lethal challenge with chikungunya virus. Vaccine. 2013;31(36):3718–25. doi:10.1016/j.vaccine.2013.05.086.
8. Chattopadhyay S, Roy A, Banerjee A, Goswami R, Basu A, Jana AM. Development and characterization of monoclonal antibody against non-structural protein-2 of chikungunya virus and its application. J Virol Methods. 2014;199:86–94. doi:10.1016/j.jviromet.2014.01.008.
9. Mavale M, Parashar D, Sudeep A, Yadav PD, Gokhale MD, Mourya DT. Venereal transmission of chikungunya virus by *Aedes aegypti* mosquitoes (Diptera: culicidae). Am J Trop Med Hyg. 2010;83(6):1242–4. doi:10.4269/ajtmh.2010.09-0577.
10. Goh LY, Tan HC, Lim XF, Ho BC, Sam IC, Chan YF, et al. Neutralizing monoclonal antibodies to the E2 protein of chikungunya virus protects against disease in a mouse model. Clin Immunol. 2013;149(3):487–97. doi:10.1016/j.clim.2013.10.004.
11. Sourisseau M, Schilte C, Casartelli N, Trouillet C, Guivel-Benhassine F, Rudnicka D, et al. Characterization of reemerging chikungunya virus. PLoS Pathog. 2007;3(6):e89. doi:10.1371/journal.ppat.0030089.
12. Gérardin P, Barau G, Michault A, Bintner M, Randrianaivo H, Choker G, et al. Multidisciplinary prospective study of mother-to-child chikungunya virus infections on the island of La Réunion. PLoS Med. 2008;5:e60.
13. Rezza G, Nicoletti L, Angelini R, Romi R, Finarelli AC, Panning M, et al. Infection with chikungunya virus in Italy: an outbreak in a temperate region. Lancet. 2007;370(9602):1840–6. doi:10.1016/s0140-6736(07)61779-6.
14. Reiter P, Fontenille D, Paupy C. Aedes albopictus as an epidemic vector of chikungunya virus: another emerging problem? Lancet Infect Dis. 2006;6(8):463–4. doi:10.1016/s1473-3099(06)70531-x.
15. Servant MJ, Tenoever B, Lin R. Overlapping and distinct mechanisms regulating IRF-3 and IRF-7 function. J Interferon Cytokine Res. 2002;22(1):49–58. doi:10.1089/107999002753452656.
16. Brito CA, Teixeira MG. Increased number of deaths during a chikungunya epidemic in Pernambuco, Brazil. Mem Inst Oswaldo Cruz. 2017;112(9):650–1. doi:10.1590/0074-02760170124.
17. Blasius AL, Giurisato E, Cella M, Schreiber RD, Shaw AS, Colonna M. Bone marrow stromal cell antigen 2 is a specific marker of type I IFN-producing cells in the naive mouse, but a promiscuous cell surface antigen following IFN stimulation. J Immunol. 2006;177(5):3260–5. doi:10.4049/jimmunol.177.5.3260.
18. Rashid S, Jarad F. Novel investigation of stochastic fractional differential equations measles model via the white noise and global derivative operator depending on mittag-leffler kernel. Comput Model Eng Sci. 2024;139(3):2289–327. doi:10.32604/cmes.2023.028773.
19. Arif MS, Abodayeh K, Nawaz Y. Construction of a computational scheme for the fuzzy HIV/AIDS epidemic model with a nonlinear saturated incidence rate. Comput Model Eng Sci. 2024;138(2):1405–25. doi:10.32604/cmes.2023.028946.

20. Jajarmi A, Baleanu D, Rezapour S, Mohammadi H. A new fractional analysis on the interaction of HIV with $CD4^+$ T-cells. Chaos Soliton Fract. 2018;115(4):1–10. doi:10.1016/j.chaos.2018.06.009.
21. Bellan SE. The importance of age dependent mortality and the extrinsic incubation period in models of mosquito-borne disease transmission and control. PLoS One. 2010;5(4):e10165.
22. Olayiwola MO, Oluwafemi EA. Modeling tuberculosis dynamics with awareness and vaccination using laplace-adomian and fractional calculus. Iran J Sci. 2025;1(1):78. doi:10.1007/s40995-025-01830-0.
23. Olayiwola MO, Tijani KR, Ogunniran MO, Yunus AO, Oluwafemi EA, Abanikanda MO, et al. Modeling the booster vaccine effect on new COVID-19 variant management employs the Atangana-Baleanu-Caputo fractional derivative operator together with the Laplace-Adomian decomposition method. Vacunas. 2025;26(3):500458. doi:10.1016/j.vacun.2025.500458.
24. Mohamed Ali H, Mahdy AM, El-Mesady A. Investigation of stability criteria and optimal control measures for a fractional-order model of human papillomavirus infection and cervical cancer. Int J Biomathematics. 2025;18:1–15. doi:10.1142/s1793524525500639.
25. El-Mesady A, Al-Shami TM, Ali HM. Optimal control efforts to reduce the transmission of HPV in a fractional-order mathematical model. Bound Value Probl. 2025;42(1):1–18. doi:10.1186/s13661-024-01991-8.
26. Buonomo B. Analysis of a malaria model with mosquito host choice and bed-net control. Int J Biomathematics. 2015;8(1550):077. doi:10.1142/s1793524515500771.
27. Chitnis N, Smith T, Steketee R. A mathematical model for the dynamics of malaria in mosquitoes feeding on a heterogeneous host population. J Biol Dyn. 2008;2(3):259–85. doi:10.1080/17513750701769857.
28. Zhang L, Zhou Q, Yang J. Necessary condition for optimal control of doubly stochastic systems. Math Control Relat Fields. 2020;10(2):379–403. doi:10.3934/mcrf.2020002.
29. Huang J, Li X, Wang G. Near-optimal control problems for linear forward-backward stochastic systems. Automatica. 2010;46(2):397–404. doi:10.1016/j.automatica.2009.11.016.
30. Yong J, Zhou X. Stochastic control: hamilton systems and HJB equations. New York, NY, USA: Springer; 1999.
31. Ji C. Dynamics of a multigroup SIR epidemic model with stochastic perturbation. Automatica. 2012;48(8):1859–67. doi:10.1016/j.automatica.2011.09.044.
32. Yang Q. The ergodicity and extinction of stochastically perturbed SIR and SEIR epidemic models with saturated incidence. J Math Anal Appl. 2012;386(2):722–38. doi:10.1016/j.jmaa.2011.11.072.
33. Dereich S, Heidenreich F, Scheutzow M. A multilevel Monte Carlo algorithm for Lévy-driven stochastic differential equations. Stochastic Process Appl. 2011;121(12):2597–17. doi:10.1016/j.spa.2011.03.015.
34. Rubenthaler S. Numerical simulation of the solution of a stochastic differential equation driven by a Lévy process. Stochastic Process Appl. 2003;103(2):313–32. doi:10.1016/s0304-4149(02)00191-6.
35. Zhou Y, Yuan S, Zhao D. Threshold behavior of a stochastic SIS model with Lévy jumps. Appl Math Comput. 2016;275:255–67.
36. Liu M, Bai C. Optimal harvesting of a stochastic mutualism model with Lévy jumps. Appl Math Comput. 2016;276(247):301–9. doi:10.1016/j.amc.2015.11.089.
37. Shu H, Jin HY, Wang XS, Wu J. Viral infection dynamics with immune chemokines and CTL mobility modulated by the infected cell density. J Math Biol. 2024;88(4):43.
38. Dubey P, Dubey US, Dubey B. Modeling the dynamics of viral-host interaction during treatment of productively infected cells and free virus involving total immune response. Nonlinear Anal Model Control. 2021;26(4):678–701. doi:10.15388/namc.2021.26.21434.
39. Handel A, Antia R. A simple mathematical model helps to explain the immunodominance of CD8 T cells in influenza A virus infections. J Virol. 2008;82(16):7768–72. doi:10.1128/jvi.00653-08.
40. Cui T, Liu P, Din A, Khan A. Impact of Lévy noise on a stochastic Norovirus epidemic model with information intervention. Math Methods Appl Sci. 2023;46(6):4715–30. doi:10.1002/mma.9655.
41. Gikhman II, Skorokhod AV. Stochastic differential equations. Berlin/Heidelberg, Germany: Springer; 2007.
42. El Fatini M, Sekkak I. Lévy noise impact on a stochastic delayed epidemic model with Crowley-Martin incidence and crowding effect. Physica A. 2020;541(2):123315. doi:10.1016/j.physa.2019.123315.

43. Din A, Li Y. Lévy noise impact on a stochastic hepatitis B epidemic model under real statistical data and its fractal-fractional Atangana–Baleanu order model. Phys Scr. 2021;96(12):124008. doi:10.1088/1402-4896/ac1c1a.
44. Zhang XB, Wang XD, Huo HF. Extinction and stationary distribution of a stochastic SIRS epidemic model with standard incidence rate and partial immunity. Physica A. 2019;531(3):121548. doi:10.1016/j.physa.2019.121548.
45. Song Y, Liu P, Din A. A novel stochastic model for human Norovirus dynamics: vaccination impact with Lévy noise. Fractal Fract. 2024;8(6):349.
46. Hafayed M, Abbas S. On near-optimal mean-field stochastic singular controls: necessary and sufficient premises for near-optimality. J Optim Theory Appl. 2014;160(3):778–808. doi:10.1007/s10957-013-0361-1.
47. Liu Z, Guo S, Tan R, Liu M. Modeling and analysis of a non-autonomous single-species model with impulsive and random perturbations. Appl Math Model. 2016;40(9–10):5510–31. doi:10.1016/j.apm.2016.01.008.
48. Kuang D, Li J, Gao D, Luo D. Stochastic near-optimal control for a system with Markovian switching and Lévy noise. Chaos Soliton Fract. 2024;178:114360. doi:10.1016/j.chaos.2023.114360.
49. Donnelly C. Sufficient stochastic maximum principle in a regime-switching diffusion model. Appl Math Optim. 2011;64(2):155–69. doi:10.1007/s00245-010-9130-9.
50. Peng S. A general stochastic maximum principle for optimal control problems. SIAM J Control Optim. 1990;28(4):966–79. doi:10.1137/0328054.
51. Li M, Wu Z. Necessary and sufficient assertions of near-optimality in a regime-switching diffusion model. Optim Control Appl Methods. 2020;41(3):793–807. doi:10.1002/oca.2571.
52. Mao X. Stochastic differential equations and applications. Amsterdam, The Netherland: Elsevier; 2007.
53. Ekeland I. On the variational principle. J Math Anal Appl. 1974;47(2):324–53.
54. Zhu Y, Wang L, Qiu Z. Dynamics of a stochastic cholera epidemic model with Lévy process. Physica A. 2022;595(1):127069. doi:10.1016/j.physa.2022.127069.
55. Ain QT, Din A, Qiang X, Kou Z. Dynamics for a nonlinear stochastic cholera epidemic model under Lévy noise. Fractal Fract. 2024;8(5):293. doi:10.3390/fractalfract8050293.
56. Mao X, Wei F, Wiriyakraikul T. Positivity preserving truncated Euler–Maruyama method for stochastic Lotka-Volterra competition model. J Comput Appl Math. 2021;394(3):113566. doi:10.1016/j.cam.2021.113566.
57. Data-Center of USA Public Health Science. Data director [Internet]. 2023 [cited 2025 Jul 16]. Available from: https://www.phsciencedata.usa/Share/en/index.jsp.
58. Florida Department of Economic and Demographic Research, U.S. Census Bureau. Population data for florida, 2005–2019 [Internet]. 2023 [cited 2025 Jul 16]. Available from: http://edr.state.fl.us/Content/population-demographics/data/index.cfm.
59. Byers NM, Fleshman AC, Perera R, Molins CR. Metabolomic insights into human arboviral infections: dengue, Chikungunya, and Zika viruses. Viruses. 2019;11(3):225. doi:10.3390/v11030225.
60. de Lima STS, de Souza WM, Cavalcante JW, Candido DDS, Fumagalli MJ, Carrera J-P, et al. Fatal outcome of Chikungunya virus infection in Brazil. Clin Infect Dis. 2021;73:2436–43.
61. Reisinger EC, Tschismarov R, Beubler E, Wiedermann U, Firbas C, Loebermann M, et al. Immunogenicity, safety, and tolerability of the measles-vectored Chikungunya virus vaccine MV-CHIK: a double-blind, randomised, placebo-controlled and active-controlled phase 2 trial. Lancet. 2018;392(10165):2718–27. doi:10.1016/s0140-6736(18)32488-7.
62. Schilte C, Staikovsky F, Couderc T, Madec Y, Carpentier F, Roux K, et al. Correction: chikungunya virus-associated long-term arthralgia: a 36-month prospective longitudinal study. PLoS Negl Trop Dis. 2013;7(3):e2137. doi:10.1371/journal.pntd.0002137.
63. Cazelles B, Chavez M, De Magny GC, Guegan J, Hales S. Time-dependent spectral analysis of epidemiological time-series with wavelets. J R Soc Interface. 2007;4(15):625–36. doi:10.1098/rsif.2007.0212.
64. Centers for Disease Control and Prevention (CDC). Population census and population estimates [Internet]. 2023 [cited 2025 Jul 16]. Available from: https://www.cdc.gov/nchs/hus/sources-definitions/census-population.htm.
65. Haario H, Laine M, Mira A, Saksman E. DRAM: efficient adaptive MCMC. Stat Comput. 2006;16(4):339–54. doi:10.1007/s11222-006-9438-0.
66. Cressie NAC. Statistics for spatial data. Revised ed. New York, NY, USA: Wiley; 1993.

67. Wikipedia. One in ten rule [Internet]. 2022 [cited 2025 Mar 26]. Available from: https://en.wikipedia.org/wiki/One_in_ten_rule.
68. McKay MD, Beckman RJ, Conover WJ. A comparison of three methods for selecting values of input variables in the analysis of output from a computer code. Technometrics. 1979;21(2):239–45. doi:10.1080/00401706.1979.10489755.
69. Huang M, Caines PE. Pontryagin's maximum principle for mean field stochastic control problems. SIAM J Control Optim. 2009;48(8):5145–75.
70. Esteva L, Vargas C. Analysis of a model for the transmission dynamics of the dengue virus in a human population. Math Biosci. 1998;149(1):41–61. doi:10.1016/S0025-5564(98)00006-6.
71. Agusto FB, Mbohwa C, Lokossou T. Modeling and analysis of age-structured population for the control of vector-borne diseases. Math Biosci Eng. 2016;13(2):263–81. doi:10.3934/mbe.2016.13.263.
72. Applebaum D. Lévy processes and stochastic calculus. 2nd ed. Cambridge, UK: Cambridge University Press; 2009.
73. Fleming WH, Rishel RW. Deterministic and stochastic optimal control. 1st ed. New York, NY, USA: Springer-Verlag; 1975.
74. Buckwar E, Riedler M. Adaptive control for stochastic epidemic models. Math Biosci Eng. 2011;8(4):935–50. doi:10.3934/mbe.2011.8.935.